MECAME 2018

4th Mediterranean Conference on the Applications of the Mössbauer Effect

In honour of Frank J. Berry

Zadar, Croatia

27-31 May 2018

BOOK OF ABSTRACTS

Edited by:

Mira Ristić

Željka Petrović

Lidija Androš Dubraja

Stjepko Krehula

MECAME 2018 Book of Abstracts

Edited by:
Mira Ristić
Željka Petrović
Lidija Androš Dubraja
Stjepko Krehula

Logo designed by:
Tea Glušica

Published by: Ruđer Bošković Institute, Zagreb, Croatia (2018)

Printed by: ART STUDIO AZINOVIĆ d.o.o., Zagreb, Croatia

ISBN: 978-953-7941-23-9

WELCOME TO MECAME 2018!

It is my great pleasure to welcome you to the 4th Mediterranean Conference on the Application of the Mössbauer Effect, MECAME 2018, which is taking place at the hotel Kolovare, Zadar, Croatia, from 27 to 31 May 2018.

MECAME 2018 is being organized in honour of Professor Frank J. Berry (University of Birmingham, UK) on the occasion of his 70th birthday to celebrate his life-long scientific contributions in the application of Mössbauer spectroscopy in materials chemistry and physics. He has made a significant contribution to the study of catalytically active mixed metal oxides, superconducting oxides, aluminosilicates, rare earth exchanged Y-zeolites, pillared clays, magnetic oxides, fluorinated perovskites, new materials derived from mineral structures and other materials. He holds the view that Mössbauer spectroscopy is an important complementary technique to other methods of characterisation including EXAFS, X-ray, neutron and electron diffraction methods.

Professor Berry has also held many important positions at national as well as international level. It is well known to all of you that for six years he served as Chairman of International Board on the Applications of Mössbauer Effect (IBAME) and at the present he is an Honorary Director of the Mössbauer Effect Data Center.

I am very happy that many of his collaborators, former students, colleagues and friends will contribute greatly to MECAME 2018 sharing with Frank and all participants the newest results of their research on the application of Mössbauer spectroscopy and related instrumental techniques in materials science, chemistry and physics. The MECAME 2018 is great platform for many young scientists to present their own research as well as to learn from the experts in the field.

I wish to thank Professors Tetsuaki Nishida (Kindai University, Fukuoka, Japan) and Virender K. Sharma (Texas A&M University, College Station, Texas, USA), co-chairs of MECAME 2018 for their significant contribution for MECAME 2018 scientific programme. I also wish to thank all members of Local Organizing Committee, who all worked hard on the conference organization, and MECAME 2018 sponsor RITVERC Gmbh, Saint Petersburg, Russia.

Finally, I am thankful to all MECAME 2018 speakers and participants for accepting our invitation making this event to be successful.

I wish you to enjoy the conference, the city of Zadar and Croatia!

Mira Ristić

MECAME 2018 Chair

CONFERENCE SCOPE

Mediterranean Conference on the Applications of the Mössbauer Effect (MECAME 2018) is organized in honour of Professor Frank Berry (University of Birmingham, UK) on the occasion of his 70th birthday to celebrate his life-long scientific contributions in the application of Mössbauer spectroscopy in materials chemistry.

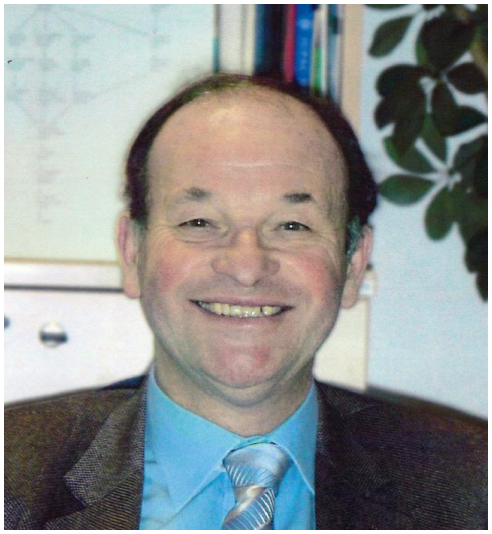

Frank J. Berry was born in London, England on 1st March 1947. He grew up and attended school in London and his interest in chemistry originated at around the age of nine years when his father gave him a chemistry set.

Subsequently Frank studied chemistry in The University of London where he graduated with a B.Sc. degree in 1972. His Ph.D. thesis entitled "Reactions and Nuclear Spectral Characteristics of Some Organotellurium Compounds" was presented to The University of London in 1975.

The first Mössbauer spectrum Frank ever recorded was the tellurium-125 spectrum from diphenylteurium dichloride on 4th January 1974 at AERE Harwell. After a brief time in Simon Fraser University in Vancouver, Canada, Frank returned to England take up a Research Fellowship in the University of Cambridge.

In 1978 he was offered a Lectureship in The University of Birmingham where he was subsequently promoted to Senior Lecturer and later to Reader in Solid State Chemistry. In 1986 he was Visiting Professor of Inorganic Chemistry in the University of Illinois at Urbana-Champagne in the USA. In 1991 Frank was appointed Professor of Inorganic Chemistry in The Open University where he also served as Head of Department for seven years. In 2010 he moved back to The University of Birmingham.

Professor Berry believes that an important component of the discipline of chemistry is the making of new materials, the structural characterisation of these materials, and the evaluation of their physical properties. His research interests have spanned chemistry, physics and materials science and he has enjoyed significant interactions with industry.

His research group has published over 430 papers, he is the Editor of two books, including one on Mössbauer spectroscopy, and has been Editor of The Royal Society of Chemistry Annual Report on the Progress of Chemistry. Frank holds in high esteem the large number of students, postdoctoral workers and visitors who have worked with him and without whom none of the exciting work would have been done. He is also highly indebted to the people with whom he has collaborated and who are now friends of him and his family.

Professor Berry has served on many national and international committees. He has chaired and served on panels reviewing science and institutions in the UK, Europe and USA. In the late 1990's he chaired the group which made the scientific case for the UK's new synchrotron DIAMOND and also chaired the Synchrotron Radiation Source Forum for several years and has been a member or chair of various committees of the UK's research funding organisations.

However, the positions he has enjoyed most are those involved with the Mössbauer community including the great honours of being Honorary Director of the Mössbauer Effect Data Center and serving for six years as Chairman of IBAME.

ORGANIZATION AND SPONSORSHIP

MECAME 2018 is organized by Ruđer Bošković Institute, Zagreb, Croatia.

MECAME 2018 is sponsored by RITVERC GmbH.

TOPICS

- Nanomaterials and Thin Films
- Magnetic and Optical Materials
- Materials Science and Industrial Applications
- Lattice Dynamics and Solid State Physics
- Coordination Chemistry and Solid State Chemistry
- Environmental Science and Catalysis
- Earth and Planetary Sciences
- Biological and Medical Applications
- Synchrotron Mössbauer Spectroscopy

MECAME 2018 COMMITTEES

Organizing Committee

Mira Ristić (chair), Ruđer Bošković Institute, Zagreb, Croatia
Virender K. Sharma (co-chair), Texas A&M University, College Station, Texas, USA
Tetsuaki Nishida (co-chair), Kindai University, Fukuoka, Japan
Stjepko Krehula, Ruđer Bošković Institute, Zagreb, Croatia
Željka Petrović, Ruđer Bošković Institute, Zagreb, Croatia
Lidija Androš Dubraja, Ruđer Bošković Institute, Zagreb, Croatia
Marijan Marciuš, Ruđer Bošković Institute, Zagreb, Croatia
Ana Vidoš, Ruđer Bošković Institute, Zagreb, Croatia

Program Committee

Cathrine Frandsen, Technical University of Denmark, Kongens Lyngby, Denmark
Israel Felner, The Hebrew University, Jerusalem, Israel
Yann Garcia, Catholic University of Louvain, Louvain-la-Neuve, Belgium
Stjepko Krehula, Ruđer Bošković Institute, Zagreb, Croatia
Ernő Kuzmann, Eötvös Loránd University, Budapest, Hungary
Adriana Lančok, Institute of Physics of the Czech Academy of Sciences, Prague, Czech Republic
Libor Machala, Palacky University, Olomouc, Czech Republic
José F. Marco, The Rocasolano Institute of Physical Chemistry, Madrid, Spain
Marcel Miglierini, Slovak University of Technology, Bratislava, Slovakia
Tetsuaki Nishida, Kindai University, Fukuoka, Japan
Israel Nowik, The Hebrew University, Jerusalem, Israel
Mira Ristić, Ruđer Bošković Institute, Zagreb, Croatia
Virender K. Sharma, Texas A&M University, College Station, Texas, USA

International Advisory Board

Cesar Barrero, University of Antioquia, Medellín, Colombia
Stewart J. Campbell, The University of New South Wales, Canberra, Australia
Massimo Carbucicchio, University of Parma, Parma, Italy
Stanislaw M. Dubiel, AGH University of Science and Technology, Krakow, Poland
Vijayendra Garg, University of Brasília, Brasília, Brazil
Mohammad Ghafari, Karlsruhe Institute of Technology, Karlsruhe, Germany
Jean Marc Grenèche, Universite du Maine Le Mans, Le Mans, France
Mohamed Yousry Hassaan, Faculty of Science, Al-Azhar University, Cairo, Egypt
Zoltán Homonnay, Eötvös Loránd University, Budapest, Hungary
Jean-Claude Jumas, University of Montpellier, Montpellier, France
Göstar Klingelhöfer, Johannes Gutenberg University, Mainz, Germany
Yoshio Kobayashi, University of Electro-Communications, Tokyo, Japan
Shiro Kubuki, Tokyo Metropolitan University, Tokyo, Japan
Guido Langouche, Catholic University of Leuven, Leuven, Belgium
Károly Lázár, Centre for Energy Research, Hungarian Academy of Sciences, Budapest, Hungary
Igor S. Lyubutin, Shubnikov Institute of Crystallography, Moscow, Russia
Ko Mibu, Nagoya Institute of Technology, Nagoya, Japan
Svetozar Musić, Ruđer Bosković Institute, Zagreb, Croatia
Dénes L. Nagy, Wigner Research Centre for Physics, Hungarian Academy of Sciences, Budapest, Hungary
Satoru Nakashima, Hiroshima University, Hiroshima, Japan
Kiyoshi Nomura, Tokyo University of Science, Tokyo, Japan
Michael Reissner, Vienna University of Technology, Vienna, Austria
Ralf Röhlsberger, DESY, Hamburg, Germany
Volker Schünemann, University of Kaiserslautern, Kaiserslautern, Germany
Bogdan Sepiol, University of Vienna, Vienna, Austria
Junhu Wang, Dalian Institute of Chemical Physics, Dalian, China
Tao Zhang, Dalian Institute of Chemical Physics, Dalian, China
Yasuhiro Yamada, Tokyo University of Science, Tokyo, Japan
Philipp Gütlich, Johannes Gutenberg University, Mainz, Germany
Michael Oshtrakh, Ural Federal University, Yekaterinburg, Russia

Conference Programme (only presenters are listed)

Sunday 27/05/2018

17:00 – 19:00 Registration at Hotel Kolovare

20:00 Welcome Reception at Hotel Kolovare

Monday 28/05/2018

09:00 – 10:30 SESSION 1

09:00 – 09:15 Opening Ceremony (M. Ristić, T. Nishida, V.K. Sharma)

09:15 – 09:45 Jose F. Marco: *Overview of the Scientific Achievements of Prof. Dr. Frank J. Berry*

09:45 – 10:30 Peter Adler: *Double Perovskite Oxides with 3d and 4d or 5d Ions: A Versatile Playground for Magnetism*

10:30 – 11:00 Coffee Break

11:00 – 13:00 SESSION 2 (Chairperson: V. Ksenofontov)

11:00 – 11:30 Yann Garcia: *Sensing Temperature, Pressure, Alcohols and Toxic Industrial Chemicals through Coordination Assemblies*

11:30 – 12:00 Satoru Nakashima: *On/Off Spin-Crossover Phenomenon and Control of the Transition Temperature in Assembled Iron(II) Complexes*

12:00 – 12:30 Yiannis Sanakis: *Heteronuclear Fe/Ni Clusters*

12:30 – 13:00 Masashi Kaneko: *Benchmarking of DFT with Mössbauer Isomer Shift Values for Heavy Metal Complexes*

13:00 – 14:30 Lunch Time

14:30 – 16:30 SESSION 3 (Chairperson: Z. Homonnay)

14:30 – 15:00 Shiro Kubuki: *^{57}Fe-Mössbauer and Magnetic Susceptibility Studies of Iron Phosphate Glass Prepared by Sol-Gel Method*

15:00 – 15:15 Tetsuaki Nishida: *Substitution Effect in Highly Conductive Barium Iron Vanadate Glass*

15:15 – 15:45 Nobuto Oka: *Local Structure of Conductive Vanadate Glass Applied to the Oxygen Electrode for Rechargeable Metal-Air Battery*

15:45 – 16:00 Yuta Kobayashi: *Relationship between Structure and Electrical Conductivity of Tin Phosphate containing Vanadate Glass Ceramics*

16:00 – 16:15 Yuka Katayama: *Chemical Structure and Visible-Light Activated Photocatalytic Effect of Iron-containing Glass Prepared from Slag*

16:15 – 16:30 Sakura Morishita: *^{57}Fe-Mössbauer and Magnetic Properties of Iron Oxide Nanoparticles in Silica Matrix Prepared by Sol-gel method*

16:30 – 17:00 Coffee Break

17:00 – 18:30 POSTER SESSION (all posters will be displayed during the entire conference)

Tuesday 29/05/2018

09:00 – 10:30 **SESSION 4** (Chairperson: M. Reissner)

09:00 – 09:45 Stanislaw M. Dubiel: *Effect of Magnetism on Lattice Dynamics*

09:45 – 10:15 Fernando Plazaola: *^{119}Sn Mössbauer Spectroscopy in the Study of Metamagnetic Alloys*

10:15 – 10:30 Judit Balogh: *On the Asymmetry of Fe-on-Ti and Ti-on-Fe Interfaces*

10:30 – 11:00 **Coffee Break**

11:00 – 13:00 **SESSION 5** (Chairperson: D.L. Nagy)

11:00 – 11:30 Vadim Ksenofontov: *Mössbauer Studies of Superconducting Iron Pnictides and Chalcogenides*

11:30 – 12:00 Yoshio Kobayashi: *In-Beam Mössbauer Study of ^{57}Mn Implanted into CaF_2*

12:00 – 12:30 Satoshi Tsutsui: *Precise Determination of Hyperfine Interaction and Second-order Doppler Shift in ^{149}Sm Mössbauer Transition*

12:30 – 13:00 Yasuhiro Yamada: *In-Beam Mössbauer Study of ^{57}Mn Implanted into Ice*

13:00 – 14:30 **Lunch Time**

15:00 **Conference Excursion** (Nin, Pag)

Wednesday 30/05/2018

09:00 – 10:45 **SESSION 6** (Chairperson Y. Garcia)

09:00 – 09:45 Pierre-Emmanuel Lippens: *Phosphate Based Electrodes for Li-Ion and Na-Ion Batteries*

09:45 – 10:15 Jean-Claude Jumas: *The Contribution of Mössbauer Spectroscopy to Study New Materials for Energy Applications*

10:15 – 10:45 Darko Hanzel: *Influence of Support Properties on $FePO_4$ Catalysts for the Selective Oxidation of Methane to Methanol*

10:45 - 11:15 **Coffee Break**

11:15 – 13:00 **SESSION 7** (Chairperson: P.-E. Lippens)

11:15 – 11:45 Junhu Wang: *Prussian Blue Analogues Derivated Multi-Metal Oxides/Nitrides as Fenton-Like Catalysts for the Degradation of Organic Pollutants and Its Mechanism*

11:45 – 12:15 Ayyakannu S. Ganeshraja: *Tin- or Iron-Doped Titania Nanocomposites: Mössbauer Spectroscopic, Magnetic and Photocatalytic Investigations*

12:15 – 12:45 Libor Machala: *Iron and Iron Oxide Based Nanomaterials in Environmental Applications - Contribution of Mossbauer Spectroscopy*

12:45 – 13:00 Virender K. Sharma: *Interactions of Ferrate(VI) with Natural Organic Matter: Mössbauer Spectroscopy Investigation*

13:00 – 14:30 **Lunch Time**

14:30 – 16:00 **SESSION 8** (Chairperson: S.M. Dubiel)

14:30 – 15:00 Dénes L. Nagy: *In-Situ Study of Electric-Field-Controlled Ion Transport in the Fe/$BaTiO_3$ Interface*

15:00 – 15:30 Ralf Witte: *Epitaxial Strain Adaption Mechanisms in FeRh Thin Films Probed by Mössbauer Spectroscopy and Nuclear Inelastic Scattering*

15:30 – 16:00 Göstar Klingelhöfer: *13 Years of Mars-Exploration-Rover Mission: Achievements and Lessons Learned*

16:00 – 16:30 **Coffee Break**

16:30 – 18:45 **SESSION 9** (Chairperson: J.-M. Grenèche)

16:30 – 17:00 Michael Oshtrakh: *Study of Some Stony and Stony-Iron Meteorites Using X-Ray Diffraction and Mössbauer Spectroscopy: Fe^{2+} Partitioning Between the M1 and M2 Sites in Silicate Phases*

17:00 – 17:15 Károly Lázár: *Iron in Minerals of Boda Claystone Formation*

17:15 – 17:30 Zoltan Homonnay: *Characterisation of Nanomagnetites Co-Precipitated in Inert Gas Atmosphere for Plant Nutrition*

17:30 – 17:45 Dalibor M. Stanković: *Magnetite Nanoflowers Decorated on Reduced Graphene Oxide for Efficient Removal of Reactive Dyes*

17:45 – 18:00 Irina Alenkina: *Mössbauer Spectroscopy and Magnetization Measurements of Spleen and Liver Tissues from Patients with Some Hematological Malignant Diseases*

18:00 – 18:15 Krisztina Kovács: *Effect of Arsenic on Iron Uptake and Distribution in Plants. A Mössbauer spectroscopic study*

18:15 – 18:45 Georges Dénès: *Oxidation and Passivating Effect in Tin(II) Fluoride and Chloride Fluoride Solid Solutions: A ^{119}Sn Mössbauer Study*

20:00 **Conference Dinner**

Thursday 31/05/2018

09:00 – 11:00 **SESSION 10** (Chairperson: J.F. Marco)

09:00 – 09:30 Jean-Marc Greneche: *Magnetisation and Mössbauer Study of Weberites $A^{2+}B^{3+}F_5$(Htaz)*

09:30 – 10:00 Jun Okabayashi: *Probing Orbital Magnetic Moments by Mössbauer and X-Ray Absorption Spectroscopies in FeV_2O_4*

10:00 – 10:30 Silvana J. Stewart: *Role of Defects on the Electronic and Magnetic Properties of Frustrated $ZnFe_2O_4$ Spinel*

10:30 – 10:45 Alex Scrimshire: *Determination of Debye Temperatures and Lamb-Mössbauer Factors for $LnFeO_3$ Orthoferrite Perovskites (Ln = La, Nd, Sm, Eu, Gd)*

10:45 Frank J. Berry: *Less Than a Half-Life Remembered*

Closing Ceremony

ABSTRACTS

Double Perovskite Oxides with 3*d* and 4*d* or 5*d* Ions: A Versatile Playground for Magnetism

P. Adler

Max Planck Institute for Chemical Physics of Solids, 01187 Dresden, Germany
(adler@cpfs.mpg.de)

Due to their great chemical and structural flexibility perovskite oxides ABO_3 constitute one of the most important materials platforms in contemporary solid state and materials research. In double perovskites (DPs) $A_2BB'O_6$ two different ions *B* and *B*' feature an ordered NaCl-like arrangement, which in case of magnetic ions provides two magnetic sublattices and in turn allows to generate a large variety of magnetic behaviour. Particularly fruitful are combinations of a 3*d* ion with 4*d* or 5*d* ions. While the former show strongly correlated localized electron behaviour, the spatially more extended 4*d* or 5*d* orbitals introduce more itinerant features. In addition spin-orbit coupling may become important. Examples which have stimulated much interest in DPs are the half-metallic ferrimagnet Sr_2FeMoO_6 [1] with large magnetoresistance effects even at room temperature as well the ferrimagnetic insulator Sr_2CrOsO_6 with a high T_C of 720 K [2].

In this lecture an overview on our work on magnetic double perovskites is given, where frequently the combination of powder neutron diffraction with a local probe like ^{57}Fe Mössbauer spectroscopy gives detailed insights into structural, magnetic, and electronic properties of this unique class of compounds. Emphasis will be on the system A_2FeOsO_6 (*A* = Sr, Ca, Ba) where a strong-magneto-structural coupling is evident. Thus Ca_2FeOsO_6 is a ferrimagnetic insulator with T_C ~ 320 K [3], Sr_2FeOsO_6 is an antiferromagnet with two competing spin structures [4], whereas Ba_2FeOsO_6 adopts the hexagonal perovskite structure with some atomic disorder and shows ferrimagnetism above room temperature (T_C ~370 K) as well as exchange bias effects [5]. Synchrotron Mössbauer spectroscopy using the synchrotron Mössbauer source at ID18 of ESRF allows insights into the high pressure magnetism of Sr_2FeOsO_6 [6] where a pressure-induced change from antiferromagnetism to ferrimagnetism was proposed to occur [7]. It is instructive to compare the properties of the system A_2FeOsO_6 with those of the ruthenium analogue A_2FeRuO_6 (*A* = Ca, Sr), where, however, the Fe^{3+} and Ru^{5+} ions are atomically disordered on the *B* sites. Also in this case strong magneto-structural correlation is apparent and the system changes from spin-glass behaviour for Sr_2FeRuO_6 to long-range antiferromagnetic ordering with features of re-entrant magnetism in Ca_2FeRuO_6 [8].

In powder neutron studies it is often difficult to separate the magnetic moments of 3*d* and 5*d* ions. In this respect studies on Os^{5+} double perovskites Sr_2BOsO_6 with diamagnetic B^{3+} ions (*B* = Y, Sc, In) are useful which give insights into the exchange pathways within the Os^{5+} sublattice [9]. Another remarkable DP is non-stoichiometric $La_2Ni_{1.18}Os_{0.82}O_6$[10], which shows ferrimagnetism with giant coercivity at 5 K and suggests that DPs may be interesting for the search of rare earth free hard magnets.

[1] K.L. Kobayashi, T. Kimura, H. Sawada, K. Terakura, Y. Tokura, Nature 395 (1998) 677.
[2] Y. Krockenberger, K. Mogare, M. Reehuis, M. Tovar, M. Jansen, G. Vaitheeswaran, V. Kanchana, F. Bultmark, A. Delin, F. Wilhelm, A. Rogalev, A. Winkler, L. Alff, Phys. Rev. B 75 (2007) 020404.
[3] H.L. Feng, M. Arai, Y. Matsushita, Y. Tsujimoto, Y.F. Guo, C.I. Sathish, X. Wang, Y. H. Yuan, M. Tanaka, K. Yamaura, J. Am. Chem. Soc. 136 (2014) 3326.
[4] A.K. Paul, M. Reehuis, V. Ksenofontov, B. Yan, A. Hoser, D.M.Többens, P.M. Abdala, P. Adler, M. Jansen, C. Felser, Phys. Rev.Lett. 111 *(*2013) 167205.
[5] H.L. Feng, P. Adler, M. Reehuis, W. Schnelle, P. Pattison, A. Hoser, C. Felser, M. Jansen, Chem. Mater. (2017) 29 886.
[6] P. Adler, S.A. Medvedev, P.G. Naumov, S. Mohitkar, R. Rüffer, M. Jansen, C. Felser, to be published.
[7] L.S.I. Veiga, G. Fabbris, M. van Veenendaal, N.M. Souza-Neto, H.L. Feng, K. Yamaura, D. Haskel, Phys. Rev. B. 91 (2015) 235135.
[8] K. Naveen, M. Reehuis, P. Adler, P. Pattison, A. Hoser, T.K. Mandal, U. Arjun, P. Mukharjee, R. Nath, C. Felser, A.K. Paul, submitted for publication.
[9] A.K. Paul, A. Sarapolova, P. Adler, M. Reehuis, S. Kanungo, D. Mikhailova, W. Schnelle, Z. Hu, C. Kuo, V. Siruguri, S. Rayaprol, Y. Soo, B. Yan, C. Felser, L.H. Tjeng, M. Jansen, Z. Anorg. Allg. Chem. 641 (2015) 197.
[10] H.L. Feng, M. Reehuis, P. Adler, Z. Hu, M. Nicklas, A. Hoser, S-C. Weng, C. Felser M. Jansen, arXiv: 1802.03874 (2018)

Effect of Magnetism on Lattice Dynamics

S.M. Dubiel

AGH University of Science and Technology, Faculty of Physics and Applied Computer Science, PL-30-059 Krakow, Poland (Stanislaw.Dubiel@fis.agh.edu.pl)

An effect of magnetism on lattice dynamics is considered as negligible. Such belief is based on calculations according to which the spin susceptibility of metal is not affected by the electron-phonon interaction (EPI) ([1] and references therein). Indeed, the effect of the EPI was estimated as $h\omega_D/\varepsilon_F \approx 10^{-2}$ ([1] and references therein) where ε_F is the Fermi energy, and $h\omega_D$ is the Debye energy. However, Kim showed [1] that the influence of the EPI on spin susceptibility can be significantly, i.e. by a factor of $\sim 10^2$, enhanced by exchange interactions between electrons. In other words, the effect of the EPI on magnetic properties of metallic systems, and *vice versa*, is much more significant than generally believed. The Mössbauer spectroscopy (MS) is a well-suited method for studying the lattice dynamics via two spectral parameters viz. (1) center shift, CS, and (2) recoil-free factor, *f*. The former gives information on an average squared velocity of vibrations, $\langle v^2 \rangle$, while the latter is related to average squared amplitude of vibrations, $\langle x^2 \rangle$. Presented and discussed will be relevant results obtained with the MS for sigma-phase Fe-Cr and Fe-V alloys [2,3], C14 Laves phase $NbFe_2$[4], spin-density waves Cr doped with ^{57}Fe [5], and last but not least, the effect of magnetism on sound velocity in the σ-FeCr alloy studied with the nuclear inelastic scattering of synchrotron radiation [5].

[1] D.J. Kim, Phys. Rep. 171 (1988) 129.
[2] S.M. Dubiel et al., EPL, 101 (2013) 16008.
[3] S.M. Dubiel, J. Żukrowski, J. Magn. Magn. Mater. 441 (2017) 557.
[4] J. Żukrowski, S.M. Dubiel, arXiv:1712.08514 (2017)
[5] S.M. Dubiel et al., J. Phys.: Condens. Matter. 22 (2010) 435403.
[6] S.M. Dubiel, A. I. Chumakov, EPL, 117 (2017) 56001.

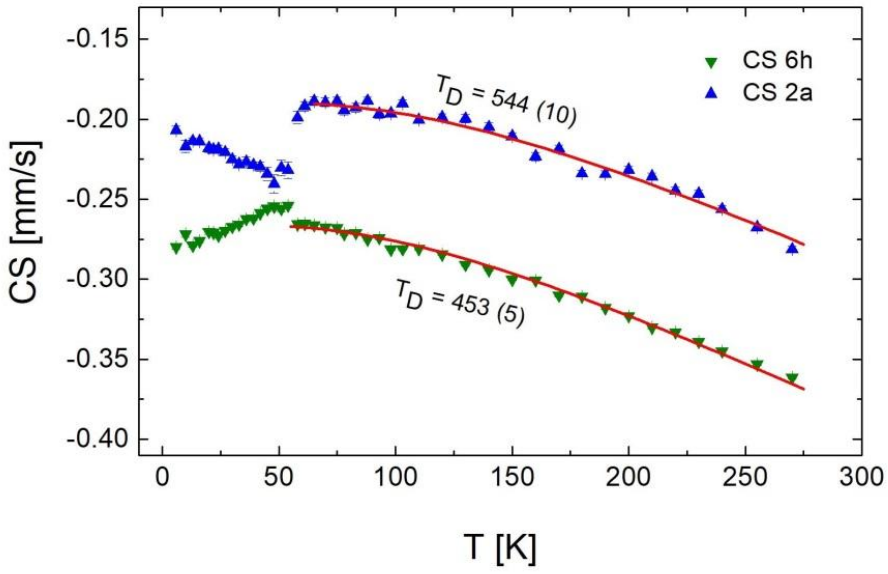

Fig. 1 Center shift, *CS*, vs. temperature, *T*, for Fe atoms occupying 2a and 6h sites in the $Nb_{0.975}Fe_{2.025}$ C14 Laves phase compound with the magnetic ordering temperature $T_C \approx 50$K [4]. T_D is the Debye temperature.

Phosphate Based Electrodes for Li-Ion and Na-Ion Batteries

P.-E. Lippens

Institut Charles Gerhardt, UMR 5253 CNRS, Université de Montpellier, Place Eugène Bataillon, 34095 Montpellier cedex 5, France
(lippens@univ-montp2.fr)

Electrochemical energy storage systems are now used for many applications, going from small and mobile electronic devices to large and stationary systems, not forgetting electric vehicles. Li-ion batteries constitute the main technology because of their high energy density but there is a main concern for lithium availability in a near future. Thus, the replacement of lithium should be considered for some applications. For example, Na-ion batteries have lower energy density but could be of interest for stationary applications (intermittent renewable energies, smart grids) because of the worldwide natural abundance of sodium and its low cost. However, both the improvement of Li-ion technology and the development of Na-ion systems require new electrolytes and electrode materials. In the latter case, this involves improved specific and volumetric capacities, rate capabilities, cycle life and safety with low cost.

Transition metal phosphates have been studied for a long time because of their open framework structures that allow fast and highly reversible insertion of Li^+ or Na^+ with a rather good structural stability in a large range of temperatures. This is mainly due to the covalent P-O bonds that strengthen the stability of the PO_4 tetrahedral units. Combined with one or more transition metals, they can form very different and open 3d stable frameworks well adapted to the diffusion of alkali metals. The versatility of the structures and the choice of the transition metals allow to tune the redox potential through the inductive effect. In addition, it is also possible to substitute other chemical elements for the transition metals, opening new perspectives for the applications of these materials.

This talk is devoted to single phosphate materials. For the application of the Mössbauer effect, different examples of iron based phosphates are considered as well as less studied tin based phosphates [1-3]. A particular attention will be focused on NASICON (Na super ionic conductors) type phosphates that offer the possibility to use the same material at different voltages depending on the redox potentials of the transition metal ions and the insertion mechanisms: solid solution, two-phase, conversion or alloying reactions. Iron and tin atoms have very different behaviors during Li (or Na) insertion due to their different electronic configurations involving 3d and 5s/5p electrons, respectively. The analysis of such complex mechanisms is only possible by combining different experimental tools especially in operando mode.

In this context, ^{57}Fe and ^{119}Sn Mössbauer spectroscopies can be used to follow changes in the oxidation states of iron and tin, respectively, and to detect modifications in their local environments or the formation of new species. For example, Fe^{3+}/Fe^{2+} reversible transformation is observed at high potential for $Na_{1.5}Fe_{0.5}Ti_{1.5}(PO_4)_3$ electrode material of Na-ion batteries, whereas Fe^{2+} is inactive at low potential (Fig. 1) [4]. Another example concerns the first sodiation of $Na_2FeSn(PO_4)_3$ that consists in the irreversible reduction of Sn^{4+} into Sn^0 followed by reversible Na-Sn alloying reactions (Fig. 2).

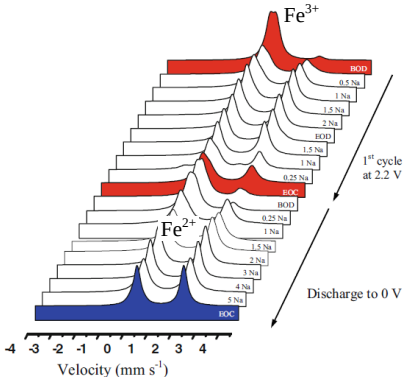

Fig. 1 Evolution of the operando ^{57}Fe Mössbauer spectra obtained during the first sodiation of $Na_{1.5}Fe_{0.5}Ti_{1.5}(PO_4)_3$.

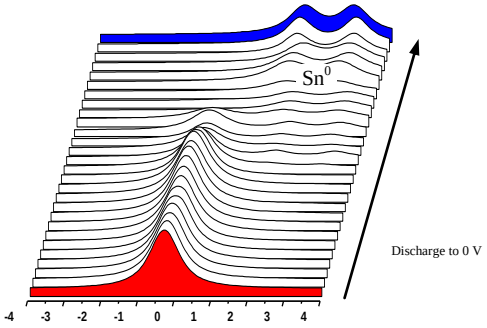

Fig. 2 Evolution of the operando ^{119}Sn Mössbauer spectra obtained during the first sodiation of $Na_2FeSn(PO_4)_3$.

[1] C. Karegeya, A. Mahmoud, B. Vertruyen, F. Hatert, R. Cloots, P. E. Lippens, F. Boschini, J. Power Sources 388 (2018) 57.
[2] S. Difi, I. Saadoune, M.T. Sougrati, R. Hakkou, K. Edstrom, P.E. Lippens, J. Phys. Chem. C 45 (2015) 25220.
[3] S. Difi, A. Nassiri, I. Saadoune M. T. Sougrati, P. E. Lippens, J. Phys. Chem. C (in press).
[4] S. Difi, I. Saadoune, M.T. Sougrati, R. Hakkou, K. Edstrom, P.E. Lippens, Hyp. Interactions 237 (2016) 61.

Tin- or Iron-Doped Titania Nanocomposites: Mössbauer Spectroscopic, Magnetic and Photocatalytic Investigations

A.S. Ganeshraja and J. Wang

Mössbauer Effect Data Center, Dalian Institute of Chemical Physics, Chinese Academy of Sciences, Dalian 116023, China (wangjh@dicp.ac.cn; ganeshraja@dicp.ac.cn)

Waste water treatment on the basis of highly efficient photocatalysts attracts progressively attention [1,2]. The improvement of stabilizations of photoinduced charge carrier/separation is the key factor of photocatalytic reactions, which convert light energy into chemical reactions [3]. Titanium dioxide and TiO_2-based materials are widely used in environmental and energy-related applications. However, the photocatalytic efficiency needs to improve in visible-light or sunlight. Hence, Mössbauer spectroscopic, magnetic and photocatalytic investigations on bulk and supported tin- or iron-doped titania nanocomposites were studied [4-9]. Following two efficient methods were used for preparing highly efficient tin- or iron-doped titania photocatalysts: (i) Sn-TiO_2, (Sn,N)TiO_2, and AgCl@Sn-TiO_2 nanocrystals/ microspheres were designed and produced by simple hydrothermal method, and (ii) FeO_x-TiO_2 nanocrystals were prepared by novel photochemical method, in which visible light are mediated reduction of surface bound ionic type iron(III)-bipyridyl complex on TiO_2 surface. The chemico-physical properties were characterized by X-ray diffraction analysis, UV−vis diffuse reflectance spectroscopy, Raman spectroscopy, X-ray photoelectron spectroscopy, N_2 adsorption-desorption measurements, high-resolution transmission electron microscopy, and photoluminescence techniques. Magnetic measurements of the as-prepared samples were performed on a Quantum Design SQUID magnetometer. In combination with all the conventional techniques, the structure-activity relationships and photocatalytic mechanism of Sn or Fe-doped TiO_2 nanocomposites were mainly explored by X-ray absorption fine structure, electron paramagnetic resonance (EPR) and Mössbauer spectroscopy under various simulated working conditions. With the efficient visible light absorption and high photocatalytic activity and stability, the tin- or iron-doped TiO_2 nanocomposites have promising application in photocatalysis for degradation of organic pollutants. However, the magnetic and photocatalytic properties of Sn- or Fe-doped TiO_2 nanocomposites depend critically on oxygen vacancy, structural defects, chemical states and various contents of Fe or Sn. We strongly believe that our work would contribute toward the fundamental understanding of structural and magnetic properties of tin- or iron-doped TiO_2 nanocomposites and would be useful for inexpensive photocatalyst materials.

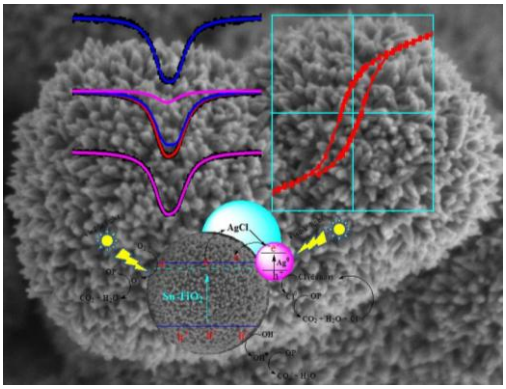

Fig. 1 HRSEM image, ^{119}Sn Mössbauer spectra, hysteresis loop of Sn and N codoped TiO_2 microsphere and photocatalytic mechanism of AgCl loaded Sn doped TiO_2 microsphere

[1] M. Dahl, Y. Liu, Y. Yin, *Chem. Rev*., **2014**, *114*, 9853−9889.

[2] M. Liu, X. Qiu, M. Miyauchi, K. Hashimoto, *J. Am. Chem. Soc*., **2013**, *135*, 10064−10072.

[3] Q. Gu, J. Long, Y. Zhou, R. Yuan, H. Lin, X. Wang, *J. Catal*. **2012**, *289*, 88–99.

[4] A.S. Ganeshraja, A. S. Clara, K. Rajkumar, Y. Wang, Y. Wang, J. Wang, K. Anbalagan, *Appl. Surf. Sci*., **2015**, *353*, 553−563.

[5] A.S. Ganeshraja, S. Thirumurugan, K. Rajkumar, K. Zhu, Y. Wang, K. Anbalagan, J. Wang, *RSC Adv*. **2016**, *6*, 409−421.

[6] A.S. Ganeshraja, K. Rajkumar, K. Zhu, X. Li, S. Thirumurugan, W. Xu, J. Zhang, M. Yang, K. Anbalagan, J. Wang, *RSC Adv*., **2016**, *6*, 72791−72802.

[7] A.S. Ganeshraja, M. Yang, K. Nomura, S. Maniarasu, G. Veerappan, T. Liu, J. Wang: *J. Phys. Chem. C*, **2017**, *121*, 6662−6673.

[8] A.S. Ganeshraja, K. Zhu, K. Nomura, J. Wang: *Appl. Surf. Sci*., **2018**, *441*, 678−687.

[9] A.S. Ganeshraja, M. Yang, W. Xu, K. Anbalagan, J. Wang: *ChemistrySelect*, **2017**, *2*, 10648 –10653.

Sensing Temperature, Pressure, Alcohols and Toxic Industrial Chemicals through Coordination Assemblies

Y. Garcia

Institute of Condensed Matter and Nanosciences, Molecules, Solids and Reactivity (IMCN/MOST), Université catholique de Louvain, 1348 Louvain-la-Neuve, Belgium (yann.garcia@uclouvain.be)

Iron(II) spin crossover (SCO) complexes continue to attract a great deal of interest,[1,2] due to their potential technological applications, for instance as pressure sensors.[3] SCO nanomaterials have emerged as an appealing class of materials considering nanostructuration processes and size reduction effects.[4] Although sophisticated techniques can be used for the preparation of SCO nanoparticles, the use of a botanic biomembrane as a soft and green support for SCO micro and nanocrystals growth of $[Fe(ptz)_6](BF_4)_2$ proved to be very efficient.[5] In this respect, Mössbauer spectroscopy allowed to identify the SCO complex along with metal salt used for the deposition.[6] Ultrasounds were also recently used to exfoliate a 2D SCO network into nanoparticles.[7] Mössbauer spectroscopy was also used to track the SCO behaviour operating above room temperature for a hybrid nanomaterial made of MCM-41 and the 1D polymer $[Fe(Htrz)_2trz](BF_4)$.[8] This later class of SCO materials, whose spin states can be switched by light,[2,9] afforded the first example of this substance class to display a thermally induced two-step spin conversion.[10] This compound was discovered in the frame of our investigation of a new range of porous metal organic frameworks including 1,2,4-triazole ligands built from amino acids building blocks.[11] Within this family, we recently isolated a 1D SCO chain switching at room temperature with a wide bistability domain of 60 K,[12] which bears great potential for aeronautoics applications. We shall also report on a mononuclear Fe(II) neutral high-spin complex which was screened for sensing abilities for a series of hazardous chemicals. Interestingly, the complex visually detects methanol and ethanol among other alcohols as well as several toxic industrial chemicals.[13] The sensing process, which involves an unexpected spin state change for the alcohols, is visually detectable, fatigue-resistant, selective, and reusable.[14] A memory effect was also detected, as shown by ^{57}Fe Mössbauer spectroscopy.[13]

[1] P. Gütlich, A.B. Gaspar, Y. Garcia, Beilstein J. Org. Chem. 9 (2013) 342.

[2] D. Unruh, P. Homenya, M. Kumar, R. Sindelar, Y. Garcia, F. Renz, Dalton Trans. 45 (2016) 14008. **Perspective.**

[3] C.M. Jureschi, J. Linares, A. Rotaru, M.H. Ritti, M. Parlier, M.M. Dîrtu, M. Wolff, Y. Garcia, Sensors 15 (2015) 2388.

[4] S. Majumdar, G. Sliwinski, Y. Garcia, In Hybrid Organic-Inorganic Interfaces: Towards Advanced Functional Materials, 7 (2018). Wiley VCH Book, Eds. M. H. Delville, A. Taubert.

[5] A.D. Naik, L. Stappers, J. Snauwaert, J. Fransaer, Y. Garcia, Small 6 (2010) 2842.

[6] A.D. Naik, Y. Garcia, Hyperfine Interact. 206 (2012) 7.

[7] S. Suarez-Garcia, N.N. Adarsh, G. Molnar, A. Bousseksou, Y. Garcia, M.M. Dîrtu, J. Saiz-Poseu, R. Robles, P. Ordejón, D. Ruiz-Molina, submitted (2018)

[8] T. Zhao, L. Cuignet, M. M. Dîrtu, M. Wolff, V. Spasojevic, I. Boldog, A. Rotaru, Y. Garcia, C. Janiak, J. Mater. Chem. C 3 (2015) 7802. **Hot paper**.

[9] Y. Garcia, F. Renz, P. Gütlich, Curr. Inorg. Chem. 6 (2016) 4.

[10] M.M. Dîrtu, F. Schmit, A.D. Naik, A. Rotaru, I. Rusu, S. Rackwitz, J. A. Wolny, V. Schünemann, Y. Garcia, Chem. Eur. J. 21 (2015) 5843.

[11] N.N. Adarsh, M. M. Dîrtu, A. D. Naik, A. F. Léonard, N. Campagnol, K. Robeyns, J. Snauwaert, J. Fransaer, B. L. Su, Y. Garcia, Chem. Eur. J. 21 (2015) 4300. **Hot pape**r.

[12] M.M. Dîrtu, A.D. Naik, A. Rotaru, L. Spinu, D. Poelman, Y. Garcia, Inorg. Chem. 55 (2016) 4278.

[13] Y. Guo, S. Xue, M.M. Dîrtu, *J. Mater. Chem. C.* **2018**, submitted.

[14] A.D. Naik, K. Robeyns, C. Meunier, A. Léonard, A. Rotaru, B. Tinant, Y. Filinchuk, B. L. Su, Y. Garcia, *Inorg. Chem.* **2014**, *53*, 1263.

FNRS (PDR and CR positions) is thanked for funding support.

Magnetisation and Mössbauer Study of Weberites $A^{2+}B^{3+}F_5(Htaz)$

M. Albino[a], L. Clark[b], J. Lhoste[a], C. Payen[c], M. Leblanc[a], P. Lightfoot[b], V. Maisonneuve[a] and J.-M. Grenèche[a]

[a] *Institut des Molécules et des Matériaux du Mans (IMMM), UMR CNRS 6283, Le Mans Université, avenue O. Messiaen, 72085 Le Mans, France*
[b] *School of Chemistry and EaStCHEM, University of St. Andrews, St. Andrews, Fife KY16 9ST, UK*
[c] *Institut des Matériaux Jean Rouxel (IMN), UMR CNRS 6502, Université de Nantes, 2 rue de la Houssinière, BP 32229, 44322 Nantes Cedex 3, France*
(jean-marc.greneche@univ-lemans.fr)

We report on a series of weberite-type fluorides isostructural of Na_2NiFeF_7. Powder $A^{2+}B^{3+}F_5(H_2O)_2$ samples have been early prepared by different methods during the 70s and 80s while a triazole fluoride weberite $A^{2+}B^{3+}F_5(Htaz)$ series was recently synthesized by means of hydrothermal route; A and B correspond to transition metal species. When B=Fe, the chemical composition was refined by combining X-ray diffraction data and hyperfine data derived from ^{57}Fe Mössbauer spectrometry. The interest of weberite structures results from the magnetic frustration of antiferromagnetic interactions originating from the cationic topology of Hexagonal Tungsten Bronze layers. Thus, magnetization measurements, neutron diffraction and ^{57}Fe Mössbauer spectrometry including zero-field and in-field conditions were performed. The magnetic ordering temperatures and the magnetic structures are strongly dependent on the nature of cations, together with the occurrence of negative and positive magnetization effects. We report on the most significant results discussed in terms of magnetic interactions and local anisotropy while a particular attention is paid to experimental conditions when performing Mössbauer spectra.

Influence of Support Properties on $FePO_4$ Catalysts for the Selective Oxidation of Methane to Methanol

D. Hanžel[a], V.D.B.C. Dasireddy[b], F. Khan[c], K. Bharut-Ram[d] and B. Likozar[b]

[a]*Jozef Stefan Institute, Department of Low and Medium Energy Physics, Jamova 39, SI-1001 Ljubljana, Slovenia*
[b]*Laboratory of Catalysis and Chemical Reaction Engineering, National Institute of Chemistry Slovenia, Hajdrihova 19, SI-1001 Ljubljana, Slovenia*
[c]*Energy Technology, Sasol, South Africa*
[d]*School of Chemistry and Physics, University of KwaZulu Natal, Durban, South Africa*
(darko.hanzel@ijs.si)

Much attention has been paid to the conversion of methane into useful chemicals and easily transportable liquid fuels from the viewpoint that the abundant methane resources will play more significant roles in the production of energy and chemicals in the new century [1]. A direct conversion process for methane to useful chemicals such as methanol would have many advantages over the indirect technology via synthesis gas. However, the current state-of-the-art technology for the direct conversion process is not competitive with the indirect one via synthesis gas. Among the direct conversion processes, the partial oxidation of methane to useful oxygenates particularly methanol, possesses great potential and is viewed as one of the biggest challenges in catalysis [2]. The direct conversion of methane to methanol has been attracting considerable attention because of its great potential application in the efficient utilization of abundant natural gas reserves. In the last decade a number of interesting approaches [2-4] was suggested for the effective implementation of this difficult transformation. To activate methane, usually high temperatures are required. At the same temperature ranges, formed methanol undergoes further oxidation down to CO_2 and H_2O.

To achieve a high selectivity towards methanol from methane in one step, $FePO_4$ catalysts supported on Al_2O_3, ZrO_2, TiO_2 and SiO_2 and with iron loading from 5 to 15 wt% were tested in selective oxidation of methane, using molecular oxygen, N_2O and CO_2 in a continuous-flow reactor, at atmospheric pressure. The main products of the reaction were methanol, CO, and CO_2. For the silica-supported catalysts, small but quantifiable amounts of formaldehyde were also identified. Catalytic activity and selectivity exhibited a clear dependence on the oxide support and on $FePO_4$ loading. $FePO_4$ on silica produced the highest yield of the desired oxygenates, while alumina-supported $FePO_4$ exhibited the lowest selectivity to formaldehyde. The highest selectivity and space-time yield to methanol was observed at lower $FePO_4$ loading levels for the ZrO_2, and TiO_2 supports. The presence of easily reducible iron, in high coordination and isolated by phosphate groups is proposed to be responsible for the superior performance of the supported $FePO_4$ catalyst [5]. Stability of the desired products on the support also plays an important role in achieving a high yield.

The location, dispersion, and environment (acidic or alkaline) of iron sites and the nature of oxidant are key factors in determining the catalytic performances of iron-containing mesoporous materials for selective oxidation reactions [2, 4]. For the partial oxidation of CH_4 by O_2, a higher dispersion of iron sites is required for obtaining a higher selectivity to HCHO. The alkaline is detrimental to HCHO selectivity. On the other hand, HCHO selectivity can be remarkably enhanced by the formation of $FePO_4$ clusters, in which the tetrahedral iron sites are surrounded by the acidic phosphate groups. In the case of CH_4 oxidation by N_2O, the catalyst with $FePO_4$ clusters is unique in achieving high selectivity to CH_3OH. The location of iron is vital in the case of using N_2O, and the catalyst containing framework iron exhibits poorer catalytic performances for the oxidation of CH_4 to CH_3OH.

[1] D.L. Chiavassa, J. Barrandeguy, A.L. Bonivardi, M.A. Baltanás, Catalysis Today, 133–135 (2008) 780-786.
[2] K. Otsuka, Y. Wang, Applied Catalysis A: General, 222 (2001) 145-161.
[3] C. Zhong, X. Guo, D. Mao, S. Wang, G. Wu, G. Lu, RSC Advances, 5 (2015) 52958-52965.
[4] G. Ertl, H. Knözinger, F. Schüth, J. Weitkamp, Handbook of Heterogeneous Catalysis, 8 Volumes, Wiley2008.
[5] M.D. Porosoff, B. Yan, J.G. Chen, Energy & Environmental Science, 9 (2016) 62-73.

The Contribution of Mössbauer Spectroscopy to Study New Materials for Energy Applications

J.-C. Jumas, J. Olivier-Fourcade and P.-E. Lippens

Institut Charles Gerhard (UMR 5253), Université Montpellier, Case Courrier 1502, Place Eugène Bataillon, 34095 Montpellier Cedex 5, France (jumas@univ-montp2.fr)

The greatness of Mössbauer Spectroscopy (MS) will be highlighted for the study of new materials for energy applications: Li-ion batteries for electrochemical storage of energy, production of hydrogen and synthetic fuels by concentrated solar energy, production of hydrogen, high-octane gasoline and fine chemicals (reforming catalysis).

Throughout its hyperfine parameters, isomer shift (IS) and quadrupole splitting (QS), the characterization of the local electronic structure, including oxidation state and coordination of the probed element, is easily achieved.

In the field of electrochemical storage of energy, the development of high energy and high power Li-ion batteries leads to intensive world-wide research. The performance of such batteries depends on many factors amongst which the important ones are the electrode materials and their structural and electronic evolution upon cycling. The highest advances of *in situ operando* measurements combining X-Ray Diffraction (XRD) and MS (Figure 1) allowed for a better understanding of electrochemical mechanisms. Several examples judiciously selected illustrate the interest of such measurements for new negative (TiSnSb) and positive ($LiMn_{0.25}Fe_{0.75}PO_4$) electrodes.

Production of hydrogen and synthetic fuels (syngas, liquid fuels) by concentrated solar energy without CO_2 emission is a strategic issue in the fight against climate change and the search for sustainable energy vectors. Thermochemical processes using a direct heating source (Solar Furnace in Odeillo, Font-Romeu, France) are able to produce hydrogen with greater efficiency than electrolysis. The tin-based redox process for hydrogen production was significantly improved by considering a novel two-step thermochemical cycle based on SnO_2 and SnO. ^{119}Sn MS is a powerful tool to characterize these nanopowders.

Catalytic reforming is a chemical process used to convert naphtha (produced during petroleum refining) into high octane number gasoline. If Pt/Al_2O_3 was the first naphtha-reforming catalyst, great progress has been achieved with the introduction of supported bimetallic-reforming catalysts in which Pt is promoted by another metal. The presence of a second metal, like tin, reduces considerably the deactivation of the catalyst by coke formation and coalescence of the metallic particles during the reaction and regeneration steps. The role played by tin seems to depend on several factors like the nature of the support, the pre-treatment the support has undergone, the preparation method and the precursors used. Some of these parameters influence the particle size and the accessibility of the noble metal, which, in turn, determine the way tin acts on the catalytic performances. In the field of Sn-based reforming catalysts (bimetallic PtSn or trimetallic PtSnIn on γ-alumina) various Sn-species have been identified thanks to the use of a (QS) – (IS) diagram previously established from reference compounds, model catalysts and *in situ* measurements.

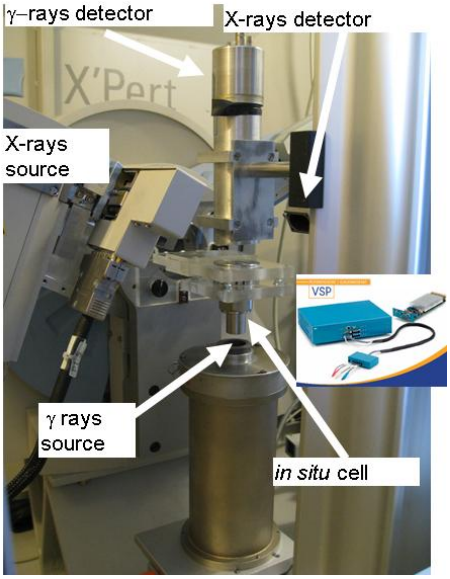

Fig. 1 New set up combining a X-ray Diffractometer (X'Pert Panalytical) and a standard Transmission Mössbauer Spectrometer.

The obtained results, in the framework of new materials for energy applications, demonstrate new potential for MS to better define phase analyses and local cationic arrangements in complex systems with actual industrial implications.

Benchmarking of DFT with Mössbauer Isomer Shift Values for Heavy Metal Complexes

M. Kaneko and M. Watanabe

Nuclear Science and Engineering Center, Japan Atomic Energy Agency, 2-4, Shirakata, Tokai-mura, Ibaraki, Japan (kaneko.masashi@jaea.go.jp)

A linear relationship between Mössbauer isomer shift (δ) values and electron densities at nucleus position (ρ_0) assures the quantitative evaluation of the covalent interaction between a Mössbauer element and the surroundings. The evaluation of the linearity between experimental δ, δ^{exp}, values and calculated ρ_0, ρ_0^{calc}, values obtained via quantum chemical methods helps us to validate the computational method for estimating the bonding property as well as to obtain $\Delta R/R$ value [1].

Our recent studies have demonstrated the benchmarking between δ^{exp} values and ρ_0^{calc} values using density functional theory (DFT) calculations for heavy metal complexes, including ^{99}Ru, ^{151}Eu, ^{189}Os and ^{237}Np Mössbauer nuclides [2, 3]. Table 1 shows the results of correlation coefficients (R^2) and root mean square error (RMSD) values, which were obtained with high reproducibility.

Table 1: R^2 and RMSD values by linear regression analysis between δ^{exp} and ρ_0^{calc}

Nuclides	R^2	RMSD / mm s^{-1}	Method
^{99}Ru	0.914	0.18	DKH2-B3LYP
^{151}Eu	0.998	0.20	ZORA-B2PLYP
^{189}Os[1]	0.980	0.22	DKH2-B3LYP
^{237}Np	0.941	3.48	ZORA-B2PLYP

[1] *δ^{exp} values of 36.2 keV transition were used*

Their R^2 and RMSD values were indicated to depend on the mixing ratio of Hartree-Fock exact exchange potential into density functional, in particular, for ^{151}Eu and ^{237}Np benchmark studies. Numerical optimization of the mixing ratio suggested that the inclusion of 30 and 60 % for Eu and Np systems, respectively, gives the smallest RMSD value [4].

Bonding property between the metal ion and the ligands has been also investigated for five sets of Eu(III) [5] and Np(IV) complexes [6]. The result indicated that the participation of the f-orbital electrons into the bonds correlates to the variation of the Mössbauer isomer shift values. We will also present the applications of this study to understanding the separation mechanism of minor actinides from lanthanides, which is an important task for partitioning and transmutation of nuclear waste, as well as the detail of these benchmarking and bonding investigations.

[1] F. Neese, Quantum Chemistry and Mössbauer Spectroscopy, in: P. Gütlich, E. Bill, A. X. Trautwein (Eds.), Mössbauer Spectroscopy and Transition Metal Chemistry – Fundamentals and Applications, Springer, Berlin, p. 150 (2011).

[2] M. Kaneko, S. Miyashita, S. Nakashima, Dalton Trans. 44 (2015) 8080.

[3] M. Kaneko, S. Miyashita, H. Yasuhara, S. Nakashima, Hyperfine Interact. 238 (2017) 36.

[4] M. Kaneko, M. Watanabe, S. Miyashita, S. Nakashima, Hyperfine Interact. 239 (2018) 20.

[5] M. Kaneko, M. Watanabe, S. Miyashita, S. Nakashima, Radioisotopes 66 (2017) 289.

[6] M. Kaneko, S. Miyashita, S. Nakashima, Croat. Chem. Acta 88 (2016) 347.

13 Years of Mars-Exploration-Rover Mission: Achievements and Lessons Learned

G. Klingelhöfer[a], B. Bernhardt[b], D. Rodionov[a,c], J. Girones Lopez[a], R.V. Morris[d], C. Schröder[e] and F. Renz[f]

[a]*Inorg.and Analyt. Chemistry, Johannes Gutenberg-University Mainz,Germany*
[b]*Von-Hoerner&Sulger GmbH, Schwetzingen, Germany*
[c]*Space Research Institute IKI, Moscow Russia*
[d]*NASA Johnson Space Center, Houston, Texas, USA*
[e] *School of Natural Sciences, University of Stirling, Stirling, Scotland, UK*
[f] *Inorganic Chemistry, Leibniz University, Hannover, Germany*
(klingel@mail.uni-mainz.de)

In 2003 the NASA Mars-Exploration Rover Twin mission MER (Fig. 1) has been launched to explore the surface of Mars. Part of the payload of the two rovers Spirit and Opportunity is the Miniaturized Mössbauer Spectrometer MIMOS-II [1], a contact instrument for placement on rock or soil samples (no sample preparation) (Fig. 2). After landing on the surface of Mars in January 2004 a large number of rocks and soils have been analyzed by the Mössbauer spectrometers [2–5]. The MER rover Opportunity is still operating after 13 Years on the surface of Mars. The instrument MIMOS II is also still functioning, but its radioactive source has been decayed not allowing measurements anymore.

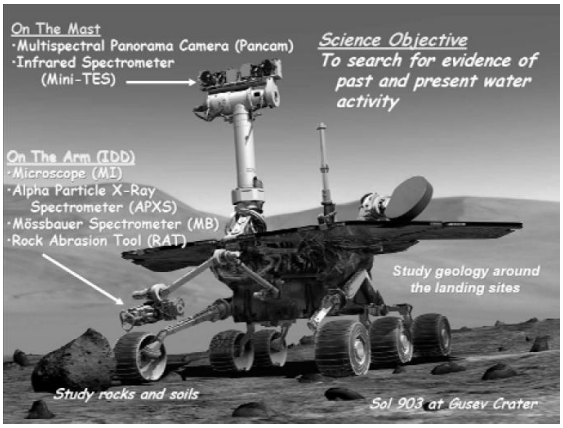

Fig. 1 Artist view of the Mars Exploration Rovers. Size of the rover is about 1m x 1m (length and width) by ~1.6m height (position of the Panorama Camera). The Mössbauer spectrometer is mounted on the robotic arm (IDD).

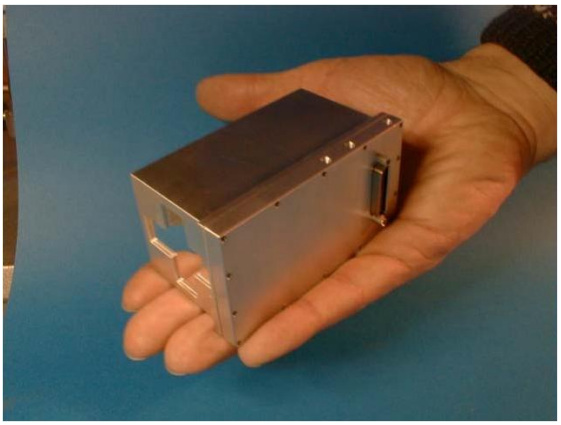

Fig. 2 The Miniaturized Mössbauer Spectrometer MIMOS II

We will discuss the achievements and lessons learned after 13 Years of operation on the surface of Mars.

[1] G. Klingelhöfe, R.V. Morris, B. Bernhardt, D.S. Rodionov, P.A. de Souza, S.W. Squyres, J. Foh, E. Kankeleit, U. Bonnes, R. Gellert, C. Schröder, S. Linkin, E. Evlanov, B. Zubkov, and O. Prilutski, *J. Geophys. Res. Planets* **108** (2003) 8067

[2] Klingelhöfer et al., Science 306 (2004), 1740-1745.

[3] Morris et al., Science 305 (2004), 833-836.

[4] Morris et al., J. Geophys. Res. 111 (2006)

[5] G. Klingelhöfer, M. Blumers, B. Bernhardt, P. Lechner, J. Girones Lopez, J. Maul, H. Soltau, L. Strüder, *Lunar Planet. Sci. Conf.*, **3** (2010) 5-6.

In-beam Mössbauer Studies of ^{57}Mn Implanted into CaF_2

Y. Kobayashi[a,b], N. Takahama[a], Y. Yamada[c], Y. Sato[c], M. K. Kubo[d], M. Mihara[e], W. Sato[f], K. Takahashi[a], K. Some[a], T. Ando[a], M. Sato[a], T. Nagatomo[c], J. Miyazaki[g], J. Kobayashi[e], S. Sato[h] and A. Kitagawa[h]

[a] *Graduate School of Engineering Science, University of Electro-Communications, Chofu, Tokyo182-8585, Japan*
[b] *Nishina Center for Accelerator-Based Science, RIKEN, Wako, Saitama 351-0198, Japan*
[c] *Department of Chemistry, Tokyo University of Science, Shinjuku, Tokyo 162-8602, Japan*
[d] *Division of Arts and Sciences, International Christian University, Mitaka, Tokyo 181-8585, Japan*
[e] *Graduate School of Science, Osaka University, Toyonaka, Osaka 560-0043, Japan*
[f] *Institute of Science and Engineering, Kanazawa University, Kanazawa, Ishikawa 920-1192, Japan*
[g] *Faculty of Pharmaceutical Sciences, Hokuriku University, Kanazawa, Ishikawa 920-1180, Japan*
[h] *National Institute of Radiological Science, Inage, Chiba 263-8555, Japan*
(kyoshio@pc.uec.ac.jp)

In-beam Mössbauer spectroscopy of solids implanted with ^{57}Mn, which decays to ^{57}Fe with a half-life of 87 s, enables *in situ* characterizations of the electronic states, the oxidation states, the site distributions and the coordination environments of extremely dilute Fe atoms in solids in which iron is insoluble. It is important to investigate the final positions and the atomic states of the dilute impurity atoms in the optical materials [1-4]. Calcium fluorite (CaF_2) is one of typical optical materials and has a simple crystalline structure, as it is a cubic and highly ionic compound. It was reported that a single line and a quadrupole doublet were ascribed to Fe^{2+} on substitutional Ca^{2+} site and in non-cubic sites, respectively [1-3]. Here, the in-beam Mössbauer spectroscopy was applied to study the site distributions and chemical states of Fe after ^{57}Mn implantation into a single-crystalline CaF_2.

The experimental procedure and setup were described in detail in Ref. 5. The sample of single crystalline CaF_2 was obtained from Pier Optics Co. and was used with no prior treatment. The sample size was $25\times25\times3^{t}$ mm.

The in-beam Mössbauer spectra of ^{57}Fe after implantation of ^{57}Mn into CaF_2 were obtained between 13 K and 230 K, as shown in Fig. 1. The spectra could be analyzed with two or three doublets, respectively. From the results of the Mössbauer parameters and DFT calculations, D1 (δ =1.62(3) mm/s, ΔE_Q = 3.22(8) mm/s at 13 K) and D2 (δ =1.62(5) mm/s, ΔE_Q = 2.03(9) mm/s at 13 K) were assigned to Fe^{2+} substituted for Ca^{2+} and Fe^{2+} at an interstitial site of *fcc* lattice, respectively. The assignment of D3 and the temperature dependence of three components will be discussed.

[1] J. R. Regnard and U. Dürr, *J. Phys*. (Paris) **40** (1979) 997.
[2] C. Garcin et al., *J. Phys*. (Paris) **47** (1986) 1977-1988.
[3] C. Garcin et al., *Hyp. Int.* **29** (1986) 1225-1228.
[4] S. Olariu et al., *J. Mod. Opt*. **52** (2005) 877-884.
[5] T. Nagatomo et al. *Nucl. Inst. Meth.* B **269** (2011) 455-459.

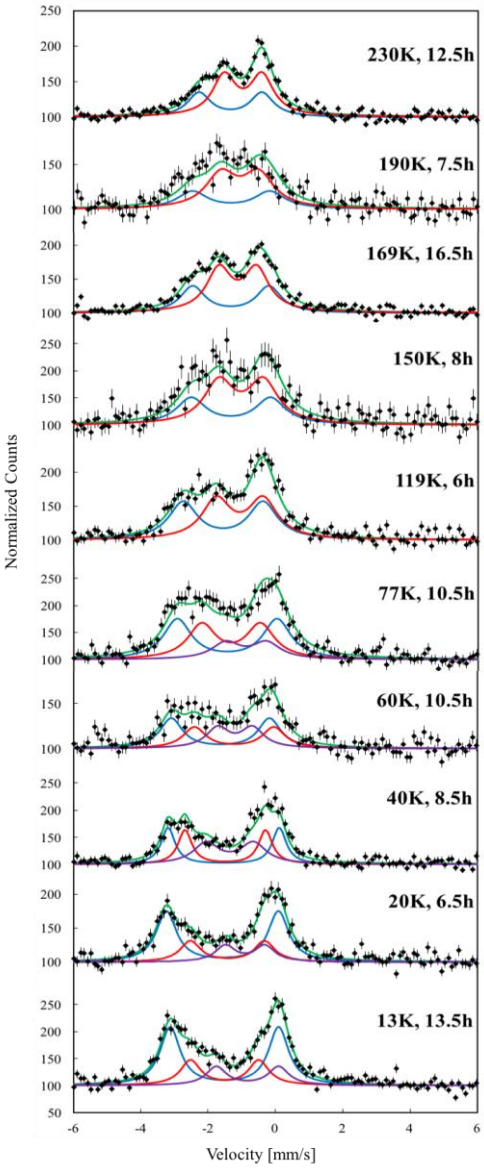

Fig. 1 In-beam emission Mössbauer spectra of ^{57}Fe after ^{57}Mn implantation in CaF_2 between 13 K and 230 K. The velocity is given relative to α-Fe at room temperature. The sign of the velocity scale is opposite to the conventional absorption experiment.

Mössbauer Studies of Superconducting Iron Pnictides and Chalcogenides

V. Ksenofontov[a], S. Shylin[a], S. A. Medvedev[b], P. Naumov[b], G. Wortmann[c] and C. Felser[b]

[a]*Institut für Anorganische und Analytische Chemie, Johannes Gutenberg-Universität, Mainz, Germany*
[b]*Max-Planck-Institut für Chemische Physik fester Stoffe, Dresden, Germany*
[c]*Department Physik, Universität Paderborn, Paderborn, Germany*
(ksenofon@uni-mainz.de)

Within the novel superconducting Fe-based systems, FeSe could be clue compounds for the understanding of the mechanisms of superconductivity (SC) in these systems. In particular, the dramatic increase of T_C under pressure from 8.5 K at ambient pressure to 36.7 K at 9 GPa [1] points to a new superconductivity mechanism in these systems. However the structural similarity of iron pnictides and chalcogenides rises a question about a possibility of SC also in isostructural chalcogenides systems.

Application of nuclear inelastic scattering (NIS) of synchrotron radiation to study of the local phonon DOS in FeSe-based SC as function of temperature and pressure could prove that electron-phonon interactions could not be the main mechanism for superconductivity in these systems [2]. Together with conventional ^{57}Fe-Mössbauer spectroscopy, we can conclude an important role of antiferromagnetic spin fluctuations which can mediate superconductivity acting as "glue" for Cooper pairs in Fe-based SC.

Mössbauer studies of FeSe intercalated with Li/NH_3 (T_C = 43 K, [3]) demonstrate that simultaneously with superconducting transition in ^{57}Fe Mössbauer spectra appears a magnetic subspectrum of dynamic nature. Conductivity measurements demonstrate that T_C decreases with increasing pressure. Pressure measurements with ^{57}Fe-Synchrotron Mössbauer Source (SMS) revealed that both the amount of magnetic fraction and the frequency of the hyperfine magnetic field fluctuations do follow the variation of T_C with pressure confirming that the superconducting pairing in FeSe-based superconductors is mediated by the antiferromagnetic spin fluctuations.

Doping of small amounts of Cu into the FeSe matrix suppresses superconductivity and introduces local static moments at the Fe sites, evidenced by glassy magnetic interactions. Application of pressure leads to restoration of superconductivity in Cu-doped FeSe [4]. High-pressure studies of non-supercondctive $Fe_{0.97}Cu_{0.04}Se$ using the SMS revealed that pressure suppresses the static spin-glass state. Apparently only nano-scale phase separation of insulating vacancy-ordered antiferromagnetic and metallic non-magnetic FeSe-similar domains provides conditions for coexistence of static magnetism and SC [5].

The structural similarity of iron pnictides and chalcogenides - the semiconducting $Rb_{0.8}Fe_{1.6}S_2$ and superconducting $Rb_{0.8}Fe_{1.6}Se_2$, is intriguing. Both compounds crystallize in the tetragonal space group I4/m and order antiferromagneticaly at T_N above 500 K. ^{57}Fe Mössbauer spectra of these two samples are very similar. They have the same constituencies, reflecting the intergrown antiferromagnetically ordered (sextet) and paramagnetic (doublet) fractions. The main issue can be briefly summarized as follows: how a formal substitution of FeSe by FeS layers inhibits superconductivity? Study a series of solid solutions $Rb_{0.8}Fe_{1.6}Se_{2-x}S_x$ ($0 \le x \le 2$) varying a Se-by-S substitution level can give an answer.

Possibility of "tuning" of magnetism, nematic order and superconductivity by doping and hydrostatic pressure application allows in several cases to clarify the interplay between them in iron-based superconductors.

[1] S. Medvedev et al., Nature Mater. 8 (2009) 630.
[2] V. Ksenofontov et al., Phys. Rev. B 81 (2010) 184510.
[3] S. I. Shylin et al., Europhys. Lett., 109, 67004 (2015).
[4] L. M. Schoop et al., Phys. Rev. B, 84, 174505 (2011).
[5] V. Ksenofontov et al., Phys. Rev. B, 84, 180508(R) (2011).

^{57}Fe-Mössbauer and Magnetic Susceptibility Studies of Iron Phosphate Glass Prepared by Sol-Gel Method

K. Sunakawa[a], R. Higashinaka[a], T. D. Matsuda[a], Y. Aoki[a], E. Kuzmann[b], Z. Homonnay[b], M. Perović[c], M. Bošković[c], T. Naka[d], T. Nakane[d], S.Krehula[e], M. Ristić[e], S.Musić[e] T. Nishida[f] and S. Kubuki[a]

[a]*Graduate School of Science, Tokyo Metropolitan University, Minami-Osawa 1-1, Hachi-Oji, Tokyo 192-0397, Japan*
[b]*Institute of Chemistry, Faculty of Science, Eötvös Loránd University, Pazmany P.s., 1/A, Budapest 1117, Hungary*
[c]*Laboratory for Condensed Matter Physics, Institute of Nuclear Science Vinča, 12-14 Mike Petrovića Street, Belgrade, Serbia*
[d]*National Institute of Materials Science, Sengen 1-2-1, Tsukuba, Ibaraki, 305-0047, Japan*
[e]*Division of Materials Chemistry, Ruđer Bošković Institute, P.O. Box 180, HR-10002, Zagreb, Croatia*
[f]*School of Humanity-Oriented Science and Engineering, Kindai University Kayanomori 11-5, Iidzuka Fukuoka 820-8555, Japan (kubuki@tmu.ac.jp)*

Oxide glasses shows some characteristic behavior at low temperature region. However, there are only few reports about the chemical states of magnetic ions effecting the magnetic properties of oxide glass because structure of oxide glass is amorphous. In this study, the relationship between the local structure and magnetic properties of iron phosphate glass ($50Fe_2O_3{\cdot}50P_2O_5$ glass, composition in mass%) prepared by sol-gel method was investigated by measuring ^{57}Fe Mössbauer spectra, X-ray diffraction pattern (XRD), dc and ac magnetic susceptibility.

Only a halo patterns were detected in the XRD diffractograms of $50Fe_2O_3{\cdot}50P_2O_5$ glass annealed (HT) at 200, 300 and 400 ^{o}C for 2 h. After the isothermal annealing at 500 ^{o}C for 2 h, in contrast, diffraction peaks due to α-Fe_2O_3 and $FePO_4$ were detected. Mössbauer spectra of $50Fe_2O_3{\cdot}50P_2O_5$ glass, recorded before the annealing (Fig. 1(a)), consisted of a doublet with isomer shift (IS) and quadrupole splitting (QS) of 0.33 and 0.63 mm s^{-1}, respectively, reflecting the presence of distorted $Fe^{III}O_4$ tetrahedra. On the other hand, Mössbauer spectra of $50Fe_2O_3{\cdot}50P_2O_5$ glass annealed at higher than 200 ^{o}C for 2 h (Fig. 1(b)-(d)) consisted of two doublets. In case of the glass HT at 200 ^{o}C, one doublet with IS and QS of 1.0 and 2.6 mm s^{-1}, respectively, was ascribed to $Fe^{II}O_6$ octahedra, and the other with IS and QS of 0.31 and 0.76 mm s^{-1}, respectively, was ascribed to $Fe^{III}O_4$ tetrahedra. The Mössbauer parameters of the glass HT at 300 ^{o}C were similar to that of the glass HT at 200 ^{o}C. However, the Fe^{III}/Fe^{II} ratio of the glass HT at 200 ^{o}C was higher than that of the glass HT at 300 ^{o}C.

From the temperature dependency of dc magnetic susceptibility under zero field cooling, the value of magnetic moment was the highest around 5 K. In measurements of ac magnetic susceptibility, this peak shifted towards higher temperatures with increasing in frequency of magnetic field. From the relationship between cusp temperature and relaxation time, the value of microscopic relaxation time and the dynamical exponent were estimated 0.22 ns and 13.9, respectively, in the case of the glass heat treated at 200 ^{o}C, when the magnetic property was ascribed to spin glass[1]. On the other hand, the value of the dynamic exponent decreased with heat treatment at higher temperature, of which the magnetic properties changed spin glass to superparamagnetism with heat treatment at higher temperature.

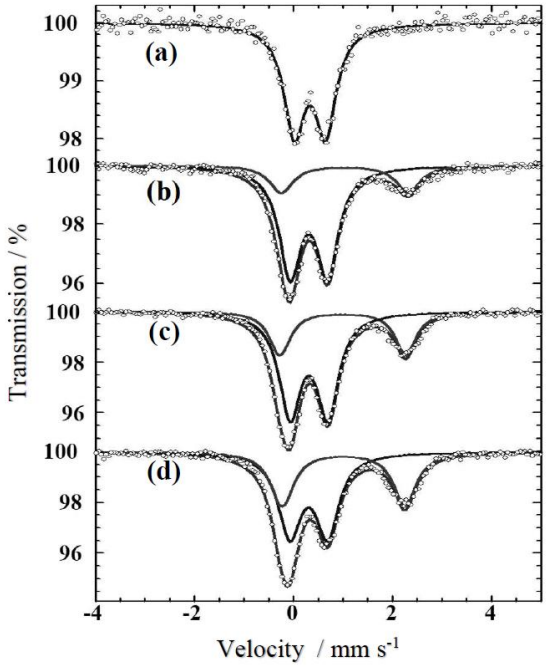

Fig. 1 ^{57}Fe Mössbauer spectra of $50Fe_2O_3{\cdot}50P_2O_5$ glass (a) before and after heat treatment for 2 h, at (b) 200, (c) 300 and (d) 400 ^{o}C.

[1] H. Akamatsu, S. Oku, K. Fujita, S. Murai, K. Tanaka, Phys. Rev. B **80** (2009) 134408.

Iron and Iron Oxide Based Nanomaterials in Environmental Applications - Contribution of Mössbauer spectroscopy

L. Machala[a], R. Prucek[a], J. Filip[a], J. Tucek[a] and R. Zboril[a]

[a] *Regional Centre of Advanced Technologies and Materials, Departments of Experimental Physics and Physical Chemistry, Faculty of Science, Palacky University, Olomouc, Czech Republic (libor.machala@upol.cz)*

Zero valent iron nanoparticles (nZVI) as well as iron oxide nanoparticles (NPs) are widely used in various environmental applications thanks to their magnetic, sorption, photocatalytic, and non-toxic properties. There are a lot approaches how to synthesize nZVI or iron oxide NPs, particularly, a large-scale production is desired for the applications. ^{57}Fe Mössbauer spectroscopy is the key experimental technique for characterization of the NPs and monitoring of processes which they are involved in, including characterization of final products. The effectivity of a process can be enhanced when so called "in-situ" approach is applied. In this case the treated sample (e.g. a pollutant in water) is present direct during the formation of NPs. Thus a pollutant is in a close contact with the NPs just after their formation and before NPs agglomerate. Moreover, it can happen that atoms of the pollutant are able to enter the crystal structure of iron oxide NPs during their formation. The pollutant can be then filtered from the solution very effectively. Magnetic separation can be considered as well.

In this paper, a few studies where iron and iron oxide based nanoparticles were successfully employed in environmental applications will be presented. Fe_2O_3 NPs prepared by a transformation of $KFeO_2$ at room temperature in air showed effective sorption and removal of copper [1]. The above described in-situ approach has been successful for almost 100% removal of copper during 20 min (Fig. 1).

Iron(III) oxide or hydroxide NPs are formed as a product of transformation of potassium ferrate(VI) in water. Oxidation properties of the ferrate(VI) together with sorption and magnetic properties of the formed Fe(III) NPs were beneficial for effective removal of arsenic [2], phosphates [3], and heavy metals [4].

Fe_2O_3 nanopowders (3-5 nm) were prepared easily by a thermal decomposition of ferrous oxalate dihydrate ($FeC_2O_4 \cdot 2H_2O$). The nanopowders were successfully tested as nanocatalysts in decomposition of H_2O_2 [5] and phenol [6]. Recently the same nanopowders were applied for photocatalytic degradation of the Cyanotoxin Microcystin-LR under visible light illumination [7]. nZVI and potassium ferrate(VI)/(III) composite were applied for a treatment of chemical warfare agents [8].

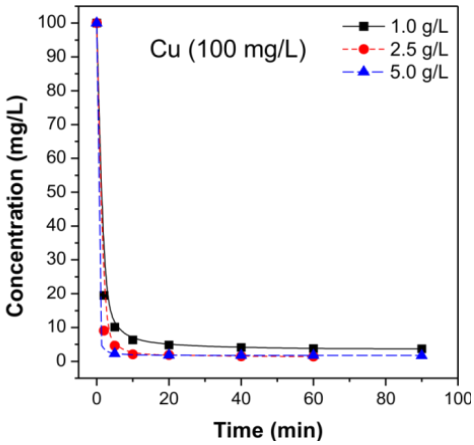

Fig. 1 The kinetics of Cu removal by sorption with amorphous Fe(III) oxyhydroxide nanoparticles (1.0; 2.5; 5.0 g/L), *in-situ* formed from $KFeO_2$. Starting concentration of Cu was 100 mg/L and pH was adjusted to 6.5

In the paper, a role of ^{57}Fe Mössbauer spectroscopy in all the above mention studies will be presented and discussed.

[1] L. Machala, J. Filip, R. Prucek, J. Tucek, J. Frydrych, V. K. Sharma, R. Zboril, Sci. Adv. Mater. 7(3) (2015) 579.

[2] R. Prucek, J. Tucek, J. Kolarik, J. Filip, Z. Marusak, V. K. Sharma, R. Zboril, Environ. Sci. Technol. 47 (7) (2013) 3283.

[3] R. P. Kralchevska, R. Prucek, J. Kolarik, J. Tucek, L. Machala, J. Filip, V. K. Sharma, R. Zboril, Water Research 103(15) (2016) 83.

[4] R. Prucek, J. Tucek, J. Kolarik, I. Huskova, J. Filip, R. S. Varma, V. K. Sharma, R. Zboril, Environ. Sci. Technol. 49(4) (2015) 2319.

[5] M. Hermanek, R. Zboril, I. Medrik, J. Pechousek, C. Gregor, J. Am. Chem. Soc. 129(35) (2007) 10929.

[6] R. Prucek, M. Hermanek, R. Zboril, Applied Catalysis A: General 366 (2009) 325.

[7] C. Han, L. Machala, I. Medrik, R. Prucek, R. P. Kralchevska, D. D. Dionysiou, Environmental Science and Pollution Research 24(23) (2017) 19435.

[8] R. Zboril, M. Andrle, F. Oplustil, L. Machala, J. Tuček, J. Filip, Z. Marušák, V.K. Sharma, J. Hazard. Mat. 211 (2012) 126.

In-Situ Study of Electric-Field-Controlled Ion Transport in the $Fe/BaTiO_3$ Interface

D.G. Merkel[a,b], D. Bessas[b,c], G. Bazsó[a] A. Jafari[b,d], R. Rüffer[b], A.I. Chumakov[b], N.Q. Khanh[e], Sz. Sajti[a], J-P. Celse[b] and D.L. Nagy[a]

[a]*Wigner Research Centre for Physics, Hungarian Academy of Sciences, POBox 49, H-1525 Budapest, Hungary*
[b]*European Synchrotron Radiation Facility, 71 avenue des Martyrs, CS 40220, F-38043 Grenoble Cedex 9, France*
[c]*Department of Radiation Science and Technology, Delft University of Technology, Mekelweg 15, 2629 JB Delft, The Netherland*
[d]*DTUSpace—National Space Institute, Technical University of Denmark, DK-2800 Kgs. Lyngby, Denmark*
[d]*Centre for Energy Research, Institute of Technical Physics and Materials Science, POBox 49, H-1525 Budapest, Hungary (nagy.denes@wigner.mta.hu)*

In multiferroic materials, the coexistence and coupling of ferroelectric (FE) and magnetic order enables the fine control and modulation of electric polarization by magnetic field or the magnetic field by electric polarization, properties with numerous potential applications. Composite multiferroic systems can be produced by combining ferromagnetic (FM) and ferroelectric thin films or by evaporating a FM layer on a FE substrate. Here we report on a study of the electric-field-controlled ion transport and interface formation of iron thin films on a FE $BaTiO_3$ (BTO) substrate with and without applied external electric field by in-situ grazing-incidence nuclear resonant scattering and x-ray reflectometry techniques [1].

The experiment was carried out at the nuclear resonant scattering beamline ID18 of the European Synchrotron Radiation Facility (ESRF) in the nuclear resonant scattering chamber of the in-beam ultrahigh-vacuum system. The electric field was applied using a special sample holder forming a parallel-plate capacitor containing the BTO crystal.

At the early stage of the ^{57}Fe deposition, below a certain thickness threshold, an iron-II oxide interface layer was observed. The hyperfine parameters of the interface layer were found to be insensitive to the evaporated layer thickness. When an electric field was applied during growth, increase of the nonmagnetic/magnetic thickness threshold from 25 Å to 35 Å and an extended magnetic transition region was measured compared to the case where no field was applied. When further evaporation occurred, the interface layer under the threshold was found to be stable, in contrast with the upper magnetic layer where the magnitude and orientation of the hyperfine magnetic field varied continuously. The increase of the thickness of the iron-II oxide layer upon electric field application during evaporation is attributed to the supported ion transfer through the interface.

The comprehensive understanding of the growth mechanism, as well as the effect of the electric field on the Fe/BTO system can lead to novel applications by the application of laterally controlled electric field. This way, custom oxide/metallic nanopatterns can be designed which are of great importance of spintronics and nanotechnology.

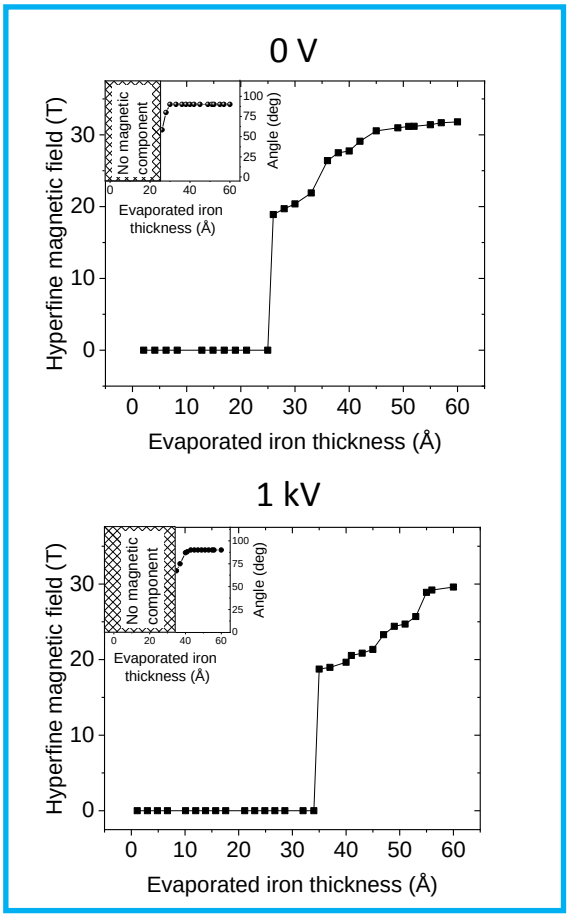

Fig. 1 The extracted mean value of hyperfine magnetic field in case of no voltage applied (top) and in case of 1 kV applied voltage (bottom). In the inset, the alignment of the hyperfine magnetic field in the FM layer is shown relative to the surface normal.

[1] D.G. Merkel, D. Bessas,, G. Bazsó A. Jafari, R. Rüffer, A.I. Chumakov, N.Q. Khanh, Sz. Sajti, J-P. Celse, D.L. Nagy, Mater. Res. Express 5 (2018) 016405.

On/Off Spin-Crossover Phenomenon and Control of the Transition Temperature in Assembled Iron(II) Complexes

S. Nakashima[a,b], M. Kaneko[c], K. Yoshinami[b], S. Iwai[b] and H. Dote[d]

[a]*Natural Science Center for Basic Research and Development, Hiroshima University, 1-4-2, Kagamiyama, Higashi-Hiroshima, Japan*
[b]*Graduate School of Science, Hiroshima University, 1-3-1 Kagamiyama, Higashi-Hiroshima, Japan*
[c]*Nuclear Science and Engineering Center, Japan Atomic Energy Agency, 2-4 Shirakata, Tokai-mura, Japan*
[a]*Graduate School of Engineering, Hiroshima University, 1-4-1 Kagamiyama, Higashi-Hiroshima, Japan*
(snaka@hiroshima-u.ac.jp)

Fe(II) spin-crossover (SCO) phenomena described as the switching behavior of two spin ground states between high-spin (HS) and low-spin (LS) have inspired lots of chemists due to their application possibilities. These possibilities come from the response abilities to several external field stimuli such as temperature, pressure and light-illumination. The investigations of coordination polymers by introducing bridging ligands have suggested not only the controlling these responsivities of SCO behavior, but also the additional potentials for fundamental and applied fields in chemistry.

The framework of coordination polymers $[Fe(NCS)_2L_2]_n$, which have *trans*-$Fe(NCS)_2$ unit bridged by 4,4'-bipyridine type ligands (L), have provided several types of SCO-on/off results. Since their assembled structures have the vacancies, which can incorporate the guest molecules, due to the systematic construction of Fe(II) octahedral sphere, the guest dependency of these compounds has been studied extensively.

In the present conference, we present the important role of local structure around iron atom on the SCO-on/off. And we present our experiments to control the local structure and then to contol the transition temperature of SCO by mixing anionic ligands.

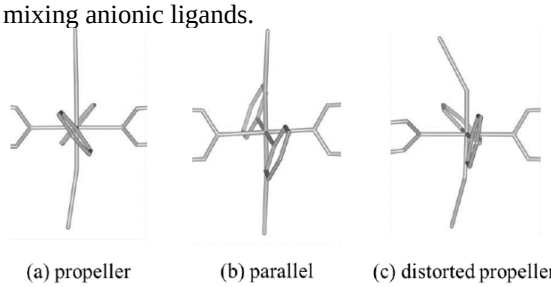

Fig. 1 Difference in the Fe-pyridine local structures observed in a variety of the assembled $Fe(NCX)_2L_2$.

Figure 1 summarizes the local structure observed in a variety of assembled $[Fe(NCX)_2L_2]_n$. It has been revealed that SCO phenomenon occurs when the coodinating pyridines facing to each other across the iron atom are propeller type, while the phenomenon does not occur when they are parallel type or distorted propeller type. The use of DFT calculation explained that, in the shortening of Fe-pyridine bonds when changing from HS state to LS state, the pyridines of propeller type can approach the iron atom with smaller steric hindrance than those of parallel and distorted propeller type complexes[1,2].

Wu et al. have reported the iron(II) assembled complex $[Fe(NCX)_2(bpb)_2]_n$ (X = S, Se, and BH_3; bpb = 1,4-bis(4-pyridyl)benzene)[3]. SCO phenomenon is observed for X = BH_3 case and incomplete SCO was also observed for NCSe case. The SCO behavior changes depending on the guest molecule in the assembled structure. We considered the changing of the local structure around iron for bpb complex. The strategy is to introduce methyl substituent to the benzene ring in the bridging ligand, which will influence the dihedral angle between benzene and pyridine. We expect such change affects the coordination of pyridine to iron. Actually the SCO-on/off was affected[4].

Next strategy is to replace benzene with anthracene in bpb. We synthesized three assembled complexes $[Fe(NCX)_2(bpanth)_2]_n$ (X = S, Se, and BH_3; bpanth = 9,10-bis(4-pyridyl)anthracene)[5]. The assembled structure is supported by the stabilization of CH-π interaction. It causes the formation of unstable parallel-type local structure which takes Fe(II)-HS state.

As an additional strategy for controlling the transition temperature from the viewpoint of ligand field strength, we synthesized NCS^- and $NCBH_3^-$ anion-mixed assembled complexes bridged by 1,2-bis(4-pyridyl)ethane[6]. SQUID measurement showed the stepwise spin transition behavior when enclathrating *p*-dichlorobenzene as guest. It is judged with the aid of DFT calculation that this might originate from the two parts of $Fe(NCS)_2$ and $Fe(NCS)(NCBH_3)$.

[1] M. Kaneko, S. Tokinobu, S. Nakashima, Chem. Lett. 42 (2013) 1432.
[2] M. Kaneko, S. Nakashima, Bull. Chem. Soc. Jpn. 88 (2015) 1164.
[3] X.-R. Wu et al., Inorg. Chem. 54 (2015) 3773.
[4] K. Yoshinami, M. Kaneko, H. Yasuhara, S. Nakashima, Radioisotopes 66 (2017) 625.
[5] S. Iwai, K. Yoshinami, S. Nakashima, Inorganics 5 (2017) 61.
[6] H. Dote, M. Kaneko, K. Inoue, S. Nakashima, Bull. Chem. Soc. Jpn. 91 (2018) 71.

Local Structure of Conductive Vanadate Glass Applied to the Oxygen Electrode for Rechargeable Metal-Air Battery

N. Oka, H. Miyamoto, Y. Fujita, S. Masuda, M. Yuasa and T. Nishida

Department of Biological and Environmental Chemistry, Kindai University, 11-6 Kayanomori Iizuka Fukuoka 820-8555, Japan
(nobuto.oka@fuk.kindai.ac.jp)

1. Introduction

Metal-air battery has a very high energy density because it could use atmospheric oxygen as the electrode active material. This rechargeable battery needs bifunctional catalytic materials, which involve effective oxygen reduction/evolution at the air electrode in the discharge/charge process. In this study, a new bifunctional catalytic material for the air electrode has been developed using conductive vanadate glass. Conductivity of vanadate glass, $20BaO{\cdot}10Fe_2O_3{\cdot}70V_2O_5$, became "*tunable*" over a wide range (10^{-7}-10^{-1} $S{\cdot}cm^{-1}$) when the local distortion of the glass skeleton was diminished by isothermal annealing [1]. Utilizing these characteristics, new catalytic materials have been developed containing MnO_2 and NiO which were introduced for the oxygen reduction and evolution, respectively.

2. Experimental

$20BaO{\cdot}5MnO_2{\cdot}5NiO{\cdot}70V_2O_5$ glass was prepared by melting the mixture composed of $BaCO_3$, MnO_2, NiO and V_2O_5 at 1100 °C for 2 h. After being quenched to 450 °C, each glass sample was annealed at 450 °C for 0-300 min. For the preparation of the air electrode, pulverized vanadate glass was mixed with powder of 7.5 mass% of poly (tetrafluoroethylene), abbreviated as PTFE, which was hot-pressed on the gas diffusion layer over a Ni metal mesh. 8M KOH aqueous solution and a Pt mesh were placed inside the Teflon cell as the electrolyte and the counter electrode, respectively. Temperature of the Teflon cell was kept constant at 60 °C. Discharge and charge polarization curves were recorded on a potentiostat.

3. Results and Discussion

The electrical conductivity of the as-prepared vanadate glass was 5.4×10^{-6} $S{\cdot}cm^{-1}$ at RT. After the annealing at 450 °C for 300 min, it increased to 1.1×10^{-2} $S{\cdot}cm^{-1}$. Figure 1 shows the discharge- (left) and charge-related polarization curves (right) obtained by using $20BaO{\cdot}5MnO_2{\cdot}NiO{\cdot}70V_2O_5$ glass as the catalyst for the air electrode. The vanadate electrode showed an excellent bifunctional oxygen reduction/evolution activity, being comparable to that of the materials reported in the literature, like polycrystalline $LaNiO_3$ [2]. This vanadate glass could be a highly potential candidate for the bifunctional catalytic material for the rechargeable metal-air battery. Some results of Mössbauer measurement will be discussed at the conference.

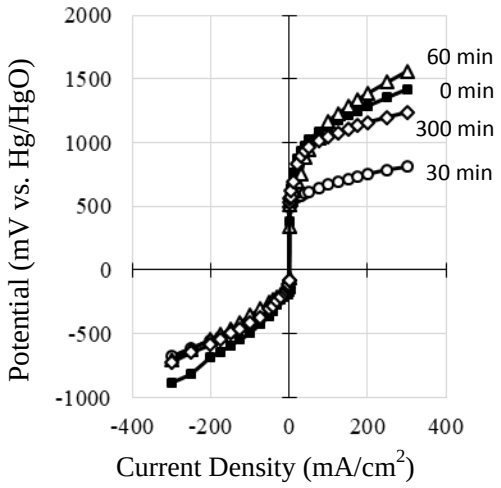

Fig. 1 Polarization curves for $20BaO{\cdot}5MnO_2{\cdot}5NiO{\cdot}70V_2O_5$. The time refers to the duration of annealing at 450 ° C.

[1] T. Nishida, Y. Izutsu, M. Fujimura, K. Osouda, Y. Otsuka, S. Kubuki and N. Oka, *Pure and Appl. Chem.* **89** (2017) 419-428.
[2] M. Yuasa, M. Nishida, T. Kida, N. Yamazoe and K. Shimanoe, *ECS* **158** (2011) A605-A610.

Probing Orbital Magnetic Moments by Mössbauer and X-Ray Absorption Spectroscopies in FeV_2O_4

J. Okabayashi

Research Center for Spectrochemistry, The University of Tokyo
(jun@chem.s.u-tokyo.ac.jp)

The orbital degree of freedom has attracted interest in the condensed-matter physics because of adding of new functional functionalities. Couplings between orbital and spin degrees of freedom in transition metal (TM) oxides exhibit a wide variety of interesting physical phenomena studied in strongly correlated electron systems. The orbital degeneracy of t_{2g} or e_g orbitals, split by the crystal field in TM oxides, gives rise to the orbital ordering phenomena in perovskite-type Fe or V oxides accompanied by Jahn-Teller distortion. Spinel-type FeV_2O_4 is a candidate to study orbital ordering since orbital magnetic moments of Fe^{2+} (d^6) are strongly affected by the Jahn-Teller distortion in the Fe sites, which brings the ferro orbital ordering in both Fe and V sites through the spin-orbit interaction. An unresolved issue related to orbital ordering of spinel-type vanadium oxides is the relationship between the orbital magnetic moments in vanadium sites and orbital ordering. In case of FeV_2O_4, the V orbital states consist of complex wave functions of degenerated *yz* and *zx* states, which expect the ferro-orbital ordering with the large orbital moments of almost 1 μ_B. On the other hand, in the case of MnV_2O_4, real wave functions in the V sites which are described as d_{yz} and d_{zx} are ordered alternatively, resulting in an antiferro orbital ordering with quenching orbital moments. Therefore, the element-specific investigations of orbital moments enable to discuss the types of orbital ordering. We employed Mössbauer spectroscopy and X-ray absorption spectroscopy (XAS) and X-ray magnetic circular dichroism (XMCD) with the sum-rule analysis, which enables to estimate the orbital moments. In this study, we investigated the element specific electronic and magnetic properties of FeV_2O_4, and examined the relationship between orbital magnetic moments and orbital ordering.

Single crystals were grown by the floating-zone method. The magnetic and orbital ordering temperatures of FeV_2O_4 were estimated to be 110 K and 70 K, respectively, accompanying the lattice distortions from tetragonal to orthorhombic structures with decreasing temperature. Temperature dependent Mössbauer spectroscopy has been conducted using ^{57}Co source in a transmission mode.

The temperature-dependent Mössbauer spectra are shown in Fig. 1 taken at room temperature (RT) (cubic phase), 100 K (orthorhombic), and 78 K (orthorhombic). We assume two kinds of components, site-1 and site-2. At RT, the single peak with the isomer shift (IS) value of 1 mm/s suggests the Fe^{2+} states with the additional peak (site-2) which is originated from the surface oxidized Fe^{3+} states. With decreasing temperature, significant hyperfine structures appear in the spectra and both intensities and peak positions are modulated between 100 and 78 K. The parameters used for the fitting; IS, quadrupole splitting (QS), and hyperfine magnetic field (H_{hf}), are adjusted. The small H_{hf} about 10 T implies the presence of the orbital angular momentum in Fe through the Jahn-Teller distortion. The appearance of orbital magnetic moments in FeV_2O_4 is also estimated from XMCD analysis. Therefore, we found that orbital magnetic moments in Fe sites are confirmed in both MS and XMCD and contribute to the ferro-orbital ordering.

We acknowledge to Prof. Masashi Takahashi (Toho University) and Prof. Shigeki Miyasaka (Osaka University).

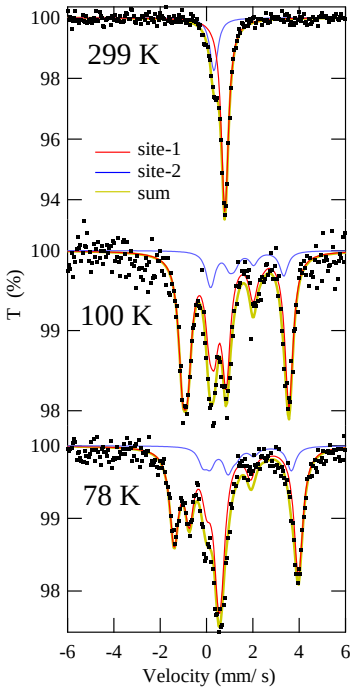

Fig. 1 Temperature-dependent Mössbauer spectra of FeV_2O_4. Dots show the experimental data. Lines represent the fitting curves.

Study of Some Stony and Stony-Iron Meteorites Using X-Ray Diffraction and Mössbauer Spectroscopy: Fe^{2+} Partitioning Between the M1 and M2 Sites in Silicate Phases

A.A. Maksimova, A.V. Chukin, E.V. Petrova and M.I. Oshtrakh

Institute of Physics and Technology, Ural Federal University, Ekaterinburg, 620002, Russian Federation (oshtrakh@gmail.com)

Stony and stony-iron meteorites consist of various iron-bearing phases with the main content of silicate crystals such as olivine $(Fe, Mg)_2SiO_4$, orthopyroxene $(Fe, Mg)SiO_3$ and clinopyroxene $(Fe, Mg, Ca)SiO_3$. These minerals have two crystallographically non-equivalent positions M1 and M2 for Fe^{2+} and Mg^{2+} cations. The information about the Fe^{2+} and Mg^{2+} partitioning between the M1 and M2 sites in silicate crystals is important for estimation of their thermal history. Therefore, evaluation of the Fe^{2+} and Mg^{2+} occupancies in silicate phases in stony and stony-iron meteorites could be used for analysis of their thermal history. Ordinary chondrites are the most frequently reached Earth stony meteorites. Pallasites are a part of stony-iron meteorites. Representatives of these meteorite types are considered in this work.

X-ray diffraction (XRD) and Mössbauer spectroscopy are very useful techniques for the study of various meteorites including the Fe^{2+} partitioning between the M1 and M2 sites in silicate phases. We present here the results of our approach to estimating the Fe^{2+} cations distribution between two nonequivalent sites in silicates using XRD and Mössbauer spectroscopy with a high velocity resolution (descretization of the velocity reference signal is 2^{12}). The latter technique has much more precise reaching the resonance and much better sensitivity to the features of the absorption line shape than conventional Mössbauer spectroscopy due to the smaller Dopler energy increment (see [1, 2]).

Samples of powdered matter were prepared from H, L and LL ordinary chondrites such as several fragments of Chelyabinsk LL5, Northwest Africa (NWA) 6286 LL6 and 7857 LL6, Tsarev L5 and Annama H5 as well as from a stony part extracted from Seymchan main group pallasite (PMG). All XRD patterns were fitted using the Rietveld full profile analysis with revealing the Fe^{2+} and Mg^{2+} occupations of the M1 and M2 sites in silicates (X_{Fe}^{M1}, X_{Fe}^{M2}, X_{Mg}^{M1} and X_{Mg}^{M2}, respectively). All Mössbauer spectra were better fitted with revealing of the main and minor spectral components. The components related to the ^{57}Fe in the M1 and M2 sites in all silicates were identified and their relative areas A^{M1} and A^{M2} were obtained for olivine, orthopyroxene and clinopyroxene.

A comparison of the Fe^{2+} partitioning between the M1 and M2 sites in silicates obtained on the basis of two techniques appeared to be similar, i.e. indicated a good agreement between XRD and Mössbauer spectroscopy. For instance, the ratios X_{Fe}^{M1}/X_{Fe}^{M2} and A^{M1}/A^{M2} for olivine were respectively 1.17 and 1.18 for Chelyabinsk LL5 (fragment No 2), 1.16 and 1.22 for NWA 7857 LL6 and 1.38 and 1.32 for Seymchan PMG. Furthermore, it is possible to estimate the distribution coefficient K_D using the values of X_{Fe}^{M1}, X_{Fe}^{M2}, X_{Mg}^{M1} and X_{Mg}^{M2} and then determine the temperature of equilibrium cations distribution T_{eq} for olivine and orthopyroxene (see details in [3, 4] and references therein). However, in contrast to XRD which permits estimation of X_{Fe}^{M1}, X_{Fe}^{M2}, X_{Mg}^{M1} and X_{Mg}^{M2}, Mössbauer spectroscopy cannot estimate X_{Mg}^{M1} and X_{Mg}^{M2} without additional data. It takes to use values of fayalite Fa and ferrosilite Fs (Fa and Fs are the molar fractions of the Fe-rich end-members of olivine and orthopyroxene solid solutions, respectively) to obtain X_{Mg}^{M1} and X_{Mg}^{M2} values from Mössbauer spectroscopy. The results obtained using two techniques appeared to be consistent. For instance, T_{eq} for olivine in Chelyabinsk LL5 (fragment No 2) was estimated of 1179 K (XRD) and 1115 K (Mössbauer spectroscopy) while that for olivine in Seymchan PMG was estimated of 684 K (XRD) and 835 K (Mössbauer spectroscopy). Thus, application of both X-ray diffraction and Mössbauer spectroscopy appeared to be a useful way for consistent analysis of Fe^{2+} partitioning between the M1 and M2 sites in silicate crystals in stony and stony-iron meteorites.

This work was supported by the Ministry of Education and Science of the Russian Federation (the Project # 3.1959.2017/4.6) and Act 211 by the Government of the Russian Federation, contract № 02.A03.21.0006.

[1] M.I. Oshtrakh, V.A. Semionkin, Spectrochim. Acta, Part A: Molec. and Biomolec. Spectrosc. 100 (2013) 78.
[2] M.I. Oshtrakh, V.A. Semionkin, AIP Conf. Proc., AIP Publishing, Melville, New York, 1781 (2016) 020019.
[3] M.I. Oshtrakh, E.V. Petrova, V.I. Grokhovsky, V.A. Semionkin, Meteorit. & Planet. Sci. 43 (2008) 941.
[4] A.A. Maksimova, M.I. Oshtrakh, A.V. Chukin, I. Felner, G.A. Yakovlev, V.A. Semionkin, Spectrochim. Acta, Part A: Molec. and Biomolec. Spectroscopy 192 (2018) 275.

^{119}Sn Mössbauer Spectroscopy in the Study of Metamagnetic Alloys

I. Unzueta[a,b], J. López-García[c,d], V. Sánchez-Alarcos[d,e], V. Recarte[d,e], J.I. Pérez-Landazába[d,e], J.A. Rodríguez-Velamazán[c], J.S. Garitaonandia[f,b], J.A. García[f,b] and F. Plazaola[a]

[a]*Department of Electricity and Electronics, University of the Basque Country UPV/EHU, 4890 Leioa, Spain*
[b]*BCMaterials, University of the Basque Country UPV/EHU, 4890 Leioa, Spain*
[c]*Institut Laue-Langevin, 71 Avenue des Martyrs, 38000 Grenoble, France*
[d]*Department of Physics, Universidad Pública de Navarra, Campus Arrosadía, 31006 Pamplona, Spain*
[e]*INAMAT, Universidad Pública de Navarra, Campus Arrosadía, 31006 Pamplona, Spain*
[f]*Department of Applied Physics II, University of the Basque Country UPV/EHU, 4890 Leioa, Spain*
(fernando.plazaola@ehu.eus)

Ni-Mn-based Heusler alloys exhibiting both long-range magnetic ordering and thermoelastic martensitic transformation (MT) are being intensively investigated over recent years, from both fundamental and applied points of view, due to the unique properties they show linked to the occurrence of a first-order structural transformation between magnetically ordered phases [1].

Different sequences of magneto structural transformations can be observed depending on both the third alloying element and the change in interatomic distances caused by the martensitic transformation. In particular, in Ni-Mn-Z (Z = In, Sn, and Sb) alloys, the so-called metamagnetic shape memory alloys, the MT takes place between a ferromagnetic austenite and weak magnetic martensitic phase, in such a way that the large magnetization drop occurring at the MT allows the induction of the martensitic transformation by an applied magnetic field. The phenomena gives rise to multifunctional properties, namely magnetic shape memory, giant magnetoresistance and large inverse magneto caloric effect, of great technical interest for practical applications in sensing and magnetic refrigeration [2].

Despite the promising features, the deficient mechanical properties of bulk samples hinder the development of practical devices. As a result, the use of micro particles is attracting an increasing interest, as it seems to be an effective method to overcome the bulk limitations [3]. However, in micro and nano regime the control of the internal stress and the defects becomes crucial to tune properly the desired multifunctional properties [4].

^{119}Sn Mössbauer Spectroscopy is a very valuable technique to study atomic level structural and magnetic characterization of metamagnetic Ni-Mn-Sn alloys.

This work studies the influence of defects and local stresses on the magnetic properties and martensitic transformation in Ni50Mn35Sn15 and Ni50Mn37Sn13 metamagnetic alloys at macroscopic and atomic scale levels, and in addition, the influence of Co introduction on its properties. This work demonstrates that the recovery of the martensitic transformation of the ternary alloys is directly related to the intensity of the non-magnetic component revealed by ^{119}Sn Mössbauer Spectroscopy, opening the possibility of quantifying the whole contribution of defects and the local stresses on the martensitic transformation in Ni-Mn-Sn alloys. In addition, the work suggests that ^{119}Sn Mössbauer Spectroscopy could be employed to track the evolution of the martensitic transformation in the quaternary alloys with Co, too.

[1] M. Acet et al., in: K.H.J. Buschow (Ed.), Handbook of Magnetic Materials, Elsevier, Amsterdam, 19 (2011) 231.
[2] X. Moya et al., Nature Materials 13 (2014) 439.
[3] C. Biffi, A. Tuissi, Opt. Laser. Technol. 78 Part B (2016) 42.
[4] V. Sánchez-Alarcos et al., J. Alloys Compd 689 (2016) 983.

Heteronuclear Fe/Ni Clusters

Y. Sanakis and C.P. Raptopoulou

Institute of Nanoscience and Nanotechnology, NCSR Demorktios, Athens, Greece
(i.sanakis@inn.demokritos.gr)

Heterometallic clusters have been widely examined as models for the active sites of important biological systems, such as nitrogenase, hydrogenases or Photosystem II. In Molecular Magnetism such clusters exhibit interesting magnetic properties. In the present talk we will present the properties of three different classes of synthetic heterometallic Fe/Ni clusters (figure 1) in which iron is found in the Fe^{II} and Fe^{III} states. Mössbauer Spectroscopy gives invaluable information concerning critical aspects of these clusters.

In the family of hetero-metallic enneanuclear clusters with general formula $[Fe_{9-x}Ni_x(\mu_4\text{-}OH)_2(O_2CMe)_8(py_2CO_2)_4]$, x = 1.00, 6.02, 7.46, 7.81 (class A) all clusters contain one 8-coordinate (rarely encountered in Fe^{II} and Ni^{II} chemistry) and eight 6-coordinate metal sites. The distribution of Fe^{II} and Ni^{II} over the two distinct metal sites and the formulation of the clusters are established via crystallography and spectroscopy. A notable site preference for iron to occupy the 8-coordinate site in low Fe-content species is observed via Mössbauer spectroscopy. Density functional theory further corroborated that Ni^{II} ions preferably occupy the octahedral sites, hence leaving the 8-coordinate site for the Fe^{II} ion. [1]

In classes B and C the heterometallic mixed-valence $Fe^{III}{}_2Ni^{II}{}_2$ and $Fe^{III}{}_3Ni^{II}$ clusters bear the defective double cubane and 'star' metal topologies, respectively (Figure 1). Static magnetic measurements indicate ferrimagnetic interactions leading to S = 3 (class B) and S = 7/2 (class C) ground states. Dynamic magnetic measurements reveal the onset of slow magnetic relaxation at liquid helium temperatures in the presence of external magnetic fields for both classes.

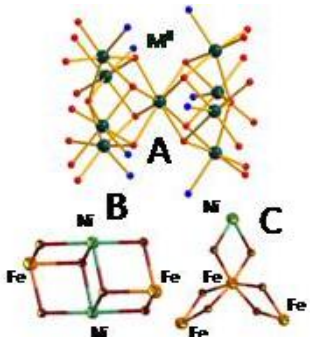

Fig. 1 The three classes of heteronuclear Fe/Ni clusters studied in the present talk.

Mössbauer spectroscopy confirms the oxidation and spin state of the iron in these clusters as well as the ligand environment around the ferric ions as determined by X-ray crystallography. Spectra recorded as a function of temperature, in the presence or absence of weak external magnetic fields are used in order to follow their spin relaxation properties. At liquid helium temperatures well-resolved sextets are observed. The analysis of these spectra in combination with the analysis of the magnetic measurements is used to assess the specific exchange coupling schemes in these clusters.

[1] A. N. Georgopoulou, K. Al-Ameed, A. K. Boudalis, D. F. Anagnostopoulos, V. Psycharis, J. E. McGrady, Y. Sanakis, C. P. Raptopoulou, Dalton Trans. 46 (2017) 12835.

Role of Defects on the Electronic and Magnetic Properties of Frustrated $ZnFe_2O_4$ Spinel

S. J. Stewart

IFLP-CCT- La Plata-CONICET and Departamento de Física, Facultad de Ciencias Exactas, Universidad Nacional de La Plata, La Plata, Argentina
(stewart@fisica.unlp.edu.ar)

$ZnFe_2O_4$ in its normal state is widely identified as an antiferromagnet with a Néel temperature around 10 K. However, its ground sate configuration has been the subject of discussion over the last decades leading to different proposals [1]. The Fe^{3+} ions at octahedral B-sites of its cubic spinel structure form a network of corner-sharing tetrahedra known as the pyrochlore lattice (Fig. 1(a). This configuration is known to give rise to 3D-geometrical spin frustration. The degeneracy of the ground state of geometrically frustrated compounds produces glassy magnetic behaviours [2] and even could lead to the inhibition of a long-range order. On the other hand, the presence of local defects like cationic inversion and vacancies as well as the broken symmetry of Fe^{3+} ions due to surface effects, modify the exchange magnetic coupling and adds randomness to $ZnFe_2O_4$ lattice [3]. These effects might lead to novel magnetic properties, for instance, the room-temperature ferromagnetism displayed by this nonmagnetic compound can be linked to this sort of defects, a phenomenon known as defect-induced magnetism (DIM).

We present here a brief overview of our results on the electronic, hyperfine and magnetic properties of defective zinc ferrite in bulk form, nanoparticles and films. The samples were investigated using near edge x-ray absorption spectroscopy, magnetic circular dichroism, Mössbauer spectroscopy, static and dynamic magnetic measurements. The experimental results were combined with *ab initio* density-functional-theory (DFT) calculations. We discuss the magnetic results in terms of the randomness and frustration introduced by the defects, and the role of these defects in triggering or enhancing the ferromagnetic order (Figs. 1 (b), (c)).

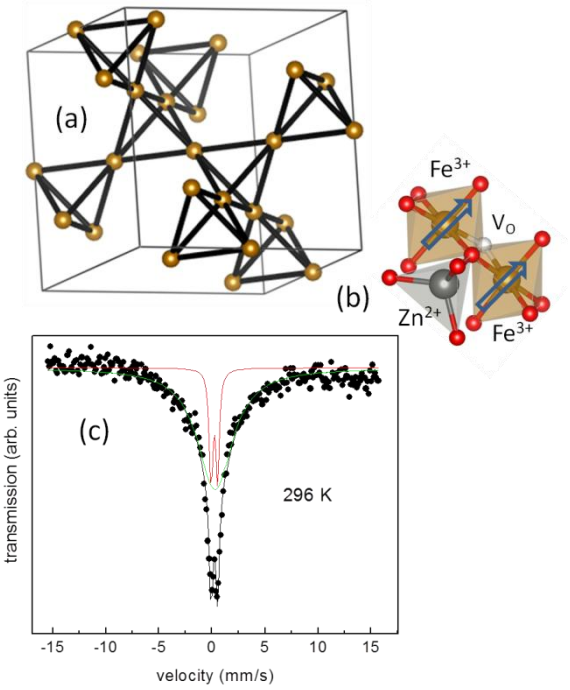

Fig. 1 (a) Lattice of corner-sharing tetrahedra formed by iron ions at B-sites of the spinel structire, (b) Ferromagnetic coupling proposed for iron ions at B-sites mediated by an oxygen vacancy Vo, (c) Mössbauer spectrum of inverted $ZnFe_2O_4$.

[1] K. Kamazawa et al., Phys. Rev. B 68 (2003) 024412
[2] H. Mamiya et al. Phys. Rev. B 90 (2014),014440.
[3] C. E. Rodríguez Torres et al, Phys. Rev. B 89, (2014) 104411; K. L. Salcedo Rodríguez et al., J. Alloys & Comp. 752, (2018) 289

Precise Determination of Hyperfine Interaction and Second-order Doppler Shift in ^{149}Sm Mössbauer Transition

S. Tsutsui

Japan Synchrotron Radiation Research Institute (JASRI), SPring-8, Sayo, Hyogo, Japan
(satoshi@spring8.or.jp)

Recent developments of nuclear resonant scattering techniques enable us to carry out various measurements using Mössbauer effect. In nuclear resonant scattering experiments, various natures of synchrotron radiation (SR) sources such as energy tunability, intense X-ray pulse and good collimation, are applicable to various measurements based on Mössbauer effect. SR-based Mössbauer spectroscopy, one of the recent developments, enables us to investigate hyperfine interactions using energy-domain Mössbauer spectra in many Mössbauer isotopes [1].

SR-based Mössbauer spectroscopy allows us to measuring Mössbauer spectra whose horizontal (vertical) axis is Doppler velocity (photon counts) like energy-domain spectra measured with radioactive sources but unlike time-domain spectra of nuclear resonant forward scattering, although Mössbauer nuclei are excited by SR sources. One of the advantages of SR-based Mössbauer spectroscopy to the experiments using radioactive sources is possibility of observing spectra in Mössbauer isotopes whose source is difficult or impossible to be prepared with nuclear reactions. In addition, intense X-ray pulse and its good collimation, which are natures of SR sources, allow us to precise measurements of hyperfine interactions using Mössbauer effects. In the present work, we have perform precise determination of hyperfine interactions through the ^{149}Sm Mössbauer transition.

Sm is known as an important element which consists of permanent magnets. For recent times, Sm is an attractive element in solid state physics such as valence fluctuating and heavy fermion compounds as well. In both cases, valence state of Sm atoms is an important parameter to discuss the physical properties in Sm compounds, because its ground state of trivalent (divalent) state is magnetic (nonmagnetic). Particularly, recent discovery of unconventional heavy fermion compounds, which are insensitive to magnetic field unlike conventional heavy fermion compounds, makes valence degrees of freedom an important parameter to consider origin of their heavy fermion behaviors [2, 3].

The ^{149}Sm Mössbauer transition is observed in the M1 transition of 22.51 keV between the ground state of I_{gd} = 7/2 and the excited state of I_{ex} = 5/2. Because of small difference of nuclear radius between the ground and excited states and small nuclear quadrupole moments in both ground and excited states, expected changes of hyperfine interactions, especially those of isomer shift and nuclear quadrupole interaction, are small. For example, the difference in the isomer shift values between Sm^{2+} and Sm^{3+} states is nearly equal to the natural linewidth (2Γ) in the ^{149}Sm Mössbauer transition. Therefore, precise determination of isomer shifts and nuclear quadrupole interactions are required in order to discuss electronic states in Sm compounds.

Change of natural linewidths in Mössbauer transitions are difficult in conventional Mössbauer spectroscopy using radioactive source. In addition, uncertainty of Doppler velocity due to beam divergence is not negligible because nuclear γ-rays are emitted isotropically from radioactive sources. Meanwhile, narrowing resonant linewidth and reducing uncertainty of Doppler velocity due to beam divergence are possible in SR-based Mössbauer spectroscopy: resonant linewidth become narrower than natural linewidth in principle when detection time window is chosen appropriately [4]; uncertainty of Doppler velocity is much smaller than measurements using radioactive sources because beam divergence of SR source is small.

Precise determination of hyperfine interactions in the ^{149}Sm Mössbauer transition has been performed using some of advantages in SR-based Mössbauer spectroscopy in the present work. Effects of the operation mode in SPring-8 and detection time window on the resonant linewidth have been investigated. These help determination of Sm valence states through isomer shift values in valence fluctuating Sm intermetallic compounds. Furthermore, second-order Doppler shift is also successfully observed by precise measurement using the effects of the operation mode and detection time window [5].

[1] M. Seto *et al*., Phys. Rev. Lett. 102 (2009) 217602.
[2] S. Sanada *et al*., J. Phys. Soc. Jpn. 74 (2005) 246.
[3] R. Higashinaka *et al*., J. Phys. Soc. Jpn. 80 (2011) 093703.
[4] M. Seto *et al*., J. Phys.: Conf. Ser. 217 (2010) 012002.
[5] S. Tsutsui *et al*., Hyperfine Int. **238**, 100 (2017).

Prussian Blue Analogues Derivated Multi-Metal Oxides/Nitrides as Fenton-Like Catalysts for the Degradation of Organic Pollutants and its Mechanism

X. Li and J. Wang

Mössbauer Effect Data Center, Dalian Institute of Chemical Physics, Chinese Academy of Sciences, Dalian 116023, China (wangjh@dicp.ac.cn)

Advanced oxidation processes (AOPs: including photocatalysis, catalytic wet oxidation, Fenton and Fenton-like reaction) are a set of chemical treatment procedures designed to remove organic pollutants through reacting with hydroxyl radicals (•OH). Among them, Fenton-like reaction is appealing since it can in-situ product large amount of highly reactive •OH and SO_4•$^-$ to degrade organic compounds with a high mineralization rate. Until now, efficient catalysts with high activity and stability are highly desired. In addition, limited mechanism understanding hinders any significant advances in Fenton chemistry.

In this study, we developed Prussian blue analogues (PBAs) derivated multi-metal nitrides (oxides) with controlled morphology, and investigated their performances in catalytic activation H_2O_2/PMS based on Fenton-like reactions for the removal of organic pollutants. Mössbauer technique was applied to investigate the mechanism of these Fenton-like reactions, as well as the structure-function relationships between the catalysts and their activities.

$Fe_xCo_{3-x}O_4$ nanocages derivated from Fe-Co PBAs were developed as excellent catalysts for removal of bisphenol A (BPA) by activation of peroxymonosulfate (PMS) [1]. Bimetallic Fe_xCo_y@C nanocages were synthesized via a one-step thermal decomposition of Fe_yCo_{1-y}-Co PBAs nanospheres in nitrogen atmosphere at different temperatures and developed as Fenton-like catalysts to activation PMS for BPA removal [2]. A novel strategy based on a one-step thermal decomposition of MOFs in N_2 atmosphere was developed for shape-controlled synthesis of graphene encapsulated transition metal nitrides (TMNs) ($Fe_xMn_{6-x}Co_4$-N@C). The catalytic oxidation performance of the as-synthesized $Fe_xMn_{6-x}Co_4$-N@C nano-dices in BPA degradation by PMS activation was found largely enhanced with the increasing of the content of Mn_4N [3].

[1] X. Li, Z. Wang, B. Zhang, A.I. Rykov, M. A. Ahmed, J. Wang, *Appl. Catal. B*, **2016**, 181, 788-799.
[2] X. Li, A.I. Rykov, B. Zhang, Y. Zhang, J. Wang, *Catal. Sci. Technol.*, **2016**, 6, 7486-7494.
[3] X. Li, Z. Ao, J. Liu, H. Sun, A.I. Rykov, J. Wang, *ACS Nano*, **2016**, 10, 11532-11540.

Epitaxial Strain Adaption Mechanisms in FeRh Thin Films Probed by Mössbauer Spectroscopy and Nuclear Inelastic Scattering

R. Witte[a], R. Kruk[a], D. Wang[a], M. E. Gruner[b], R. A. Brand[a,b], H. Wende[b] and H. Hahn[a]

[a]*Institute of Nanotechnology, Karlsruhe Institute of Technology, 76344 Eggenstein-Leopoldshafen, German*
[b]*Faculty of Physics and Center for Nanointegration Duisburg-Essen, University Duisburg-Essen, 47048 Duisburg, Germany (ralf.witte@kit.edu)*

Recently we reported on an adaptive nano-twinned structure observed in FeRh thin films [1]. The first part of the presentation will elucidate how this adaptive nanostructure is obtained by an epitaxial strain-induced martensitic transformation in thin films of a chemically (substitutionally) disordered FeRh alloy. The epitaxial strain is applied via the growth of the FeRh thin film on a W-buffer layer (+6% epitaxial mismatch). Along with the martensite transformation an unexpected suppression of magnetic order is observed in the epitaxial thin films.

Evidence for epitaxial and fully strained growth is provided by X-ray diffraction (XRD) measurements, while the magnetic properties are studied employing conversion electron ^{57}Fe Mössbauer spectroscopy (CEMS) measurement and SQUID magnetometry. Extensive XRD measurements and transmission electron microscopy (TEM) reveal that the lowering of symmetry (from cubic to tetragonal) imposed by the epitaxial relation leads to a further, unexpected, tetragonal-to-orthorhombic transition.

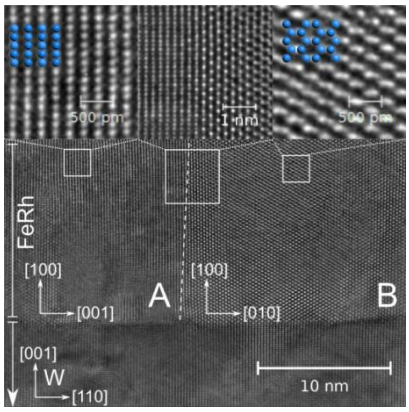

Fig. 1 High resolution TEM cross-sectional view of the multilayer. Two 90° oriented nano-twins are identified in the FeRh thin film [1].

The resulting orthorhombic phase (spacegroup *Cmcm*) forms a finely twinned nanostructure in order to adapt to the lattice constant of the W buffer-layer below, similar to the nano-twinned martensites observed in FePd [2]. This is illustrated by the high-resolution TEM cross-sectional micrograph shown in Fig. 1, featuring two epitaxial 90° oriented (in-plane) grains of about 15 nm size. The transformation together with the microstructural arrangement displays thus a strain-adaption mechanism of the material.

First principle calculations indicate that the transition is triggered by a band-Jahn-Teller type mechanism as shown by the disappearance of a peak-like feature in the Rh-density-of-states (DOS) at the Fermi level upon the transition (see Fig. 2) taken from [1]), similar to lattice instabilities in other intermetallics (e.g. FePd [3]). The combination of a specific shuffling of atomic planes with the disappearance of peak-like structures in the DOS is reminiscent of nesting-induced electron-phonon coupling and phonon softening.

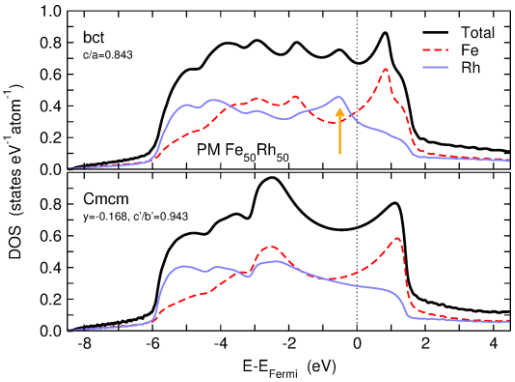

Fig. 2 Calculated electronic DOS for the tetragonal distorted bct and the Cmcm phase. The feature in the Rh-DOS (arrow) has clearly disappeared in the Cmcm case [1].

In the second part recent measurements of the Fe partial phonon density of states by nuclear inelastic scattering will be presented, which provide first evidence for a change in phonon spectra upon the structural transition. Moreover by varying the Fe-Rh composition thin films in different structural states were synthesized. The observed composition dependent strain-adaption behaviour and the resulting phonon spectra will be discussed with reference to the equilibrium phase diagram and the known metastable phases in the Fe-Rh alloy system.

We acknowledge funding by the DFG, contract HA-1344. Allocation of beamtime at the ESRF is gratefully acknowledged, as well as expert scientific support from the ID18 beamline stuff: R. Rüffer, A. I. Chumakov and D. Bessas.

[1] R. Witte et al., PRB 93, (2016) 104416.
[2] S. Kauffmann-Weiss et al., PRL 107, (2011) 206105.
[3] Buschbeck et al., PRL 103, 216101 (2009).

In-Beam Mössbauer Spectra of ^{57}Mn Implanted into Ice

Y. Yamada[a], Y. Sato[a], Y. Kobayashi[b,c], M. Mihara[d], M. K. Kubo[e], W. Sato[f], J. Miyazaki[g], T. Nagatomo[c], S. Tanigawa[b], D. Natori[b], J. Kobayashi[d], S. Sato[h] and A. Kitagawa[h]

[a] *Department of Chemistry, Tokyo University of Science, Shinjuku, Tokyo 162-8602, Japan*
[b] *Graduate School of Engineering Science, University of Electro-Communications, Chofu, Tokyo182-8585, Japan*
[c] *Nishina Center for Accelerator-Based Science, RIKEN, Wako, Saitama 351-0198, Japan*
[d] *Graduate School of Science, Osaka University, Toyonaka, Osaka 560-0043, Japan*
[e] *Division of Arts and Sciences, International Christian University, Mitaka, Tokyo 181-8585, Japan*
[f] *Institute of Science and Engineering, Kanazawa University, Kanazawa, Ishikawa 920-1192, Japan*
[g] *Faculty of Pharmaceutical Sciences, Hokuriku University, Kanazawa, Ishikawa 920-1180, Japan*
[h] *National Institute of Radiological Science, Inage, Chiba 263-8555, Japan*
(yyasu@rs.kagu.tus.ac.jp)

In-beam Mössbauer spectroscopy using short-live nuclei is a very powerful tool to investigate a local structure of a solid. Behavior of Fe atom in ice has attracted a basic interest for a long time in relation with solvation of Fe in water. Mössbauer studies of Fe in ice had been reported, in which hexaquo ferrous ions, $Fe(H_2O)_6^{2+}$, are trapped in the ice lattice [1]. It was reported that Fe^0 atoms form HFeOH species on the surface of ice [2]. In this study, ^{57}Mn atoms were implanted into a solid ice, and the in-beam Mössbauer spectra were measured to study the position and the chemical state of Fe in ice.

The experiment was performed using the heavy ion synchrotron accelerator facility (HIMAC) at the National Institute of Radiological Science (NIRS). The ^{57}Mn nuclei were produced by a projectile fragmentation reaction of the primary beam of ^{58}Fe ions and a target of ^{9}Be. A beam pulse of 1.2×10^6 particles was generated at 0.3 Hz with 250 ms duration. A parallel-plate avalanche counter (PPAC) was employed as a detector, and high-quality spectra were obtained by the anti-coincidence method [3]. A cell equipped with a polyimide film window was filled with water and was fitted onto a cryostat. The ice sample was cooled down using a vibration-isolated pulse-tube helium refrigerator. In-beam Mössbauer spectra of ^{57}Mn implanted into ice were measured at 13, 77, and 150 K.

The Mössbauer spectra measured at 13 K (Fig. 1) showed two sets of doublets. The major doublet (I) corresponded to Fe^{2+} species, but its ΔE_Q value was obviously smaller than that of $Fe(H_2O)_6^{2+}$ in ice (ΔE_Q = 3.46 mm/s at 77 K) reported in the literature [1]. This species was assigned to Fe^{2+} ion trapped in a vacancy of the lattice of the ice, which has smaller coordination number than six. The doublet (I) was also observed in the Mössbauer spectra observed at 77 and 150 K, while the intensity decreased with increasing the temperature of the sample because of the decrease of a recoil-free fraction. Another component (II) had smaller ΔE_Q value; the large change of the value was observed with varying the temperature. This species might change the trapping site depending on the temperature. Density functional calculations are now in progress to make the reasonable assignments of the species.

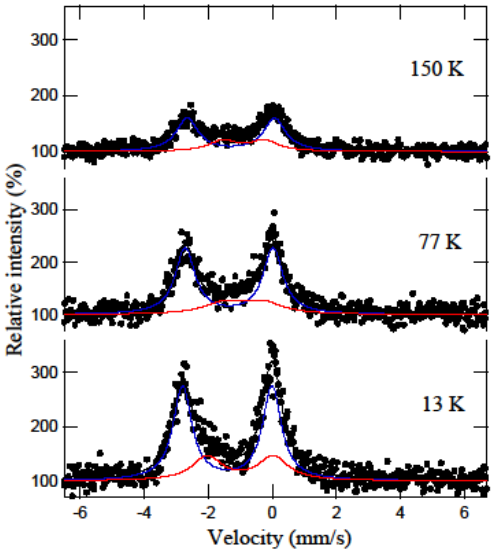

Fig. 1 In-beam Mössbauer spectra of ^{57}Fe implanted into ice. The temperatures of the sample are indicated in the figure.

Table 1 Mössbauer parameters of ^{57}Fe implanted into ice

Temp. K		δ mm/s	ΔE_Q mm/s	Γ mm/s	Int.
150	I	-1.29(2)	2.73(3)	0.83(5)	71%
	II	-0.90(6)	1.3(1)	1.1(2)	29%
77	I	-1.35(1)	2.74(2)	0.74(4)	75%
	II	-0.90(9)	1.2(2)	1.4(5)	25%
13	I	-1.41(1)	2.80(3)	0.71(4)	71%
	II	-1.00(8)	2.1(2)	1.1(2)	29%

[1] J. Nozik, M. Kaplan, *J. Chem. Phys.* 47(8) (1967) 2960-2977.
[2] G. S. Parkinson, Y.K. Kim, Z. Dohnalek, R.S. Smith, B.D. Kay, *J. Phys. Chem.* C 113 (2009) 4960-4969.
[3] T. Nagatomo, Y. Kobayashi, M.K. Kubo, Y. Yamada, M. Mihara, W. Sato, J. Miyazaki, S. Sato, A. Kitagawa, *Nuclear Instruments and Methods in Physics Research* B 269 (2011) 455-459.

Mössbauer Spectroscopy and Magnetization Measurements of Spleen and Liver Tissues from Patients with Some Hematological Malignant Diseases

I.A. Alenkina[a], A.V. Vinogradov[b,c], I. Felner[d], E. Kuzmann[e], T.S. Konstantinova[c], V.A. Semionkin[a] and M.I. Oshtrakh[a]

[a]*Department of Experimental Physics, Institute of Physics and Technology, Ural Federal University, Ekaterinburg, 620002, Russian Federation*
[b]*Sverdlovsk Regional Ministry of Health, Weiner str., 34b, Ekaterinburg, 620014, Russian Federation*
[c]*Sverdlovsk Regional Clinical Hospital No 1, Volgogradskaya str., 185, Ekaterinburg, 620102, Russian Federation;*
[d]*Racah Institute of Physics, The Hebrew University, Jerusalem, 91904 Israel*
[e]*Laboratory of Nuclear Chemistry, Institute of Chemistry, Eötvös Loránd University, Budapest, Hungary*
(alenkina-ira@mail.ru)

Large amounts of iron in mammalians can be found in iron-storage proteins (ferritin and hemosiderin) in spleen and liver tissues. Ferritin molecule consists of a nano-sized ferrihydrite ($5Fe_2O_3 \times 9H_2O$) core (up to 8 nm) inside of the protein shell (initially apoferritin). Hemosiderin can be considered as denatured ferritin. The structural peculiarities of the iron core in ferritin were extensively studied using various physical techniques. Nevertheless, its exact structure has not been agreed yet. Moreover, it is well accepted, that different conditions of organism development, especially some diseases, influence: (i) the iron core formation, resulting in variations in the iron core structure regarding the number of iron ions and the core size, (ii) variations in the core crystallinity, (iii) variations in number of different core regions, (iv) in the FeOOH packing, etc.

The presence of ferritin in tissues especially spleen and liver allows application of Mössbauer spectroscopy and magnetization measurements to study the iron state in these tissues. In this case both physical techniques provide important information about the iron core structure. Based on ^{57}Fe hyperfine parameters, magnetic moment and its behavior, quantitative and qualitative variations of the iron status in these tissues from various healthy donors and patients can be studied.

In the present work we discuss the results obtained from Mössbauer spectroscopy and magnetization measurements on spleen and liver tissues from: healthy donors (NOR), patients with acute myeloid leukemia (AML), non-Hodgkin B-cells mantle cell lymphoma (MCL), marginal zone B-cell lymphoma (MZL) and primary myelofibrosis (PMF).

Magnetization measurements performed on different tissue samples showed similar behavior. All samples contained paramagnetic and ferrimagnetic components embedded in diamagnetic matrices. The ferrimagnetic component can be associated with the presence of magnetite (Fe_3O_4) in the range 920–150 ppm estimated on the basis of determination of the saturation magnetic moment. Two liver samples NOR and AML demonstrated unusual magnetic behavior where the field-cooled curve crossed the zero-field-cooled curve in the temperature range of ~40–70 K (the first observation for AML liver was given in [1]).

Mössbauer spectra of the studied samples were measured at room temperature and at 20 K. The fit of the 295 K spectra was performed in terms of simple heterogeneous iron core model [2] considering only 2 quadrupole doublets with equal line width. Small variations of Mössbauer hyperfine parameters as well as variations of some more or less close-packed FeOOH regions in the core were considered for ferritin-like iron in spleen and liver tissues from healthy donors and patients. The largest amount of ferritin-like iron was observed in spleen from patient with PMF. Therefore, measurements of spectra of this sample, as well as of some other tissues having larger ferritin-like iron content, were performed at 20 K in order to check the presence of relaxation effects. The obtained results demonstrated that the cores in ferritin molecules in spleen from patient with PMF and in liver from patients with AML and MCL contained slightly larger amount of iron ions, while the number of ferritin molecules was larger than those in other tissues. The largest number of ferritin molecules in PMF spleen may be related to physiopathology of disease [3].

This work was supported by the Ministry of Education and Science of the Russian Federation (the Project # 3.1959.2017/4.6) and Act 211 of the Government of the Russian Federation, contract № 02.A03.21.0006.

[1] I. Felner, I.V. Alenkina, A.V. Vinogradov, M.I. Oshtrakh, J. Mag. Mag. Mat. 399 (2016) 118.
[2] I.V. Alenkina, M.I. Oshtrakh, I. Felner, A.V. Vinogradov, T.S. Konstantinova, V.A. Semionkin, AIP Conf. Proc., AIP Publishing, Melville, New York, 1781 (2016) 020010.
[3] M.I. Oshtrakh, I.V. Alenkina, A.V. Vinogradov, T.S. Konstantinova, E. Kuzmann, V.A. Semionkin, Biometals 26 (2013) 229.

On the Asymmetry of Fe-on-Ti and Ti-on-Fe Interfaces

J. Balogh, L. Bujdosó and D. Kaptás

Institute for Solid State Physics and Optics,Wigner RCP, Budapest P.O.Box 49, Hungary
(balogh.judit@wigner.mta.hu)

The asymmetry of the Fe-on-Ti and Ti-on-Fe interfaces has been revealed [1] both experimentally by Mössbauer spectroscopy (MS) and x-ray reflectometry (XRR) on Ti/Fe/Ti trilayers grown on Si(111) substrates by vacuum evaporation and by molecular dynamics (MD) simulations of layer growth on Fe or Ti underlayers of different orientations. The MD simulations show a concentration distribution along the layer growth direction which is atomically sharp at the Ti-on-Fe interface for the (001) and (110) crystallographic orientations of the Fe layer, while it varies over a few atomic layers for Fe(111) substrate and at the Fe-on-Ti interface for all basic crystallographic orientations of Ti. Conversion electron MS and XRR measurements are indicative of wider inter faces, but support the asymmetry in the width of the bottom and top interface of the Fe layer (Fe-on-Ti and Ti-on-Fe, respectively).

The asymmetry of the interfaces is also revealed by Fe-Ti-Ag multilayers with different sequence of the elemental layer. The room temperature spectra of two samples,

a.) Si/10nmAg/(15 nm Ti/1.5nm Fe/15nm Ag)$_4$
b.) Si/10nm Ag/(1.5nm Fe/15 nm Ti/15nm Ag)$_4$

are shown in Fig. 1.

The alloys formed at the interfaces are identified as amorphous Fe_xTi_{1-x}, which has Curie temperature below room temperature and bcc-Fe_xTi_{1-x} with high Ti concentration. The formation of these alloys at the Fe-on-Ti and Ti-on-Fe interfaces will be discussed and compared to the trilayer studies [1].

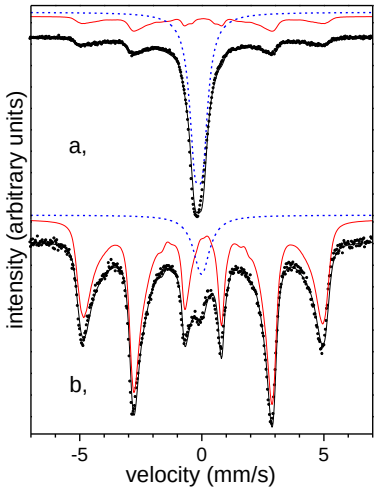

Fig. 1 Room temperature Mössbauer spectra of the Fe-Ti-Ag sample pair with different sequence of the layers, Ti/Fe/Ag (a) and Fe/Ti/Ag (b). Subspectra indicated by continuous and dashed lines belong to bcc-Fe_xTi_{1-x} and amorphous Fe_xTi_{1-x}, respectively.

[1] P. Süle, L. Bottyán, L. Bujdosó, Z. E. Horváth, D. Kaptás, A. Kovács, D.G. Merkel, A. Nakanishi, Sz. Sajti, J. Balogh, arXiv:1712.06870

Oxidation and Passivating Effect in Tin(II) Fluoride and Chloride Fluoride Solid Solutions: A ^{119}Sn Mössbauer Study

G. Dénès[a], A. Muntasar[a], M.C. Madamba[a] and H. Merazig[b]

[a] *Laboratory of Solid State Chemistry and Mössbauer Spectrocopy, Department of Chemistry and Biochemistry,Concordia University, 7141 Sherbrooke Street West, Montréal, Qc, H4B 1R6, Canada*

[b] *Unité de Recherche de Chimie de l'Environnement et Moléculaire Structurale CHEMS, Université des Frères Mentouri de Constantine, 25000 Constantine, Algeria*

(madenes@videotron.ca, georges.denes@concordia.ca)

Although divalent tin fluorides and chloride fluorides have quite a low recoil-free fraction, it is usually high enough to give a reasonably strong Mössbauer spectrum at ambient temperature. These compounds appear to be stable relative to oxidation to tetravalent tin at ambient temperature. Their X-ray diffraction pattern shows only the line of the tin(II) compound, however the ^{119}Sn Mössbauer spectrum of all the tin(II) polycrystalline samples has a small broad peak at ca. 0 mm/s. This is the case of polycrystalline α−SnF_2, even if prepared by grinding single crystals while the spectrum of a large single crystal polished sufficiently thin enough to allow the γ−ray beam through and to avoid giving rise to line broadening by saturation, shows only the tin(II) doublet, with no SnO_2 peak at 0 mm/s [1 & 2]. This shows that there is surface oxidation of each solid particle, to give a thin amorphous layer of SnO_2 stannic oxide. However, the Mössbauer peak of SnO_2 does not grow with prolonged exposure to air at ambient temperature, therefore it must be assumed that the layer of SnO_2 has a passivating effect and it prevents contact of the tin(II) compound to air, the same way as does a layer of paint, however oxidation increases at higher temperatures [3].

We have investigated in this work the passivating effect of a layer of SnO_2 in two types of solid solutions: (i) in the fluorite type $M_{1-x}Sn_xF_2$, the amount of tin at low *x* values is not sufficient to provide full coverage of the surface of the particles, and (ii) in the PbClF type doubly disordered solid solution, $Ba_{1-x}Sn_xCl_{1+y}F_{1-y}$ [4 & 5]. No crystalline SnO_2 was ever detected by X-ray diffraction in either type of solid solution. On the other hand, due to the very high recoil-free fraction of tin(IV) oxide, compared to that of tin(II) halides, and since Mössbauer spectroscopy is a local probe and it detects amorphous or nanocrystalline species as well as crystalline material, it allows the detection of very small amounts of SnO_2, regardless of crystallinity. In addition, the peak for tin(IV) bonded to oxygen (δ ≈ 0 mm/s) is very well separated from tin(II) peaks (δ ≈ 3-4 mm/s). $M_{1-x}Sn_xF_2$ solid solutions passivate well, despite the insufficient amount of tin to provide full coverage of the particles by SnO_2. On the other hand, passivation does not work as well for the $Ba_{1-x}Sn_xCl_{1+y}F_{1-y}$ and it is strongly dependent on the method of preparation and the mode of bonding, and also on the tin(II) recoil-free fraction. The solid solution prepared by precipitation passivates best, although not perfectly (fig. 1). When prepared by the dry method, covalently bonded tin(II) passivates best, and the lower the tin(II) recoil-free fraction, the faster tin(II) is oxidized to tin(IV).

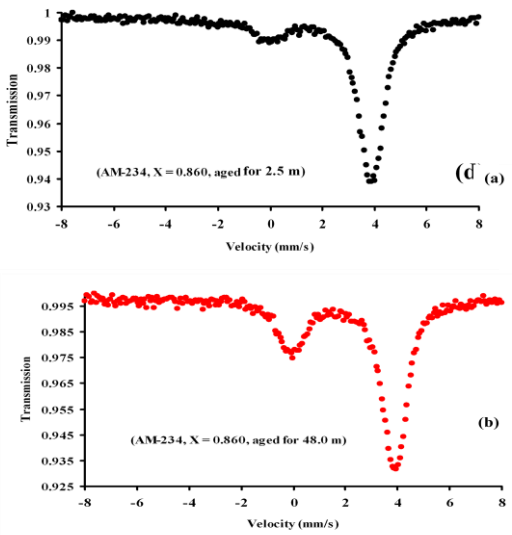

Fig. 1 Ambient temperature ^{119}Sn Mössbauer spectra of "young" (a) and "aged" (b) $Ba_{1-x}Sn_xCl_{1+y}F_{1-y}$ barium tin(II) chloride fluorides obtained by precipitation (age *m* in months) of (AM-234, X = 0.860, Ba → Sn): (a) 2.5 *m*, (b) 48.0 *m*.

This presentation is dedicated to the memory of Prof. Krzysztof Ruebenbauer (1947-2018).

[1] T. Birchall, G. Dénès, K. Ruebenbauer, J. Pannetier, J. Chem. Soc. Dalton (1981) 1831-1836.

[2] T. Birchall, G. Dénès, K. Ruebenbauer, J. Pannetier, J. Chem. Soc. Dalton (1981) 2296-2299.

[3] G Dénès, A. Laou, Hyperf. Interac. **92** (1994), 1013-1018.

[4] G. Dénès, M. Muntasar, Hyperf. Interac. **153** (2004), 91-119.

[5] G. Dénès, M. Muntasar, M.C. Madamba, H. Merazig, Mössbauer Spectroscopy: Applications in Chemistry, Biology and Nanotechnology, **ed. 1** (2013) 202-246.

Characterisation of Nanomagnetites Co-Precipitated in Inert Gas Atmosphere for Plant Nutrition

A. Lengyel[a,b], Z. Homonnay[a], K. Kovács[a], Z. Klencsár[c], Sz. Németh[a], R. Szalay[a], V. Kis[c], Á. Solti[d], F. Fodor[d], M. Ristić[e], S. Musić[e] and E. Kuzmann[a]

[a]*Institute of Chemistry, Eötvös University, Budapest, Hungary*
[b]*Wigner Research Centre for Physics, HAS, Budapest, Hungary*
[c]*Centre for Energy Research, HAS, Budapest, Hungary*
[a]*Institute of Biology, Eötvös University, Budapest, Hungary*
[e]*Ruđer Bošković Institute, Zagreb, Croatia*
(homonnay@caesar.elte.hu)

Our future aim is to ascertain the effects of selected nanoparticles on plants of agricultural importance. In the future study we intend (a) to prepare the nanoparticles containing iron and (b) to obtain data about iron metabolism in the plant(s) and (c) to propose different iron utilization strategies in agriculture. In this sense the experiments involving the plants grown in hydroponics or soil conditions will be conducted. In our previous work [1] we reported about iron(III)-oxyhydroxide and non-stoichiometric magnetite nanoparticles with the aim to use them as possible nutrition source for plants. ^{57}Fe Mössbauer spectra of magnetite nanoparticles synthesized under different preparation conditions at ambient atmosphere showed that the magnetite nanoparticles are highly oxidized.

In order to obtain more efficient magnetite nanoparticles with higher Fe^{II} content, magnetite nanoparticles were prepared in N_2 gas atmosphere. The chemical co-precipitation method was utilized, starting with stoichiometric ratio of $FeSO_4$ and $FeCl_3$ solutions for magnetite formation. Then, ammonia solution was slowly and continuously added to the iron salts solution. After the reaction was completed, the precipitates were filtered, washed several times with deionized water and lyophilized. Citric acid coated nanoparticles were also prepared similarly, but adding the citric acid dissolved in deionized water before the addition of ammonia solution.

^{57}Fe Mössbauer spectra (Fig. 1) of washed and lyophilized nanomagnetite prepared in inert gas atmosphere undoubtedly indicated the presence of considerable fraction of Fe^{II}, close to the stoichiometric magnetite composition, both at room temperature (RT) and at 80K. XRD pattern of the same sample corresponded to nanomagnetite crystal structure. Mössbauer spectra in Fig. 1 also showed that after lyophilization the unwashed citric acid coated samples contained some Fe^{II} which disappeared when the sample was washed before lyophilisation. The washed samples, however, showed a poorly crystalline character.

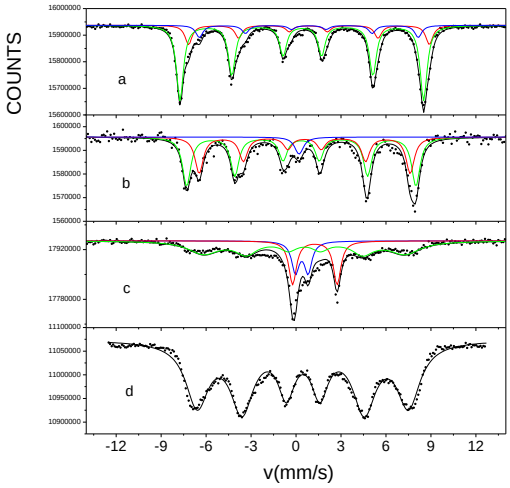

Fig. 1 ^{57}Fe Mössbauer spectra of liophylized washed nano magnetite recorded at 80K (a) and at 295 K (b) and liophylized non-washed (c) and washed (d) citric acid coated nano iron oxides recorded at 80 K.

The samples are intended to be subject to tests using them as possible nutrition source for plants.

Financial support from the National Research, Development and Innovation Office - NKFIH/OTKA (K115913 and K115784) and Hungarian-Croatian Intergovernmental S & T (No. TET 16-1-2016-0002) is gratefully acknowledged.

[1] Z. Homonnay, Gy. Tolnai. F. Fodor, A. Solti, K. Kovács, E. Kuzmann, A. Ábrahám. E. Gy. Szabo, P. Németh, L. Szabo, Z. Klencsár, Hyperfine Interact (2016) 237:127

Chemical Structure and Visible-Light Activated Photocatalytic Effect of Iron-containing Glass Prepared from Slag

Y. Katayama[a], S. Ishikawa[a], K. Akiyama[a], S. Nemeth[b], E. Kuzmann[b], T. Homonnay[b], S. Krehula[c], M. Ristić[c], S. Musić[c], K. Nomura[a] and S. Kubuki[a]

[a]*Graduate School of Science, Tokyo Metropolitan University, Minami-Osawa 1-1, Hachi-Oji, Tokyo 192-0397, Japan*
[b]*Institute of Chemistry, Eötvös Loránd University, 1117 Pázmány P.s.1/A Budapest, Hungary*
[c]*Division of Materials Chemistry, Ruđer Bošković Institute, P.O. Box 180, HR-10002, Zagreb, Croatia*
(katayama-yuka2@ed.tmu.ac.jp)

In recent years, disposal of general garbage exhausted from households is one of the serious environmental problems. Ishikawa *et al.* reported that iron-containing glass ceramics prepared from household waste slag denoted as Slag + $10Na_2O$ + xFe_2O_3 (SlagNaFe*x*) showed photocatalytic effect under visible-light irradiation after the samples were heat treated at 800 °C for 100 min. It was turned out that the photocatalytic effect of SlagNaFe*x* after heat treatment is closely related to the precipitated amount of α-Fe_2O_3 nanoparticles [1]. In this study, a relation between chemical structure of Fe and photocatalytic effect of Slag + xFe_2O_3 (SlagFe*x*, x = 0, 5, 10 in mass%) was investigated by means of Mössbauer spectroscopy, XRD, UV-Vis and ESI-MS.

SlagFe*x* was prepared by conventional melt-quenching method. Mixture of slag collected from Tamagawa incineration plant and Fe_2O_3 was placed in a platinum crucible, and was melted at 1400 °C for 1 h in the electric furnace. Dark brown samples were obtained by dipping the bottom of the crucible in ice. Each sample was heat-treated at 800 °C for 100 min or 1000 min after being purverized. Photocatalytic activity of SlagFe*x* before and after heat treatment was evaluated by soaking 40 mg of the powdered samples into 20 mL methylene blue (MB) aqueous solution with the concentration of 20 μmol/L. The MB concentration and decomposition products were detremined by UV-Vis and ESI-MS, respectively. ^{57}Fe Mössbauer spectra (^{57}FeMS) were recorded by constant acceralation method at both room temperature and 80 K, using ^{57}Co(Rh) and α-Fe as a source and a reference. X-ray diffraction (XRD) patterns were obtained between 2Θ of 10 and 80 °, by using Cu-K_α rays (λ = 0.1541 nm).

As shown in Fig. 1, MB concentration in aqueous solution decreased when it was reacted with SlagFe*x* under the visible-light irradiation. The largest first-order rate constant, k of 1.3×10^{-3} min^{-1} was recorded for SlagFe5 after heat treatment at 800 °C for 100 min. According to ESI-MS the MB solution after the degradation test showed a peak at m/z of 257, indicating that MB was decomposed into Azure A.

XRD patterns of heat-treated SlagFe*x* showed that the peaks assinged to iron oxides (Fe_3O_4 and γ-Fe_2O_3) and $CaFeAlSiO_6$. ^{57}Fe MS of heat treated SlagFe*x* measured at 80 K (Fig. 2) are composed of magnetically relaxated of sextets and doublet peaks of Fe(III). The doublet with quadrupole splitting of 1.00 mms^{-1} and isomer shift of 0.46 mm s^{-1} are assinged to paramagnetic $CaFeAlSiO_6$ and the another doublet to superparamagnetic component, γ-Fe_2O_3. In comparison with previous study, SlagFe*x* showed relatively smaller photocatalytic effect than SlagNaFe*x* containing Na [1]. It is concluded that the smaller nanoparticles of γ-Fe_2O_3 precipitated in SlagFe*x* is effective to promote photocatalytic effect under visible-light irradiation.

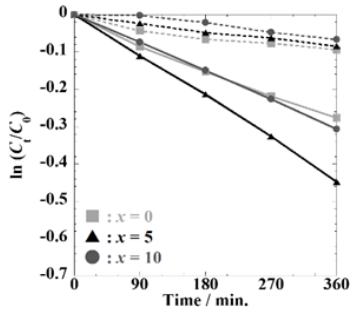

Fig.1 ln C_t/C_0 vs. t plot of MB degradation test carried out under the visible light (solid line) and in the dark (dotted line) using SlagFe*x* heat ` at 800 °C for 100 min.

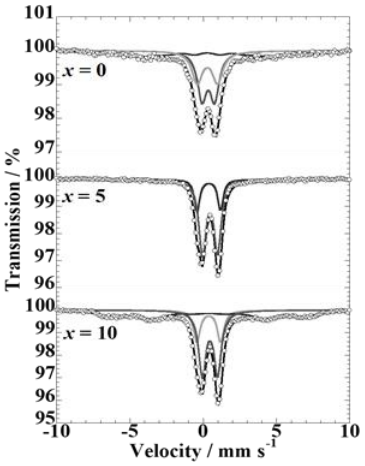

Fig.2 ^{57}Fe Mössbauer spectra measured at 80 K of SlagFe*x* heat treated at 800 °C for 100 min.

[1] S. Ishikawa et al., Pure and Applied Chemistry, 89, 535-544 (2017).

Relationship between Structure and Electrical Conductivity of Tin Phosphate Containing Vanadate Glass Ceramics

Y. Kobayashi[a], S. Shiba [a], K. Akiyama[a], K. Nomura[a] S. Kubuki[a] and T. Nishida[b]

[a]*Graduate School of Science, Tokyo Metropolitan University, Minami-Osawa 1-1, Hachi-Oji, Tokyo 192-0397, Japan*
[b]*Faculty of Humanity-oriented Science and Engineering, Kindai University, kayanomori 11-6, Iizuka, Fukuoka 820-8555, Japan*
(kobayashi-yuta@ed.tmu.ac.jp)

Vanadate glasses are known to a semiconductor caused by electron hopping from V^{4+} to V^{5+}. They are expected as cathode materials for secondary battery due to relatively high electrical conductivity, amorphous structure and various oxidation states of vanadium[1],[2]. In our previous study, sodium containing phosphovanadate glasses were prepared and applied to cathode materials for Na-ion batteries. In this study, sodium tin phosphovanadate glasses with the composition of yNa$_2$O•x(PO$_{5/2}$•SnO$_2$)•(100-2x-y)V$_2$O$_5$ (abbreviated as Na$_y$(PSn)$_x$V$_{100-2x-y}$; x= 5, 7.5, 10 mol% y=0, 5, 10 mol%) was prepared, and relationship between the local structure and electrical property was investigated.

At first, tin phosphate glass with the composition of 50PO$_{5/2}$•50SnO$_2$ (PSn) was prepared by sol-gel method. Next, Na$_y$(PSn)$_x$V$_{100-2x-y}$ was synthesized by melting the mixture composed of prepared PSn, Na$_2$CO$_3$ and V$_2$O$_5$ at 1200 ^{o}C for 1 hour and quenching in ice water. The structure of prepared samples was analysed by X-ray diffraction (XRD) and ^{119}Sn-Mössbauer spectroscopy (^{119}SnMS). XRD patterns were obtained between 2θ of 10 and 80 ^{o}, by using Cu-K$_\alpha$ rays (λ = 0.1541 nm). ^{119}SnMS were recorded at room temperature using ^{119m}Sn and BaSnO$_3$ as a source and a reference, respectively. Electrical conductivity (σ) was measured by a dc four-probe method, recording the voltage by changing the electrical current from 0 to 20 μA.

Fig. 1 shows XRD patterns of Na$_y$(PSn)$_x$V$_{100-2x-y}$ with 'y' of 0 and 5. Sharp peaks due to V$_2$O$_5$, NaV$_6$O$_{15}$ and SnO$_2$ were observed for almost all XRD patterns, indicating that prepared samples contained crystalline phases. With increase in PSn content, V$_2$O$_5$ and NaV$_6$O$_{15}$ phases decreased, and SnO$_2$ phases and amorphous phase (halo pattern) increased.

From the ^{119}SnMS of Na$_0$(PSn)xV$_{100-2x}$, it was found that isomer shift (δ) of 0.09-0.07 mm s^{-1} is almost constant and quadrupole splitting (Δ) of 0.50-0.45 mm s^{-1} decreases with increase in 'x' from 5 to 10, as shown in Fig. 2(a). Similar results were obtained for Na$_5$(PSn)$_x$V$_{95-2x}$. These results suggest that only Sn^{4+} is incorporated into the studied samples.

The conductivity (σ) of Na$_0$(PSn)xV$_{100-2x}$ showed 1.4×10^{-3} (x=5), 1.8×10^{-4} (x=7.5) and 4.3×10^{-5} S cm^{-1} (x=10). This indicates the decrease in σ with increase in 'x'.

On the other hand, σ of Na$_5$(PSn)$_x$V$_{95-2x}$ showed 1.7×10^{-2} (x=5), 4.3×10^{-3} (x=7.5) and 3.9×10^{-5} Scm^{-1} (x=10). From this, it was found that σ increases with increase in 'y' from 0 to 5 in Na$_y$(PSn)$_x$V$_{100-2x-y}$ with 'x' of 5 and 7.5. These results show that when Na is introduced into the tin phosphovanadate, σ increases due to the formation of vanadium bronze (NaV$_6$O$_{15}$) as shown in XRD patterns (Fig. 1 (b), top).

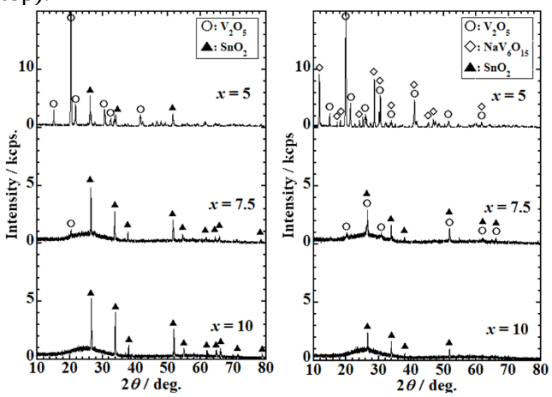

Fig. 1 X-ray diffraction patterns of Na$_y$(PSn)$_x$V$_{100-2x-y}$ with 'y' of (a) 0 (b) 5.

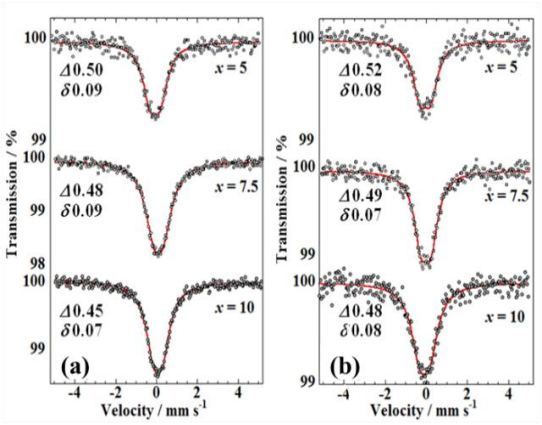

Fig. 2 ^{119}Sn Mössbauer spectra of Na$_y$(PSn)$_x$V$_{100-2x-y}$ with 'y' of (a) 0 and (b) 5.

[1] N. F. Mott, Adv. Phys., 16 [61] (1967) 49-144.
[2] T. Nishida et al., J. Radioanal. Nucl. Chem., 275[2] (2008) 417-422.

Effect of Arsenic on Iron Uptake and Distribution in Plants: A Mössbauer Spectroscopic Study

K. Kovács[a], Á. Solti[b], K. Ágostai[a] and F. Fodor[b]

[a] *Department of Analytical Chemistry, Institute of Chemistry, ELTE Eötvös Loránd University, Pázmány Péter lane 1/A, 1117 Budapest, Hungary*

[b] *Department of Plant Physiology and Molecular Plant Biology, ELTE Eötvös Loránd University, Pázmány Péter lane 1/C, 1117 Budapest, Hungary*

(kkriszti@caesar.elte.hu)

Arsenic is a nonessential, toxic element for plants. However, due to natural and anthropogenic pathways, arsenic is widely distributed in the environment and its accumulation in food crops may pose a health risk also for humans [1,2]. For this, many efforts are made to understand its metabolism in plants, especially in rice [2,3]. However, less is known on the possible effects of arsenic on the uptake of other essential elements, like iron.

In the present study, the influence of arsenic on the iron uptake of plants belonging to reduction based (strategy I) and complex forming (strategy II) iron uptake mechanisms was studied with the help of Mössbauer spectroscopy. Two model plants were chosen: cucumber (*Cucumis sativus*, strategy I model plant) and wheat (*Triticum aestivum*, strategy II model plant).

Plants were grown in aerated hydroponics (modified Hoagland solution), both in iron sufficient and iron deficient conditions. Arsenic was supplied as arsenate (AsO_4^{3-}) since this is the major form of arsenic at aerobic conditions. Arsenate was applied together with iron in the same concentration range. In the case of plants, grown without iron, arsenate was added only for the short-time iron treatment but at higher concentrations (100 and 500 μM). Iron was supplied as $^{57}Fe^{3+}$-citrate or $^{57}Fe^{2+}$-ascorbate complex. Roots of the plants were excised, stored and measured at liquid nitrogen temperature to avoid any changes in the chemical state of iron.

The Mössbauer spectra of the iron sufficient cucumber and wheat roots grown in the presence of arsenate showed no differences compared to those grown without arsenic. In the case iron deficient roots supplied with $^{57}Fe^{3+}$-citrate for 30 min at 100 μM or 500 μM concentration, the accumulation of a high spin Fe^{2+}-component was also found (Figure 1) which is in good agreement with previous results on strategy I plants [4]. This suggests no significant effect of arsenate on the iron reduction in a short-time range and was further confirmed with the iron reductase activity measurements, too.

In the case of $^{57}Fe^{2+}$-ascorbate supply, the oxidation of Fe^{2+} could be demonstrated which resulted in 50% Fe^{3+} of the total iron taken up by the root. The oxidation rate was found to be the same as without arsenate supply. No differences could be found in iron distribution of roots if arsenate (pre)treatment was performed only before the iron supply. In any cases, no sign of iron deposits on the root surface (iron plaque) could be observed.

The results indicate that the effects of arsenate may arise only after longer arsenic supply thus further experiments on this are planned in the next future.

This work was supported by Hungarian National Science Fund grants National Research, Development and Innovation Office – NKFIH PD 111979

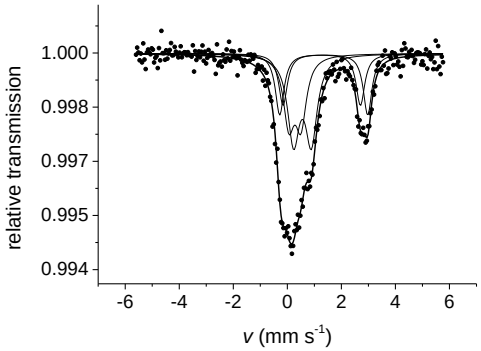

Fig. 1 Mössbauer spectrum of iron deficient cucumber root supplied with 500 μM $^{57}Fe^{3+}$-citrate for 30 min in the presence of arsenate (500 μM).

[1] F. J. Zhao, J. F. Ma, A. A. Meharg, S. P. McGrath, New Phytologist 181 (2009) 777-794.

[2] W. J. Liu, Y. G. Zhu, Y. Hu, P. N. Williams, A. G. Gault, A. A. Meharg, J. M. Charnock, F. A. Smith, Environ. Sci. Technol. 40 (2006) 5730-5736.

[3] N. Khan, B. Seshadri, N. Bolan, C. P. Saint, M. B. Kirkham, S. Chowdhury, N. Yamaguchi, D. Y. Lee, G. Li, A. Kunhikrishnan, F. Qi, R. Karunanithi, R. Qiu, Y. G. Zhu, C. H. Syu, Adv. Agr. 138 (2016) 1-96.

[4] K. Kovács, J. Pechousek, L. Machala, R. Zboril, Z. Klencsár, Á. Solti, B. Tóth, B. Müller, H. D. Pham, Z. Kristóf, F. Fodor Planta 244 (2016) 167-179.

Iron in Minerals of Boda Claystone Formation

K. Lázár[a] and Z. Máthé[b]

[a]*Department of Nucear Analysis, Research Centre for Energy Science, HAS, 29-33 Konkoly Thege Miklós street, 1121 Budapest, Hungary*
[b]*Mecsekérc Environmental Ltd, 19 Esztergár Lajos street, 7633 Pécs, Hungary*
(lazar.karoly@energia.mta.hu)

Boda Claystone Formation is an extended huge stone block located in ca. 10 x 20 km area with ca. 800 m average thickness in Mecsek mountains, SW of Hungary. The formation of the block was a long process, it started at the upper Permian and was finished in the lower Triassic period, principally by erosion of igneous basement rocks under arid, semi-arid conditions by sequential flooding and drying of a salty playa lake in mostly oxidizing atmosphere [1]. The conditions were periodically modified during the long diagenesis, different dominant rock types can be distinguished at various locations [2]. The main iron bearing clay minerals are illite, chlorite, hematite (rarely pyrite). The occurrence and proportions of ferric and ferrous iron are different in samples obtained from various regions. Certain aspects of the history of the formation can be followed by distinguishing the species of iron present in the minerals. Namely the process of the commencement of the formation of clay minerals can be tracked by analysing the type of constituting minerals (ferric or ferrous iron is incorporated). Furthermore later stages of diagenesis can also be evidenced (e.g. reduction before final consolidation), or occasional submergence of strata to deeper regions – experiencing higher temperature resulting larger extent of transformations in clay minerals.

The mentioned processes are illustrated in the Mössbauer spectra obtained on samples at different depth of a borehole (Fig. 1). In the sample representing the layer close to the surface (10.2 m) hematite is the dominant component, displaying additionally mostly ferric ions in illite and ferrous iron is only minor constituent. The situation is the opposite in 151.6 m depth, iron is present exclusively in ferrous form, in chlorite and pyrite. In strata of deeper regions (369.8 m) partial relocation and reduction of ferric ions to ferrous sites can be observed due to secondary processes and raised local temperatures.

In the presentation spectra obtained on several samples collected from various regions and depths of Boda Claystone will be interpreted, variations in the state of iron shall be compared with data of other methods (primarily X-ray diffraction), and the results will be discussed in the frame of possible transformations of clay minerals during secondary diagenetic processes.

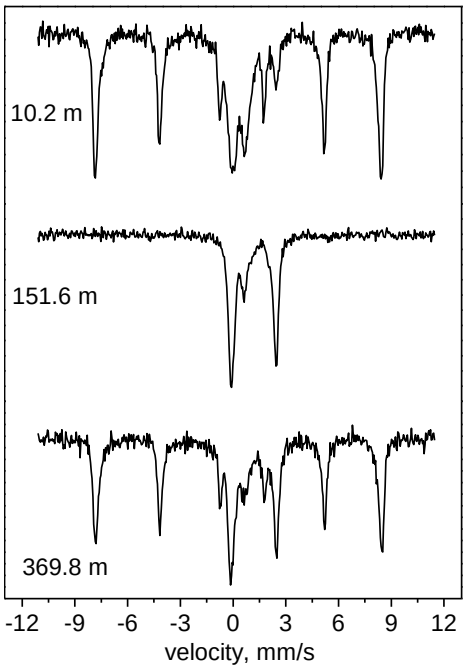

Fig. 1 Mössbauer spectra of samples obtained from different depths of borehole BAF-1 in Boda Claystone Formation

[1] A.R. Varga et al., Acta Geologica Hungarica, 48 (2005) 49.

[2] T. Németh et al., Open Geoscience, 8 (2016) 259.

^{57}Fe-Mössbauer and Magnetic Properties of Iron Oxide Nanoparticles in Silica Matrix Prepared by Sol-gel method

S. Morishita[a], K. Sunakawa[a], K. Akiyama[a], R. Higashinaka, T. D. Matsuda[a], Y. Aoki[a], T. Naka[b], T. Nakane[b], S. Krehula[c], M. Ristić[c], S.Musić[c], K. Nomura[a] and S. Kubuki[a]

[a]*Graduate School of Science, Tokyo Metropolitan University, Minami-Osawa 1-1, Hachi-Oji, Tokyo 192-0397, Japan*
[b]*National Institute of Materials Science, Sengen 1-2-1, Tsukuba, Ibaraki, 305-0047, Japan*
[c]*Division of Materials Chemistry, Ruđer Bošković Institute, P.O. Box 180, HR-10002, Zagreb, Croatia*
(morishita-sakura@ed.tmu.ac.jp)

In recent years, iron oxide nanoparticles have been interested in various applications, such as magnetic storage media, drug delivery, MRI contrast medium and hyperthermia. It is known that iron oxide nanoparticles are produced in the pores of the silica matrices, which is possible to control the size of iron oxide nanoparticles homogeniously, using sol-gel method[1]. In this study, iron oxide nanoparticles in amorphous silica matrix (Fe_2O_3 : SiO_2 = 40 : 60 in mass%, abbreviated as 40Fe60Si) were prepared by sol-gel method and investigated by powder X-ray diffractometry (XRD), transmission electron microscopy (TEM), ^{57}Fe Mössbauer spectroscopy at room temperature (^{57}Fe MS), and magnetic susceptibility.

Only a halo was detected from the XRD patterns of 40Fe60Si heat treated at 400 and 600 ^{o}C for 2 h. Based on the fringes of the observed TEM images, the averaged crystalline size of iron oxide nanoparticles in 40Fe60Si heat treated at 400 and 600 °C were estimated to be 4 and 5 nm, respectively. Mössbauer spectra of 40Fe60Si recorded before (Fig. 1(a)) and after heat treatment at 400 ^{o}C (Fig. 1(b)) and 600 °C (Fig. 1(c)) for 2 h consisted of a doublet. The Mössbauer parameter of 40Fe60Si heat treated at 400 °C was similar to that heat treated at 600 °C. As the obtained value of the isomer shift was 0.32 mm s^{-1} at room temperature, it was determined that 40Fe60Si contained only Fe^{3+}.

From the temperature dependence of dc magnetic susceptibility under zero field cooling, the highest magnetic susceptibility of 40Fe60Si after heat treatment at 400 and 600 °C were recorded at the blocking temperature of 33 and 37 K, respectively.

In ac magnetic susceptibility measurements, the blocking temperatures became higher with increase in magnetic field frequency. From the relationship between blocking temperature and relaxation time, in the case of 40Fe60Si heated at 400 °C, the value of microscopic relaxation time and the dynamical exponent were estimated to be 9.8 ns and 9.1, respectively, of which the magnetic property was ascribed to superparamagnetism [2].

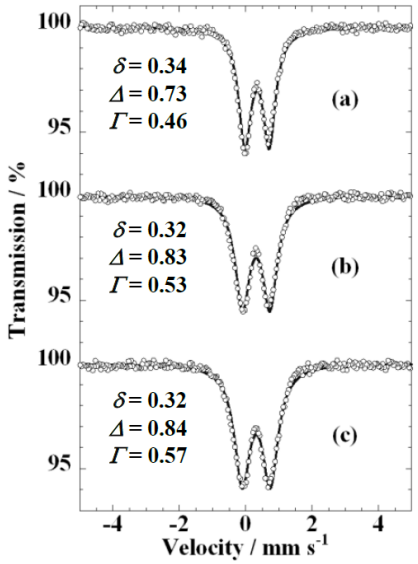

Fig. 1 ^{57}Fe Mössbauer spectra of 40Fe60Si (a) before and after heat treatment for 2 h, at (b) 400 and (c) 600 ^{o}C.

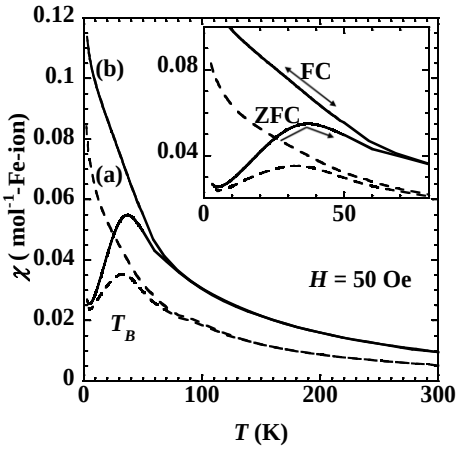

Fig. 2 Temperature dependence of the ZFC and FC magnetic susceptibility of 40Fe60Si heat-treated at (a) 400 and (b) 600 ^{o}C under the applied field of 50 Oe.

[1] L.Kopanja, et al., *Applied Surface Science*, 362, 380-386 (2016)
[2] H. Akamatsu, S. Oku, K. Fujita, S. Murai, K. Tanaka, *Phys. Rev. B*, 80, 134408, (2009)

Substitution Effect in Highly Conductive Barium Iron Vanadate Glass

T. Nishida[a], Y. Fujita[a], S. Kubuki[b] and N. Oka[a]

[a]*Department of Biological and Environmental Chemistry, Faculty of Humanity-Oriented Science and Engineering, Kindai University, 11-6 Kayanomori, Iizuka, Fukuoka 820-8555, Japan*
[b]*Department of Chemistry, Graduate School of Science and Engineering, Tokyo Metropolitan University, 1-1Minami-Osawa, Hachi-Oji, Tokyo 192-0397, Japan*
(nishida@fuk.kindai.ac.jp)

Heat treatment of vanadate glass at a given temperature higher than glass transition temperature (T_g) or crystallization temperature (T_c) causes a marked increase in the conductivity (σ) by several orders of magnitude [1-10]. The σ values are "*tunable*" by changing the temperature of the heat treatment. These highly conductive vanadate glasses have a lot of industrial applications such as conductive glass paste in place of Ag paste, bus-bar electrode for solar battery, cathode active material for LIB, air electrode catalyst for air battery, plasmatic discharge electrode, electron-emitting needle for air cleaning, substrate for hyperfine processing of submicron scale in association with FIB (focused ion beam), antistatic device, *etc*.

It was found that Fe^{III} atoms with a symmetric electron configuration of $3d^5$ were favorable to improve the conductivity of vanadate glass [6-9]. Substitution of metal oxides for Fe_2O_3 in BaO-Fe_2O_3-V_2O_5 glasses was investigated for developing highly conductive vanadate glass [7-9]. As a result, it proved that substitution of CuO, Cu_2O and ZnO, in which the metal atoms had electron configurations of $3d^9$ and $3d^{10}$, for Fe_2O_3 were effective to attain the higher conductivity [7,8].

Regarding the conduction mechanism of vanadate glass with a resistivity (ρ) of MΩ·cm, "*small polaron hopping theory*" [11] has so far been applied. As for the highly conductive vanadate glasses containing Fe_2O_3, CuO, Cu_2O and ZnO, *etc*., this authors' group suggested that the well-known "*n-type semiconductor model*" could be effective to comprehend the conduction behavior in conjunction with the activation energy (E_a) for conduction and the band gap energy of the metal oxides (E_g) [6-10]. In case of as-quenched CuO- and Cu_2O-containinig vanadate glasses, E_a's of 0.16 and 0.22 (±0.01) eV were respectively obtained, and the ρ's were 2.6×10^5 and 2.0×10^5 Ω·cm, respectively. After isothermal annealing at 450 °C for 30 min, the E_a's respectively decreased to 0.10 and 0.09 (±0.01) eV, and the ρ's were only 3.1 and 5.0 (±0.1) Ω·cm, respectively. It proved that smaller E_g's of 1.2-1.5 eV (CuO) and 2.1 eV (Cu_2O) were involved with the smaller E_a and the smaller ρ values [7-10].

^{57}Fe Mössbauer spectrum of CuO-containing vanadate glass measured at *RT* showed a decrease in Δ of Fe^{III} from 0.66 to 0.54 (±0.02) mm·s^{-1} after the annealing at 450 °C for 30 min [7]. In case of Cu_2O-containing vanadate glass, ^{57}Fe Mössbauer spectrum showed a similar decrease in the Δ from 0.69 to 0.54 (±0.02) mm·s^{-1} after the same isothermal annealing [7]. These results reflect decreased distortion of FeO_4 tetrahedra or improved "*structural relaxation*" of the *3D*-network since the Fe^{III} atom has a symmetric electron configuration of $3d^5$ in the outer-most orbital, and hence the *electric field gradient* caused by valence electrons (eq_{val}) is essentially "zero". This *structural relaxation* is also the case for VO_4 tetrahedra since they are connected to FeO_4 tetrahedra by sharing corner oxygen atoms. It is noted that the marked decrease in ρ's observed after the annealing is due to the *structural relaxation*, and not due to crystallization.

At MECAME2018, substitution of heavy metal oxides, *e.g.*, MnO_2, CuO, Cu_2O, ZnO, WO_3, MoO_3, Ga_2O_3, GeO_2 and SnO_2, for Fe_2O_3 will be discussed in conjunction with E_g, E_a, ρ, Δ. Substitution of Li_2O, Na_2O and K_2O for BaO will also be discussed.

[1] T. Nishida, J. Kubota, Y. Maeda, F. Ichikawa and T. Aomine, *J. Mater. Chem.*, **6** (1996) 1889-1896.
[2] T. Nishida, *Chemical Applications*, in: *Introduction to the Mössbauer Spectroscopy –Principles and Applications-* (*ed*. F.E. Fujita), Agne Gijutsu Center, Tokyo (1999) *pp*. 169-266 (in Japanese).
[3] K. Fukuda, A. Ikeda and T. Nishida, *Solid State Phenom.*, **90/91** (2003) 215-220.
[4] T. Nishida, *Japan Patent* Nos. 3854985 (2006) & 5164072 (2012), and related ones.
[5] S. Kubuki, H. Sakka, K. Tsuge, Z. Homonnay, K. Sinkó, E. Kuzmann, H. Yasumitsu and T. Nishida, *J. Ceram. Soc. Jpn.*, **115** (2007) 776-779.
[6] T. Nishida and S. Kubuki, *Mössbauer Study of New Electrically Conductive Glass*, in: *Mössbauer Spectroscopy: Applications in Chemistry, Biology, Nanotechnology, Industry and Environment* (*eds*. V. K. Sharma, G. Klingelhöfer and T. Nishida), John Wiley & Sons, Hoboken, NJ (2013) *pp*. 542-551.
[7] K. Matsuda, S. Kubuki and T. Nishida, *AIP Conf. Proc.*, **1622** (*msms2014*) (2014) 3-7.
[8] T. Nishida, S. Kubuki, K. Matsuda and Y. Otsuka, *Croat. Chem. Acta*, **88**(4) (2015) 427-435.
[9] T. Nishida, Y. Izutsu, M. Fujimura, K. Osouda, Y. Otsuka, S. Kubuki and N. Oka, *Pure Appl. Chem*., **89**(4) (2017) 419-428.
[10] T. Nishida, I. Furumoto, Y. Fujita, S. Kubuki and N. Oka, *J Mater Sci: Mater. Electron.*, **29** (2018) 2654–2659.
[11] N.F. Mott. *Adv. Phys*., **16** (1967) 49-144.

Determination of Debye Temperatures and Lamb-Mössbauer Factors for $LnFeO_3$ Orthoferrite Perovskites (Ln = La, Nd, Sm, Eu, Gd)

A. Scrimshire, A. Lobera, A. M. T. Bell, A. H. Jones, I. Sterianou, S. D. Forder and P. A. Bingham

Materials and Engineering Research Institute, Faculty of Arts, Computing, Engineering and Sciences, Sheffield Hallam University, Howard Street, Sheffield S1 1WB, UK
(alexscrimshire@gmail.com)

Lanthanide orthoferrites have wide-ranging industrial uses including solar, catalytic and electronic applications [1], [2]. Here a series of lanthanide orthoferrite perovskites, $LnFeO_3$ (Ln = La; Nd; Sm; Eu; Gd), prepared through a standard stoichiometric wet ball milling route using oxide precursors, has been studied. Characterisation through X-ray diffraction and X-ray fluorescence confirmed the synthesis of phase-pure or near-pure $LnFeO_3$ compounds. ^{57}Fe Mössbauer spectroscopy was performed over a temperature range of 10 K to 293 K to observe hyperfine structure and to enable calculation of the recoil-free fraction and Debye temperature (θ_D) of each orthoferrite. Debye temperatures (Ln = La 474 K; Nd 459 K; Sm 457 K; Eu 452 K; Gd 473 K) and recoil-free fractions (Ln = La 0.827; Nd 0.817; Sm 0.816; Eu 0.812; Gd 0.826) were approximated through minimising the difference in the temperature dependent experimental Centre Shift (CS) and theoretical Isomer Shift (IS), by allowing the Debye temperature and Isomer Shift values to vary. This method of minimising the difference between theoretical and actual values yields Debye temperatures consistent with results from other studies determined through thermal analysis methods. This displays the ability of variable-temperature Mössbauer spectroscopy to approximate Debye temperatures and recoil-free fractions, whilst observing temperature induced transitions over the temperature range observed. X-ray diffraction and Rietveld refinement show an inverse relationship between FeO_6 octahedral volume and approximated Debye temperatures. Raman spectroscopy show an increase in the band positions attributed to soft modes of A_g symmetry, $A_g(3)$ and $A_g(5)$ from La to $GdFeO_3$ corresponding to octahedral rotations and tilts in the [010] and [101] planes respectively.

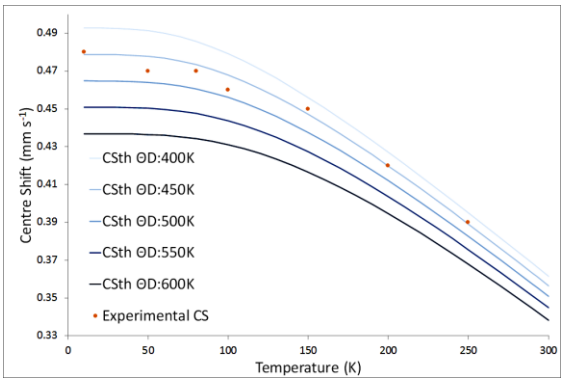

Fig. 1 Theoretical trend lines of Centre Shifts for given θ_D (solid lines) and experimental data for $LaFeO_3$ (circles) with intrinsic Isomer Shift = 0.60 mm s^{-1}.

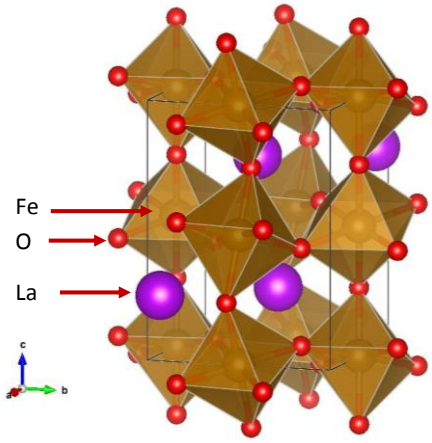

Fig. 2 Polyhedral schematic of $LaFeO_3$ orthorhombic perovskite unit cell rendered in VESTA © [3], [4].

[1] F.J. Berry, X. Ren, J.F. Marco, *Czechoslov. J. Phys.* 55 (2005) 771–780.
[2] X. Niu, H. Li, G. Liu, *J. Mol. Catal. A Chem.* 232 (2005) 89–93.
[3] K. Momma, F. Izumi, *J. Appl. Crystallogr.* 41 (2008) 653–658.
[4] P. Coppens, M. Eibschütz, *Acta Crystallogr.* 19 (1965) 524–531.

Interactions of Ferrate(VI) with Natural Organic Matter: Mössbauer Spectroscopy Investigation

V.K. Sharma[a], B. Darko[a], L. Machala[b] and R. Zboril[b]

[a]*Department of Environmental and Occupational Health, School of Public Health, College Station, Texas 77843, USA*
[b]*Regional Centre of Advanced Technologies and Materials, Departments of Experimental Physics and Physical Chemistry, Faculty of Science, Palacky University, 78371 Olomouc, Czech Republic*
(vsharma@sph.tamhsc.edu)

Natural organic matter (NOM) is the generic term for a mixture of organic components, which are slightly water soluble. Different geological and microbial process result in NOM. It mostly consists humic (humic and fulvic acid) and non humic fractions which are carbohydrates, amino acids and proteins [1]. They are classified based on their solubilities as humic acid, fulvic acid and humins. Fulvic acids (FA's) are soluble at all pH, humic acids (HA's) are insoluble at pH lower than 2 but soluble at higher pH, whereas humins are insoluble in water at all pH. Humic substances are heterogeneous mixture of carbon (45-55%), oxygen (30-45%), hydrogen (3-6%), nitrogen (1-5%) and sulfur (1%) in complex carbon chains. Of the different humic fractions of NOM, humic acids have the highest molecular weight compared to fulvic acids. The organic functional groups present in humic acid include carboxylic, carbonyl, phenols, catechol, amines, and quinones.

NOM is one of the major concerns in water treatment because they can cause taste and odor, color, and bacterial growth in the water distribution system [2]. Other concern related to NOM is the formation of disinfection by products (DBPs). NOM is considered precursor of DBPs [2]. These DBPs are formed when NOM reacts with conventional disinfectants such as chlorine, chlorine dioxide, chloramines, and ozone used in water treatment. Because of such drawbacks in these disinfectants, we have been investigating emerging oxidant and disinfectant, ferrate(VI) ($Fe^{VI}O_4^{2-}$) [3-5]. The focus of the presentation is to study the interaction of ferrate(VI) with NOM using Mössbauer Spectroscopy. An attempt was made to learn the formation of intermediate oxidation states of iron in the reduction of ferrate(VI) by moieties of NOM (for example, iron(V) and iron(IV)) and to elucidate the final reducing product phase of iron(III) oxides. Other spectroscopic techniques were also applied to investigate the fate of NOM in its interaction with ferrate(VI).

Initially, the Mössbauer Spectrum was collected after mixing ferrate(VI) with Suwannee River Fulvic Acid (SRFA) at different time intervals. A spectrum at 4 s after the mixing is shown in Fig. 1. A singlet peak indicates the presence of Fe(VI) whereas doublet represents Fe(III). The percentages (spectrum area) represent the number of atoms of either state of Fe (that is either Fe(VI) or Fe(III)) present in the solution.

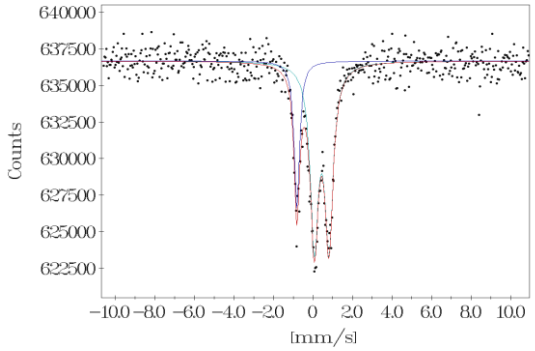

Fig. 1 Mössbauer spectrum of (3.3 M SRFA : 0.673 M Fe(VI) reaction at pH 9.0. (reaction time = 4 s and T = 100 K).

The presentation will show variation of the areas of different Mössbauer spectra with time. These results in conjunction with fluorescence and electron paramagnetic resonance (EPR) measurements will be discussed.

Addition of different concentrations of ferrate(VI) to a constant concentration of SRFA solution showed a decrease in fluorescence intensities in all different molar ratios of the reactants. Significantly, EPR spectra suggested the formation of radicals in the ferrate(VI)-SRFA system. The transmission electron microscopy (TEM) technique confirmed the presence of amorphous nanoparticles of sizes approximately 3 nm as the final oxides or hydroxides of Fe(III).

[1] V.K. Sharma, R. Zboril, R. Varma. Chem. Soc. Rev. 44 (2015) 8410-8423.
[2] V.K. Sharma, X. Yang, L. Cizmas, T.J. McDonald, R. Luque, C.M. Sayes, B. Yuan, and D.D. Dionysiou, Chem. Eng. J. 317 (2017) 777-792.
[3] V.K. Sharma, R. Zboril, and R.S. Varma, Acc. Chem. Res, 17 (2015), 182-191.
[4] V.K. Sharma, L. Chen, and R. Zbořil, ACS Sustain. Chem. Eng., 4 (2016), 18-34.
[5] M. Feng, V.K. Sharma, Chem. Eng. J., 341 (2018), 137-145.

Magnetite Nanoflowers Decorated on Reduced Graphene Oxide for Efficient Removal of Reactive Dyes

D.M. Stanković[a], M. Ognjanović[a], B. Dojčinović[b] and B. Antić[a]

[a] *The Vinča Institute of Nuclear Sciences, University of Belgrade, Mike Petrovića Alasa 12-14, Belgrade, Serbia*
[b] *ICTM, University of Belgrade, Njegoševa 12, Belgrade, Serbia*
(daliborstankovic@vin.bg.ac.rs)

In this study, for the first time, we proposed novel platform for the removal of synthetic organic dyes based on screen printed electrode (SPCE) supported with a nanocomposite obtained by decoration of reduced graphene oxide (RGO) with magnetite (Fe_3O_4) nanoflowers (Fe_3O_4@RGO/SPCE). Magnetite nanoflowers were synthesized by polyol mediated reduction of iron(III) chloride and characterized. Fe_3O_4@RGO nanocomposite was synthesized using microwave hydrothermal assisted procedure. Materials were characterized using transmission electron microscopy, X-ray diffraction, Z-sizer and electrochemical methods (Fig. 1). Impedance tests (EIS) indicate that synergetic effect of these materials reduces resistivity of the system and improves catalytic activity of the composite, which was confirmed with cyclic voltammetry (CV tests) where is obvious high increase of the electrochemically active surface area sites (Fig. 2).

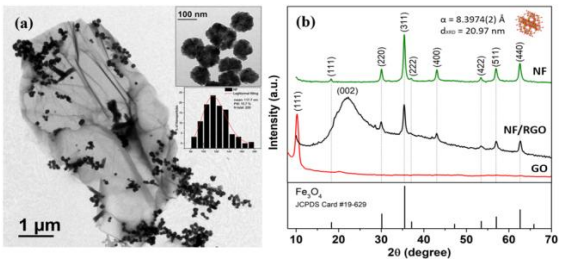

Fig. 1 Morphology and microstructure of NFs and the NF/RGO composite (a) TEM micrographs of RGO decorated nanoflowers with log-normal size distribution (inset), (b) XRD of NFs, GO and NF/RGO composite.

Obtained results clearly indicate that with this approach the optimum removal time of selected pollutant was for only 30 min, including potential of 3 V (Fig. 3) and potassium chloride as supporting electrolyte, with color removal efficiency of 99 %, while chemical oxygen demand (COD) with more than 40 % and total organic carbon with around 20 % decrease, were noticed, after only one hour of the treatment. Nonetheless, the high stability (service life) of the prepared system using Fe_3O_4@RGO/SPCE electrode was noticed and the remains almost unchanged after 50 cycles of usage to achieve same removal efficiency. Overall, electrochemical removal procedure proposed in this study can be found as reliable novel system, opening a new approach to use screen printed based electrodes.

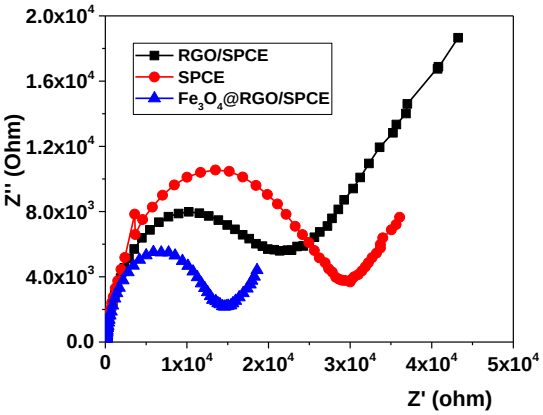

Fig. 2 EIS spectra of the electrodes

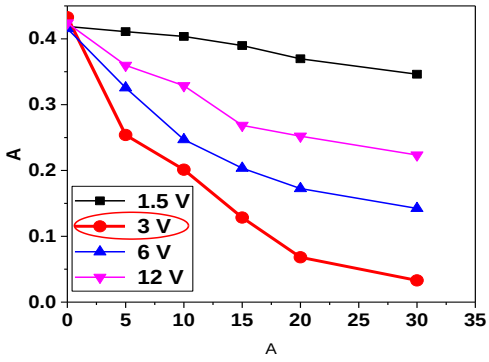

Fig. 3 Effect of different potentials for the Reactive blue 52 removal efficiency using developed method.

Electrochemical Tuning of Magnetism in Ordered Mesoporous Transition Metal Ferrite Films

L. Androš Dubraja[a], C. Reitz[b], L. Velasco[b], R. Witte[b], R. Kruk[b], H. Hahn[b] and T. Brezesinski[b]

[a]*Ruđer Bošković Institute, Bijenička cesta 54, 10000 Zagreb, Croatia*
[b]*Institute of Nanotechnology, Karlsruhe Institute of Technology, Hermann-von-Helmholtz-Platz 1, 76344 Eggenstein-Leopoldshafen, Germany*
(Lidija.Andros@irb.hr)

Ferrite materials based on the spinel-type structure with general formula MFe_2O_4 (M = Fe^{2+}, Mn^{2+}, Ni^{2+}, Zn^{2+}, or Cu^{2+},) are due to their exciting chemical, structural, electrical and magnetic properties, used for various technological applications, ranging from magnetic memory, energy storage and conversion, catalysis to biomedicine. Another interesting feature observed in the spinel ferrite structures is *in situ* control of magnetism through electrochemical insertion of lithium. For some nanocrystalline spinel oxides (γ-Fe_2O_3, $CuFe_2O_4$, $ZnFe_2O_4$ and α-$LiFe_5O_8$), it has already been shown that large and reversible changes in magnetization variation can be achieved by careful choice of lithium amount for insertion.[1,2]

Using the same strategy, we have extended these experiments to spinels produced in the form of mesoporous thin films. In the search for materials with well-defined magnetic properties and good electrochemical performance, we have selected $CoFe_2O_4$, $Co_{0.5}Ni_{0.5}Fe_2O_4$ and $NiFe_2O_4$ as suitable candidates for further *in situ* tuning measurements. One of the most promising synthetic strategies to achieve mesoporous oxides involves the solution-phase coassembly of molecular inorganic building blocks with either a surfactant or an amphiphilic polymer structure-directing agent using an evaporation-induced self-assembly (EISA) process.[3] The mesoporous transition metal ferrite thin films were prepared by dip-coating under defined conditions (relative humidity, temperature etc.) and subsequent calcination. Structural and compositional characterization was performed on samples heated to 650 °C ($CoFe_2O_4$ and $Co_{0.5}Ni_{0.5}Fe_2O_4$) and 700 °C ($NiFe_2O_4$) by electron microscopy, synchrotron-based GISAXS and GIWAXD. Insight into the cation distribution was gained from conversion electron ^{57}Fe Mössbauer spectroscopy. The model used to fit the spectra is based on work by *Sawatzky et al*[4] where it was shown that octahedral (B) sites which have all six neighboring tetrahedral (A) sites occupied by Fe^{3+} are different from those having some of the tetrahedral neighbors occupied by e.g., Co^{2+}. Assuming comparable Lamb-Mössbauer factors for the A and B site, occupations of A and B sites can be calculated based on the ratio between relative spectral areas, giving value of inversion parameter $\lambda \approx 0.7$ (Fig. 1). The magnetic properties of cobalt and nickel ferrite are predominantly determined by antiferromagnetic exchange interactions between the metal centers on tetrahedral and octahedral sites. When lithium is inserted into the lattice, it probably occupies the larger octahedral sites. For each lithium ion (in the reversible potential range), an Fe^{3+} is reduced to Fe^{2+} and the lithiated phase is created (Fig 2). Our results demonstrate that insertion of lithium ions into the spinel lattice of these nanocrystalline oxides allows reversible manipulation of magnetization, rendering them interesting for application in the field of tuneable nanomaterials.

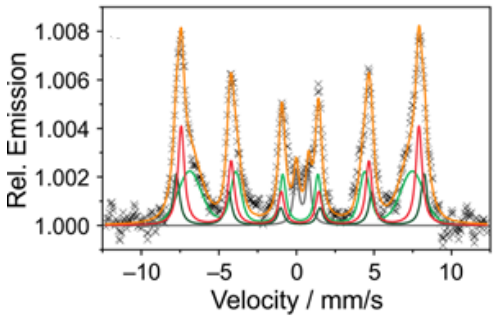

Fig. 1 Room temperature conversion electron Mössbauer spectra obtained on mesoporous $CoFe_2O_4$ thin films. The red line corresponds to Fe^{3+} on tetrahedral (A) sites. For octahedral Fe^{3+}, two sextets can be distinguished as indicated by the dark green (B1) and light green (B2) lines, corresponding to sites with six or one to five Fe^{3+} nearest neighbors, respectively. The gray line represents the Fe^{3+} doublet component and the orange line is the sum of all subspectra.

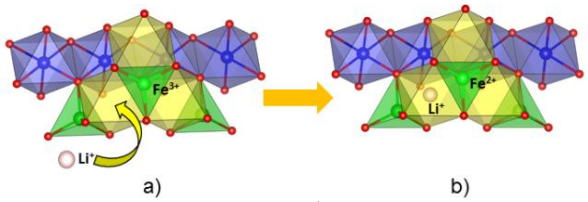

Fig 2. Representation of the Li^+ insertion into $CoFe_2O_4$: Fe^{3+}/Co^{2+} octahedra are depicted in blue, Fe^{3+}/Co^{2+} tetrahedra are depicted in green, empty octahedral sites are depicted as yellow.

[1] S. Dasgupta, B. Das, M. Knapp, R. A. Brand, H. Ehrenberg, R. Kruk, H. Hahn, *Adv. Mater.* 26 (2014) 4639–4644.
[2] C. Reitz, C. Suchomski, D. Wang, H. Hahn, T. Brezesinski, *J. Mater. Chem. C* 4 (2016) 8889–8896.
[3] Y. Lu, R. Ganguli, C. A. Drewien, M. T. Anderson, C. J. Brinker, W. Gong, Y. Guo, H. Soyez, B. Dunn, M. H. Huang, J. I. Zink, *Nature* 389 (1997) 364−368.
[4] G. A. Sawatzky, F. van der Woude, A. H. Morrish, *J. Appl. Phys.* 39 (1968) 1204–1206.

Magnetic Interactions in $Fe_{1-x}M_xSb_2O_4$, M=Mg,Co, Deduced from Mössbauer Spectroscopy

F.J. Berry[a], B.P. de Laune[a], C. Greaves[a], H.-Y. Hah[b], C.E. Johnson[b], J.A. Johnson [b], S. Kamali[b], J.F. Marco[c], M.F. Thomas[d] and M.J. Whittaker[a]

[a]*School of Chemistry, The University of Birmingham, Birmingham B15 2TT, UK*
[b] *Center for Laser Applications, University of Tennessee Space Institute, Tullahoma, Tennessee 37388, USA*
[c]*Instituto de Quimica Fisica "Rocasolano", CSIC, Serrano 119, 28006 Madrid, Spain*
[d]*Department of Physics, University of Liverpool, Liverpool L69 3BX, UK*
(f.j.berry.1@bham.ac.uk)

Magnesium- and cobalt- substituted $FeSb_2O_4$, of composition $Fe_{1-x}Mg_xSb_2O_4$ (x = 0.25, 0.50, 0.75) and $Fe_{0.25}Co_{0.75}Sb_2O_4$ have been examined by ^{57}Fe Mössbauer spectroscopy. The complex spectra recorded from the magnetically ordered materials are interpreted in terms of two models in which the dominant magnetic interactions occur along the rutile-related chains of FeO_6 octahedra in the magnetic structure of $FeSb_2O_4$. In materials of the type $Fe_{1-x}Mg_xSb_2O_4$, the diamagnetic Mg^{2+} ions have no magnetic moment and behave as non-magnetic blocks which disrupt the magnetic interactions in the chains along the *c*-axis forming segments of iron-containing chains separated by Mg^{2+} ions. In contrast, Co^{2+} ions in $Fe_{0.25}Co_{0.75}Sb_2O_4$ have a magnetic moment and, whilst segmenting the chains of Fe^{2+} ions, the segments magnetically couple *via* Fe^{2+}-O-Co^{2+} interactions and a modified spectral interpretation is proposed.

Design and Construction of Dynamic Hysteresis Magnetometer

M. Bošković[a], M. Perović[a] and V. Ćosić[b]

[a]*Laboratory for Theoretical and Condensed Mater Physics, Institute of Nuclear Sciences Vinca, P.O.Box 522, Belgrade, Serbia*
[b]*Custom Electronics Shack, Belgrade, Serbia*
(markob@vin.bg.ac.rs)

Magnetic hyperthermia presents one of the most promising applications of magnetic nanoparticles in medicine [1]. Crucial particle characteristic for this purpose is specific power absorption (SPA), which shows how much power is absorbed from external magnetic field and transformed into heat. Common and widely used method for determination of SPA is calorimetry, i.e., by measurement of the sample's temperature change during external AC field application. The method is relatively simple to implement, but posses a number of hard to assess disadvantages [2].

In this work we present a setup which enables determination of SPA by alternative route - from hysteresis loop surface area. The setup consists out of three parts: LC circuit, detection circuit, and transport. LC circuit produces high amplitude high frequency AC field (up to 300 kHz and 20 mT) by utilizing resonant current magnification of parallel LC circuit. Detection circuit (Fig. 1) contains coils wound in the first-order gradiometer configuration. This nullifies signal induced by external AC field and enables measurement of the minute response of the sample. Transport system centers detection coil and sample in the optimum position inside field-producing coil.

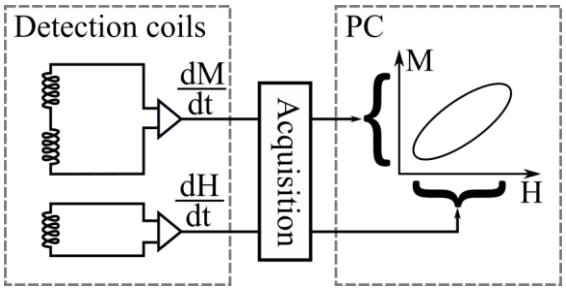

Fig. 1 Detection system block diagram

Signals from detection circuit are acquired by digital oscilloscope and further conditioned using custom-built software. Surface area of the reconstructed M(H) loops gives absorbed energy during one field cycle.

[1] S. Dutz, R. Hergt, Nanotechnology 25 (2014) 452001.

[2] F. Soetaert, S.K. Kandala, A. Bakuzis, R. Ivkov, Sci. Rep. 7 (2017) 6661.

Study on the Nature of Particulate Matters in Fly and Bottom Ashes from Power Plants

Z. Cherkezova-Zheleva, D. Paneva, N. Velinov and I. Mitov

Institute of Catalysis, Bulgarian Academy of Sciences, "Acad. G. Bonchev" St., Bld.11, 1113 Sofia, Bulgaria (zzhel@ic.bas.bg)

Air quality is improving in Bulgaria, but there are still problems in Sofia and other cities especially in winter [1]. It was also recognized that the main specific air pollutant in Bulgaria are the fine particles [2]. The unresolved problem with urban air pollution and relatively small number of regional studies encourage us to give efforts in better understanding of urban air pollution and to identify individual species that can contribute significantly to health effects in humans [3-5]. Coal combustion in power plants has been recognized to be one of the main sources of excessive particulate matters (PM) pollution [2] but their contribution to deposition fluxes remain still unclear [3-7]. In this paper, we report a preliminary investigation on the nature of particulate matter in fly and bottom ashes from two regional power plants in order to study the impact of different fossil fuel use on the atmospheric iron-bearing compounds. The paper has been focused on the powder grains bellow 0.1 mm.

It is well known that the iron is not the only transition metal found in particulate matter, but it is one of the predominant ones [4]. In this regard ^{57}Fe Mössbauer spectra registered at room and liquid nitrogen temperature allow us to become deeper into the PM characteristics. Analysis was based on [4-7]. Powder X-ray diffraction (XRD), elemental analysis and scanning electron microscopy (SEM) were also applied. The techniques applied proved to be useful in better description of iron-bearing species in the products of different coal combustion [3-7]. The results of Mössbauer spectrometry and chemical analysis allowed achieving of a better understanding of the mineral transformations that occur during the combustion of coal. The analysis suggested that the fly and bottom ashes are different in their phase composition. The relatively high total content of iron was found for both bottom and fly ashes. It was registered that samples vary in size, morphology, surface area and chemical composition, depending on the coal type used. It may be concluded that the fly and bottom ash produced as a result of the combustion of high-rank (HR) and low-rank (LR) coal have similar elemental composition, but exhibited different morphology, size-distribution and ratio between the registered phases. The Fe^{3+} iron-bearing components identified in fly ash were magnetite, maghemite, superparamagnetic ferric iron in the oxide phases, an aluminosilicate glass and a small amount of hematite. Octahedrally coordinated Fe^{2+} ions were presented in HR coal ashes in higher amount in comparison to LR coal combustion ashes. Fe^{2+} compounds are probably in hercynite/glass/silicates phases [5]. Paramagnetic iron phases are predominantly presented in bottom ash samples in comparison to fly ash samples. Higher amount of ultrafine nanoparticles was registered in the first case. SEM study confirmed the existence of inhomogeneous distribution of nanocrystallites in studied samples. XRD analysis indicates coexistence of amorphous and crystalline phases in all studied samples. X-ray amorphous phases are predominant due to the small crystallite size. It was difficult to give an exact phase composition of studied PM due to registered mixed mineralogy. Nevertheless the results could be used to identify the regional PM pollution sources and to prevent their production.

The financial support by the Bulgarian National Science Fund at the Ministry of Education and Science - Project № DN 18/16/ 2017 is gratefully appreciated.

[1] European Environment Agency, Air pollution fact sheet - Bulgaria (2017).
[2] N. Dimov, Report of the Ministry of Environment and Water (2017) (in Bulgarian).
[3] J. M. Veranth, K. R. Smith, A. A. Hu, J. S. Lighty, A. E. Aust *Chem. Res. Toxicol. 13* (2000) 382.
[4] H. Chen, A. Laskin, J. Baltrusaitis, C. A. Gorski, M. M. Scherer, V. H. Grassian Environmental Science & Technology 46 (4) (2012) 2112.
[5] R. Vandenberghe, V. G. De Resende, E. De Grave Hyperfine Interactions (2009) 191(1-3) 44.
[6] T. Szumiata, K. Brzózka, B. Górka, M. Gawroński, M. Gzik-Szumiata, R. Świetlik, M. Trojanowska, *Hyperfine Interactions 226*(1) (2014) 483.
[7] M. Kądziołka-Gaweł, D. Smolka-Danielowska, Nukleonika 62(2) (2017) 101.

Strontium Hexaferrite Platelets: Between Domains and Simulations

G. Delgado Soria[a], A. Mandziak[b] , M. Sanchez-Arenillas[a] , J. F. Marco[a], M. Foerster[b], L.Aballe[b], M. Valvidares[b] , H. B. Vasili[b] , E. Pereiro[b], J. E. Prieto[c] , P. Prieto[c], P. Janus[d], M. Christensen[e] , A. Quesada[f] and J. de la Figuera[a]

[a]*Instituto de Química Física "Rocasolano", CSIC, Madrid E-28006, Spain*
[b]*Alba Synchrotron, CELLS, Barcelona E-08290, Spain*
[c]*Universidad Autónoma de Madrid, Madrid E-28049, Spain*
[d]*Institut "Jozef Stefan", 1000 Ljubljana, Slovenia*
[e]*Aarhus University, 8000 Aarhus C, Denmark*
[f]*Instituto de Cerámica y Vidrio, CSIC, Madrid E-28049, Spain*
(gdelgadosoria@iqfr.csic.es)

Strontium hexaferrite ($SrFe_{12}O_{19}$) is a highly studied material due to its interesting magnetic properties (high magnetocrystalline anisotropy and Curie temperature), excellent thermal and chemical stability, low cost and low toxicity [1]. Besides, it has been recognized that it can be used in recording media, in permanent magnets, in applications for telecommunications, and as components in high-frequency, microwave, and magneto-optical devices. It was discovered in 1950 by Phillips and belongs to hexagonal type M ferrites [2]. It has the crystalline structure of the magnetoplumbite, a compact packing of oxygen and strontium ions with iron cations in five interstitial positions. In $SrFe_{12}O_{19}$, the axis of easy magnetization is along the C axis.

In this work we have studied this compound in the form of micrometer sized platelets which gives it the particular characteristic of driving the magnetization out-of-plane. Platelets are obtained from hydrothermal synthesis before and after annealing at high temperature to increase the grain size. We first characterized the structure and compositions by means of Mössbauer spectroscopy (see figure) and scanning transmission X-ray microscopy (STXM). We have determined the magnetic moment using X-ray absorption spectroscopy (XAS) and X-ray magnetic circular dichroism (XMCD), employing photoemission electron microscopy (PEEM) as well as total yield detection.

Micromagnetism simulations [3] have also been carried out for a better understanding of the behavior of the experimental system and for studying possible changes in the magnetization when depositing layers of materials such as Cobalt or Nickel on the ferrite.

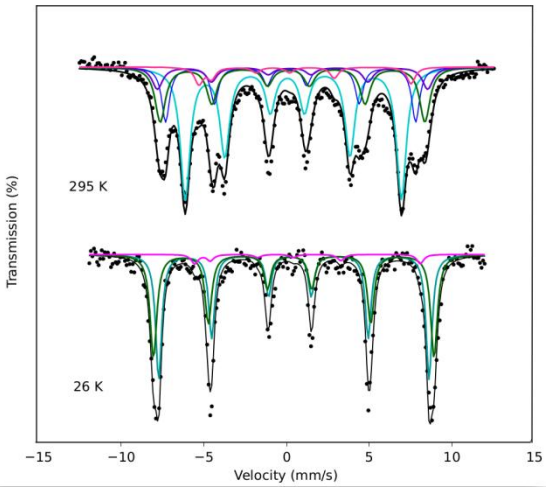

Fig. 1 Mössbauer spectra of the SFO platelets at 295 and 26 K

We acknowledge funding from the European Commission through the AMPHIBIAN project (H2020-NMBP-2016-720853) and the Spanish Ministry of Economy and Competitiveness through project (MAT2015-64110-C2-1-P).

[1] V.A.M Brabers, Handbook of Magnetism and Advanced Magnetic Materials, (2007), pp 1-19.
[2] R.C. Pullar, Progress in Materials Science 57 (2012), pp 1191–1334.
[3] A. Vansteekiste et al, AIP Advances 4, (2014), pp 107133.

Synthesis and Microstructural Properties of Cu-Doped Goethite and Cu-Doped Hematite Nanoneedles

S. Krehula, M. Ristić, Ž. Petrović and S. Musić

Division of Materials Chemistry, Ruđer Bošković Institute, P.O. Box 180, HR-10002 Zagreb, Croatia (Stjepko.Krehula@irb.hr)

Goethite (α-FeOOH) and hematite (α-Fe_2O_3) are the most stable and the most ubiquitous iron oxyhydroxide and iron oxide, respectively [1]. A number of favourable properties (nontoxicity, stability, low cost, band gap in the visible range, etc.) make these compounds promising candidates for different applications (catalysts, photocatalysts, gas sensors, battery electrodes, supercapacitors, etc.). Properties of goethite and hematite can be improved and tuned by modification of particle size and shape, as well as by incorporation of various metal cations into their crystal structure. For example, elongated (1D) hematite nanoparticles (nanorods) showed higher visible-light photocatalytic activity compared to hematite nanoplates (2D) or nanocubes (3D) [2]. Also, smaller hematite and goethite 1D nanoparticles (nanorods) showed higher visible-light photocatalytic activity compared to larger hematite and goethite 1D particles (microrods) [3]. Substitution of Fe^{3+} ions in iron oxides with divalent metal cations can significantly modify their electronic properties. As a consequence of modified electronic properties, Cu-doped goethite [4,5] and hematite [6,7] showed improved catalytic, photocatalytic and gas sensing properties compared to pure phases. In this work Cu-doped goethite and hematite 1D nanoparticles (nanoneedles) were prepared and studied.

Cu-doped goethite nanoneedles (with Cu content up to 4 mol%) were synthesized by precipitation in a highly alkaline medium. Cu-doped hematite nanoneedles were prepared by calcination of Cu-doped goethite samples at 500 °C (Fig. 1). Phase composition of prepared samples was determined using X-ray powder diffraction (XRPD) and Mössbauer spectroscopy (Fig. 2). Cu^{2+}-for-Fe^{3+} substitution in the goethite crystal structure was confirmed by the determination of the unit cell expansion using XRPD and by the measurement of the hyperfine magnetic field reduction using Mössbauer spectroscopy. An increased Cu^{2+}-for-Fe^{3+} substitution in goethite caused a gradual elongation and narrowing of nanorods with formation of nanoneedles at 3 and 4 mol% Cu. The shape and size of nanoneedles were not changed by goethite to hematite thermal transformation (Fig. 1). Thermal analysis showed a decrease in the temperature of goethite dehydroxylation by Cu doping. Cu^{2+}-for-Fe^{3+} substitution in goethite and hematite affected an increased absorption of visible and near IR radiation compared to pure phases, as well as a decrease in the optical band gap energy.

This research has been supported by the Croatian Science Foundation (project number IP-2016-06-8254).

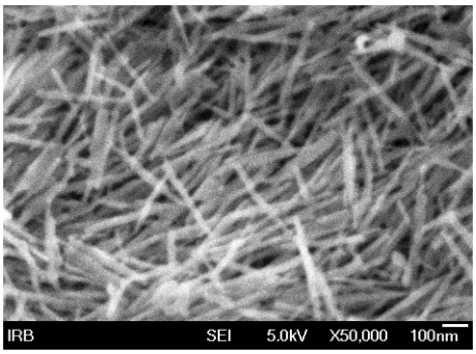

Fig. 1 FE-SEM image of Cu-doped (4 mol%) hematite nanoneedles

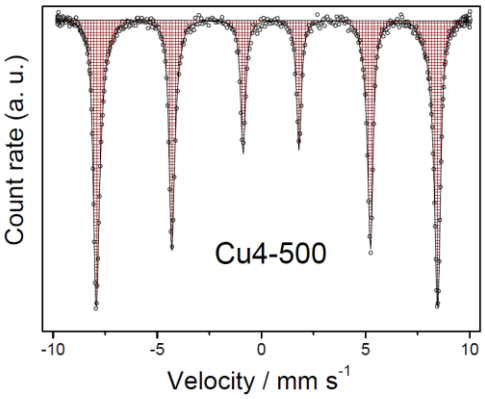

Fig. 2 RT ^{57}Fe Mössbauer spectrum of Cu-doped (4 mol%) hematite nanoneedles.

[1] R.M. Cornell, U. Schwertmann, The Iron Oxides, Structure, Properties, Reactions, Occurrence and Uses, second ed., Wiley-VCH, Weinheim, 2003.
[2] X. Zhou, J. Lan, G. Liu, K. Deng, Y. Yang, G. Nie, J. Yu, L. Zhi, Angew. Chem. Int. Ed. 51 (2012) 178–182.
[3] X. Zhou, H. Yang, C. Wang, X. Mao, Y. Wang, Y. Yang, G. Liu, J. Phys. Chem. C 114 (2010) 17051–17061.
[4] I.R. Guimaraes, A. Giroto, L.C.A. Oliveira, M.C. Guerreiro, D.Q. Lima, J.D. Fabris, Appl. Catal. B: Environ. 91 (2009) 581–586.
[5] J. Xu, Y. Li, B. Yuan, C. Shen, M. Fu, H. Cui, W. Sun, Chem. Eng. J. 291 (2016) 174–183.
[6] V.M.S. Rocha, M.G. Pereira, L.R. Teles, M.O.G. Souza, Mater. Sci. Eng. B 185 (2014) 13–20.
[7] H. Liu, T. Peng, H. Sun, R. Xie, G. Ma, RSC Adv. 7 (2017) 11414–11419.

Synthesis and Properties of Ni-doped Goethite and Ni-doped Hematite Nanorods

S. Krehula[a], M. Ristić[a], I. Mitar[b], M. Perović[c], M. Bošković[c], B. Antić[c], C. Wu[d,f], X. Li[d,e,g], L. Jiang[d,e], J. Wang[d,f], G. Sun[d], T. Zhang[f,g] and S. Musić[a]

[a] *Division of Materials Chemistry, Ruđer Bošković Institute, P.O. Box 180, HR-10002 Zagreb, Croatia*
[b] *Faculty of Science, University of Split, HR-21000, Croatia*
[c] *Condensed Matter Physics Laboratory, Institute of Nuclear Sciences Vinca, University of Belgrade, Belgrade, Serbia*
[d] *Dalian National Laboratory for Clean Energy, Dalian Institute of Chemical Physics, Chinese Academy of Sciences, Dalian 116023, China*
[e] *College of Material Science and Engineering, Qingdao University of Science and Technology, Qingdao 266042, China*
[f] *Mössbauer Effect Data Center, Dalian Institute of Chemical Physics, Chinese Academy of Sciences, Dalian 116023, China*
[g] *University of the Chinese Academy of Sciences, Beijing 100039, China*
(Stjepko.Krehula@irb.hr)

Iron oxides and oxyhydroxides are common and widespread compounds in nature. Goethite (α-FeOOH) and hematite (α-Fe_2O_3) are the most stable and the most ubiquitous iron oxyhydroxide and iron oxide, respectively [1]. A number of favourable properties (nontoxicity, stability, low cost, band gap in the visible range, etc.) make these compounds promising candidates for different applications (catalysts, photocatalysts, gas sensors, battery electrodes, supercapacitors, etc.). Properties of goethite and hematite can be enhanced by modification of particle size and shape, as well as by incorporation of different metal cations into their crystal structure. For example, elongated (1D) hematite nanoparticles (nanorods) showed higher visible-light photocatalytic activity compared to hematite nanoplates (2D) or nanocubes (3D) [2]. Substitution of Fe^{3+} ions with other metal ions can also significantly modify different properties [1,3].

Ni-doped goethite (α-FeOOH) nanorods were synthesized from mixed Fe(III)-Ni(II) nitrate aqueous solutions by a hydrothermal treatment in a highly alkaline medium using a strong organic alkali tetramethylammonium hydroxide (TMAH). Small amounts of Ni-containing ferrihydrite and Ni ferrite were present as minor phases in samples with 10 mol% Ni and more. Ni-doped hematite (α-Fe_2O_3) nanorods were obtained by calcination of Ni-doped goethite nanorods at 400 °C. Ni-for-Fe substitution in the structure of goethite and hematite was confirmed by the determination of the unit cell expansion using XRPD and by the measurement of the hyperfine magnetic field (HMF) reduction using Mössbauer spectroscopy. Ni-doped goethite and hematite nanorods were smaller compared to reference samples for 5 mol % Ni but significantly larger for higher Ni contents. Electrochemical measurements showed significant increase in oxygen evolution reaction (OER) catalytic activity of Ni-doped goethite and Ni-doped hematite nanorods compared to pure phase.

This research has been supported by the Croatian Science Foundation (project number IP-2016-06-8254).

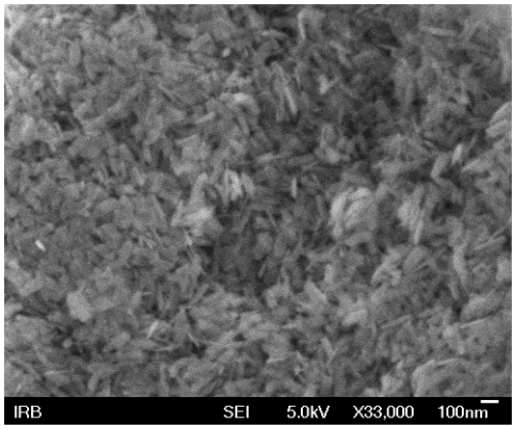

Fig. 1 FE-SEM image of Ni-doped (5 mol%) hematite nanorods

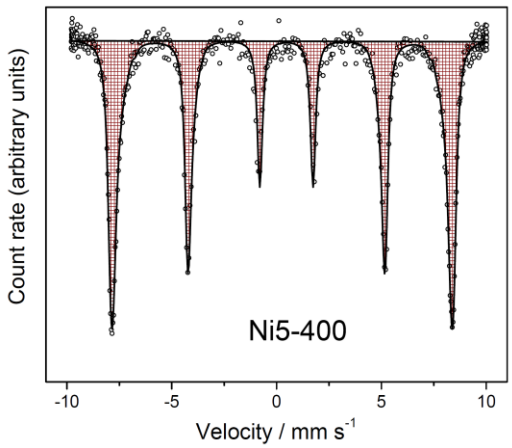

Fig. 2 RT ^{57}Fe Mössbauer spectrum of Ni-doped (5 mol%) hematite nanorods.

[1] R.M. Cornell, U. Schwertmann, The Iron Oxides, Structure, Properties, Reactions, Occurrence and Uses, second ed., Wiley-VCH, Weinheim, 2003.

[2] X. Zhou, J. Lan, G. Liu, K. Deng, Y. Yang, G. Nie, J. Yu, L. Zhi, Angew. Chem. Int. Ed. 51 (2012) 178–182.

[3] S. Musić, M. Ristić, S. Krehula, *^{57}Fe Mössbauer spectroscopy in the investigation of the precipitation of iron oxides*, in the book: *Mössbauer Spectroscopy - Application in Chemistry, Biology and Nanotechnology*, edited by V.K. Sharma, G. Klingelhofer, T. Nishida, Wiley & Sons, 2013.

^{119}Sn Mössbauer Study of Sn-containing Radiopharmaceutical Kits

E. Kuzmann[a], Z. Homonnay[a], Sz. Keresztes[b], M. Antalffy[b] and J. Környei[b]

[a]*Institute of Chemistry, Eötvös University, Budapest, Hungary*
[b]*Institute of Isotopes Co., Ltd., Budapest, Hungary*
(kuzmann@caesar.elte.hu)

Tin(II) is a crucial ingredient of radio-pharmaceutical kits to be labelled with ^{99m}Tc radionuclide 'on the spot' i.e. in the hospital labs just before patient's administration. MULTIBONE kit, composed from stannous chloride dihydrate and EDTMP (ethylene-diamine-tetramethylene phos-phonate), is designed as a "theranostic kit" that can be labelled with 99mTc and with trivalent beta-emitter radionuclides for imaging and for palliative treatment of painful bone metastases, respectively. PHYTON kit, composed from stannous chloride dihydrate and PHYTATE (myo-inositol-hexaphosphate ester), is for 99mTc-labelling and used for gamma-camera/SPECT imaging of the liver as well as monitoring of the liver tumour therapy. ^{119}Sn Mössbauer study of these two radiopharmaceutical kits were aimed in order to show the chemical microenvironment as well as interactions between the EDTMP or PHYTATE ligands and stannous chloride.

The ^{119}Sn Mössbauer spectra of Sn-PHYTATE and Sn-MULTIBONE samples were obtained in transmission geometry, using a 300 MBq activity $Ba^{119}SnO_3$ The patterns were recorded at 80 K, and evaluated by the Mosswinn code. Isomer shifts are given relatively to $BaSnO_3$.

Both ^{119}Sn Mössbauer spectra (Fig. 1) of liophylized Sn-PHYTATE and Sn-MULTIBONE samples were decomposed into two doublets corresponding to tin(II) and tin(IV) components according to their Mössbauer parameters depicted in Table 1. In both compounds tin(II) microenvironments are dominating. The occurrence of tin(IV) in Sn-MULTIBONE was as low as measured in the precursor stannous chloride dehydrate (3.2 %).

There are small but significant differences between both the isomer shifts and quadrupole splitting of Sn-PHYTATE and Sn-MULTIBONE radiopharmaceuticals. This reveals differences in the Sn microenvironments between the compounds.

The linewidths of all components are narrow enough and indicate that identical tin(II) microenvironments are present in each individual compounds.

The obtained isomer shift and quadrupole splitting data of tin(II) components (Table 1) are close to those which were reported for stannous phosphate and related compounds [1,2], but the parameters are very far from those of the precursor stannous chloride and its hydrate derivatives. This is consistent with the expectation that tin(II) is located in the vicinity of phosphonate/phospate groups in both radiopharmaceuticals, thus the appropriate compounds were prepared.

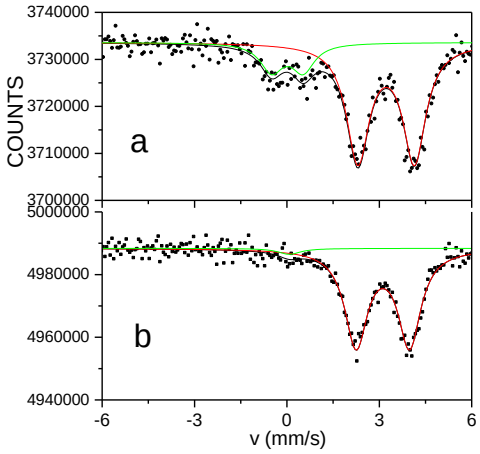

Fig. 1 ^{119}Sn Mössbauer spectra, recorded at 80 K, of liophylized Sn-PHYTATE (a) and Sn–MULTIBONE (b) radio-pharmaceuticals.

Table 1 80 K Mössbauer parameters of radiopharmaceuticals

Sample	A/ %	δ/mms^{-1}	Δ/mms^{-1}	W/mms^{-1}
Sn-PHYTATE	80.7	3.12	1.84	0.89
	19.3	-0.08	1.02	0.89
Sn-MULTIBONE	96.8	3.01	1.73	0.88
	3.2	-0.04	0.48	0.88

The characteristic ^{119}Sn Mössbauer parameters determined for Sn-PHYTATE and Sn-MULTIBONE can also serve for the quality control of these pharmaceutical kits.

[1] P. A. Flinn, in: Mössbauer Isomer Shifts, G. K. Shenoy and F. E. Wagner (Eds), North Holland, (1978) p. 593.
[2] L. Szirtes, J. Megyeri., E. Kuzmann, A. Beck, Radiation Physics and Chemistry 80 (2011) 786–791.

Spin-State and Structure of Tris(Glyoximato) Iron Complexes

E. Kuzmann[a], N. N. Gerasimchuk[b], Z. Homonnay[a], Cs. Várhelyi Jr[c], R. Szalay[a], F. Goga[c], L.-M. Golban[c], M. Várhelyi[c], P. Huszthy[d] and Gy. Pokol[d]

[a]*Institute of Chemistry, Eötvös University, Budapest, Hungary*
[b]*Department of Chemistry, Missouri State University, Springfield, MO 65897, USA*
[c]*Faculty of Chemistry and Chemical Engineering, Babes-Bolyai University, Cluj, Romania*
[d]*Faculty of Chemical and Bioengineering, Budapest University of Technology and Economics, Budapest, Hungary*
(kuzmann@caesar.elte.hu)

The future aim of our study is to develop novel metal coordination compounds that could be useful for medical therapy of cancer. Drugs containing glyoximato metal complexes have potential in cancer therapy. In our previous works [1, 2] a number of novel bis(glyoximato) iron complexes were prepared and characterized, where square planar geometry is characteristic for the $[Fe(RGlyoxH)_2]$ moiety (where R are alkyl groups). ^{57}Fe Mössbauer spectroscopy of these bis(glyoximato) iron complexes showed that iron is in low-spin iron(II) state when short chained alkyls (R = methyl or ethyl) are in the glyoxime plane, however, the incorporation of branching alkyl chains (isopropyl) in the complexes alters the Fe–N bond length and results in high-spin iron(II) state.

In the present work novel tris(glioximato) iron complexes of general formula $[Fe(R^1R^2glyoxime)_3(BOR^3)_2]$ (R^1 = methyl or ethyl, R^2 = methyl, ethyl, propyl or isobutyl, R^3 = H, methyl or ethyl) were prepared from the aqueous solution of corresponding glyoxime, $FeSO_4{\cdot}7H_2O$ and H_3BO_3 refluxed in inert gas atmosphere. FTIR, UV-VIS, TG-DTA-DTG, MS, PXRD measurements are consistent with the expected structure of the novel complexes.

In the case of $[Fe(dimethylglyoxime)_3(BOH)_2]$ we have succeeded to determine the crystal structure by the help of single crystal X-ray diffractometry. Accordingly, a centrosymmetric triclinic cell was obtained with P-1 space group #2. and with cell constants a = 12.949(7) Å, b = 22.445(13) Å, c = 22.824(13) Å, α = 78.684(9)°, β = 86.674(9)°, γ = 87.517(8)°, with volume = 6490.(6) Å^3. Interestingly, 5 crystallographically independent Fe(II)-tris-oximato centers could be distinguished. One of these is depicted in Fig. 1. In all centres the Fe-N bond lengths are in the range being diagnostically characteristic of low-spin iron(II) states.

^{57}Fe Mössbauer spectra (Fig. 2) of Fe-tris (glyoximato) complexes showed low-spin iron(II) state in the investigated complexes even if groups of branching alkyl chains were incorporated in the complexes. A decreases of quadrupole splitting was observed in $[Fe(R^1R^2glyoxime)_3(BOH)_2]$ compounds having R^1R^2 as dimethyl, methylisobutyl, methylethyl and dimethyl, which can be associated with structural changes in the complexes.

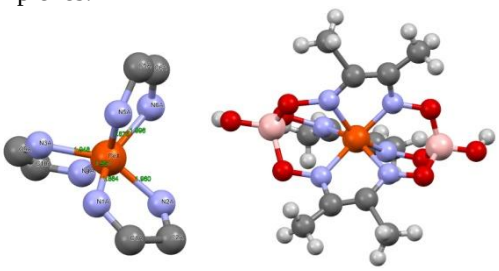

Fig. 1 Right side: Side view for only one iron(II) centre in the complex of $[Fe(dimethylglyoxime)_3(BOH)_2]$. Fe, N, C, B, O and H atoms are orange, blue, grey, pink, red and light grey colored, respectively. Left side: Geometry around the selected center of Fe with the Fe-N bond lengths.

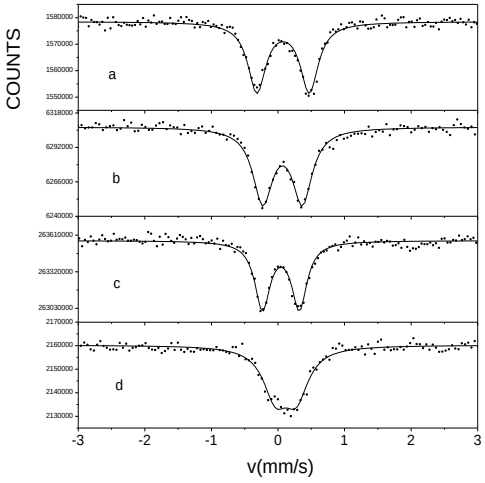

Fig. 2 ^{57}Fe Mössbauer spectra, recorded at 295 K, of $[Fe(dimethylglyoxime)_3(BOH)_2]$ (a), $[Fe(methylisobutyl-glyoxime)_3(BOH)_2]$ (b), $[Fe(methylethylglyoxime)_3(BOH)_2]$ (c) and $Fe(diethylglyoxime)_3(BOH)_2]$ (d)

Financial support from the National Research, Development and Innovation Office-NKFIH/OTKA (K115913 and K115784), Hungarian-Croatian Intergovernmental S & T (No. TET 16-1-2016-0002) and Domus Hungarica is gratefully acknowledged.

[1] Kuzmann E, Lengyel A, Homonnay Z, Várhelyi Cs. Jr, Klencsár Z, Kubuki S, Szalay R., Hyperfine Interact 226 (2014) 181–185

[2] Várhelyi C , Kuzmann E , Homonnay Z , Lengyel A , Pokol G, Izvekov V , Szalay R , Kun A , Tomoaia-Cotisel M , Covaci E , Garg VK , Oliveira AC , Goga F, Journal of Radioanalytical and Nuclear Chemistry 304 (2015) 745-750

Mössbauer Characterisation of Synthetic Analogues of the Helvite Minerals $Fe_4M_4[BeSiO_4]_6X_2$ (M=Fe, Mn, Zn; X=S , Se)

J.A Armstrong[a], S.E. Dann[a], K.U. Neumann[b] and J.F. Marco[c]

[a]*Department of Chemistry, Loughbourough University, Leicestershire, UK LE11 3TU*
[b]*Department of Physics, Loughbourough University, Leicestershire, UK LE11 3TU*
[c]*Instituto de Química Física "Rocasolano", CSIC, c/ Serrano, 119. 28006 Madrid. Spain*
(jfmarco@iqfr.csic.es)

The helvite group of minerals, with formula $(Fe,Mn,Zn)_8(BeSiO_4)_6S_2$ exist in nature within a significant compositional range of iron, manganese and zinc depending on the geology of the region where they occur. While the zinc (genthelvite) and manganese end members exist in nature and have been prepared synthetically using 2kbr hydrothermal pressure and 750°C, the pure iron species (danalite) does not occur geologically and had not been prepared using high pressure hydrothermal synthesis. Using high temperature in the laboratory, it has been possible to prepare the iron-rich materials, control their stoichometry and also prepare selenium and tellurium analogues. The materials crystallise with the sodalite structure, with a framework of vertex-sharing alternating beryllium and silicon tetrahedra, at the centre of the sodalite cage lies an M_4X tetrahedron (M= Fe, Mn and Zn) and X = S, Se or Te. The metal ions are tetrahedrally coordinated to three framework oxygens and the central chalcogen giving the metal species a tetrahedral coordination. This leads to an ordered array of tetrahedral M_4X clusters within the framework. Since the transition metal cations within the cluster contain unpaired electrons, this leads to the possibility of unusual magnetic interactions; since antiferromagnetic pairwise exchange cannot be satisfied in all three directions simultaneously in a tetrahedron, it leads to the possibility of magnetic frustration. Previous work on the manganese analogue showed strong interactions within the manganese clusters with a paramagnetic Curie temperature of 100K, however no Neel temperature was observed down to 4.2K indicating strong coupling within cages but no coupling between them. The difference in the strength of interaction presumably results from the distances over which such interactions take place. In this material, consideration of the iron-iron separations within the cage, intra-cage (3.93Å) and inter-cage (4.54 Å) indicates why the strength of these interactions may be different. In addition, there is the possibility for a through bond interaction via sulphur within a sodalite cage, while the intercage interaction would have to proceed via one or more framework oxygen atoms. Thus for electronically and magnetically active centres, the possibility exists for two distinct types of interaction – local for the four metal centres within a sodalite cage and a true long-range three-dimensional interaction between the units within the cages. The ability to prepare iron containing analogues of these materials means that Mössbauer spectroscopy could be used to further probe the local structure and interaction between the units.

We report on this paper on the Mössbauer characterisation of the family of synthetic helvite analogues, $Fe_4M_4[BeSiO_4]_6X_2$ (M=Fe, Mn, Zn; X=S , Se). The data show iron to be present as high spin Fe(II) in tetrahedral coordination. The room temperature Mössbauer spectra are composed either by singlets or doublets with small quadrupole splitting values suggesting a small valence contribution at that temperature. From the dependence of the quadrupole splitting with temperature the separation Δ between the two e_g orbitals, split by the presence of tetragonal distortion, has been estimated. The values of Δ range from 46.3 cm^{-1} for the material $Fe_8[BeSiO_4]_6S_2$ to 58.2 cm^{-1} for the material $Fe_4Zn_4[BeSiO_4]_6S_2$. No magnetically split spectra were observed for any of the various samples in the temperature range16K-298K. The lack of long magnetic order observed in the Mössbauer spectra was confirmed by neutron diffraction data which suggests that the M_4X units are largely magnetically isolated within their cages leading to a frustrated magnetic with no long range interaction for the sulfide species.

Manganese Doped Feroxyhyte Nano-Urchins Produced by Chemical Methods

N. Nishida[a], S. Amagasa[a], H. Ito[a], Y. Kobayashi[b,c] and Y. Yamada[a]

[a]*Department of Chemistry, Tokyo University of Science, 1-3 Kagurazaka, Shinjuku-ku, Tokyo, Japan*
[b]*Department of Engineering Science, The University of Electro-Communications, 1-5-1 Chofugaoka, Chofu, Tokyo, Japan*
[c]*Nishina Center for Accelerator-Based Science, RIKEN, 2-1 Hirosawa, Wako, Saitama, Japan*
(nnishida@rs.tus.ac.jp)

Feroxyhyte (δ-FeOOH) nanoparticles have attracted attention owing to their unique properties and potential application. In addition, iron oxide doped with foreign atoms is intriguing because it is known to exhibit unique magnetic and optical properties. It has also been reported that feroxyhyte doped with foreign atoms enhances those properties that are significant for photocatalysts and adsorbents of heavy metals. In this study, we examined the preparation of manganese doped feroxyhyte nano-urchins under an ambient atmosphere at room temperature.

Manganese doped feroxyhyte nano-urchins were prepared by a modified hydrazine reduction system under ambient atmosphere at room temperature. The synthesis was performed by starting with a mixture of $MnCl_2{\cdot}4H_2O$ and $FeCl_2{\cdot}4H_2O$ with various molar ratios of Mn/Fe. Four samples were prepared by employing initial mixtures with Mn/Fe = 7/3, 5/5, 3/7 and 1/9, respectively. A mixture of $MnCl_2{\cdot}4H_2O$ and $FeCl_2{\cdot}4H_2O$ (10 mmol in total metal salt), 2.3 g of $Na_2C_4H_4O_6{\cdot}2H_2O$, 0.4 g of gelatin and 3 g of NaOH were dissolved in 50 mL of pure water. Then, hydrazine solution was added slowly dropwise while ultrasonicating the mixture.

The X-ray diffraction pattern of prepared samples exhibited the characteristic peaks of feroxyhyte (JCPDS Card No. 13-87). Transmission electron microscopic observation showed that the resulting samples were needle-like particles around 100 nm in length, which formed nano-urchins structure. The Mn/Fe molar composition ratios of the nano-urchins measured by ICP-AES were compatible with the starting materials ratio.

Mössbauer spectra of the sample 3/7 were acquired at 293 and 3 K (Fig. 1). The spectrum acquired at 293 K showed a doublet, which was attributed to the superparamagnetic behavior of small crystallite. The Mössbauer spectrum at 3 K showed a sextet as the specimen no longer exhibited superparamagnetism at low temperature. The sextet had broad linewidth and was fitted assuming the distributed hyperfine magnetic fields. The mode of hyperfine magnetic fields was 480 kOe, which was smaller than those of our previously reported feroxyhyte nanoparticles (9 K: 487 and 519 kOe). Generally, the hyperfine magnetic field decreases when iron atoms are substituted by foreign atoms. As the manganese was successfully doped into the feroxyhyte nanoparticles, the decrease of the hyperfine magnetic fields were observed in this case.

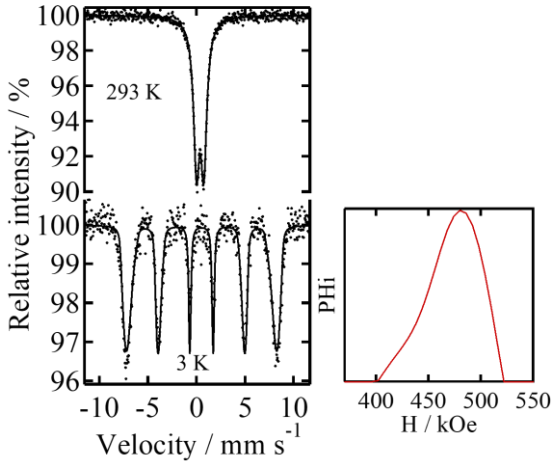

Fig. 1 Mössbauer spectra of manganese feroxyhyte nano-urchins obtained at 293 and 3 K.

We have previously reported that feroxyhyte nanoparticles were formed by oxidation of magnetite as intermediate species: the formation of feroxyhyte was associated with the rapid oxidation of the divalent iron. We have also reported a similar synthetic study using copper instead of manganese [2]; copper ferrite was obtained because Fe^{2+} in the intermediate species, magnetite, was substituted by Cu^{2+}, which prevented further oxidation of the species. In the present study, Fe^{2+} and Fe^{3+} were substituted by Mn^{2+} and Mn^{3+}, respectively, in the precursor, and rapid oxidation of both Fe^{2+} and Mn^{2+} in the precursor resulted in the production of manganese doped feroxyhyte.

[1] N. Nishida, S. Amagasa, Y. Kobayashi, Y. Yamada, Appl. Surf. Sci. 387 (2016) 996.
[2] N. Nishida, S. Amagasa, Y. Kobayashi, Y. Yamada, Hyperfine Interact. 237 (2016) 111.

Bifunctional Mg-Doped Magnetite Nanoparticles: Tuning Their Efficiency toward Potential Application in Magnetic Hyperthermia and Electrochemical Biosensors

M. Ognjanović[a], D. Stanković[a], B. Dojčinović[b] and B. Antić[a]

[a] *The Vinča Institute of Nuclear Sciences, University of Belgrade, Mike Petrovića Alasa 12-14, Belgrade, Serbia*
[b] *ICTM, University of Belgrade, Njegoševa 12, Belgrade, Serbia*
(miloso@vin.bg.ac.rs)

Superparamagnetic iron oxide nanoparticles (SPIONs) are in focus of scientific interest because of their potential biomedical applications such as MRI contrasting, targeted drug delivery, magnetic hyperthermia and others.

In this work we present a novel synthesis route and optimization of synthesis procedure in order to obtain magnetic nanoparticles of superior properties for application in magnetic hyperthermia as well as electrochemical biosensors. Synthesis parameters whose influence is examined are temperature and time of heating in a microwave field, the effect of surfactants and chemical composition on the morphology, particle size distribution, cytotoxicity, specific absorption and non-enzymatic glucose biosensing. Mg-doped Fe_3O_4 nanoparticles represented as $Mg_xFe_{3-x}O_4$ (x = 0, 0.1, 0.2, 0.4, 0.6, 0.8 and 1.0) series were prepared by two-stage procedure, coprecipitation method followed by hydrothermal treatment in microwave field at 100 °C for 10 minutes. The x values were conventionally determined, based on the assumption that the amount of Mg- doped into Fe_3O_4 is directly related to the molar ratio of Mg and Fe atoms in appropriate pure powders used for following experiment. Microstructural parameters of the samples were analysed by use of X-ray powder diffraction (XRD). Particle size and their morphology were examined using transmission electron microscopy (TEM) and ImageJ software. Electrosteric stabilization of samples was done by coating nanoparticles with citric acid (CA), oleic acid (OA) and polyethylene glycol (PEG) and heating abilities were compared by calculating Specific Absorption Rate (SAR) and Intrinsic Loss Power (ILP) from analysis of heating curves. The cytotoxic activity of the nanoparticles was done *in vitro* against the target malignant (HeLa LC174 and A549) cells as well as for normal MRC5 cells. Finally, nanoparticles were used for fabrication of modified carbon paste electrodes as novel system for electrochemical non-enzymatic detection of gallic acid [1]. Effect of Mg content (x) on the analytical performance of the modified electrodes toward gallic acid determination was tested.

Results of XRD and TEM analysis clearly demonstrate that nanoparticles were single phase, crystallizing in the spinel structure type (S.G. Fd-3m) with crystallite size ranging from 2–20 nm, which strongly depends on Mg concentration. The obtained results for cytotoxicity show that the tested nanoparticles display moderate cytotoxic activity according to tested malignant cells *in vitro*. In contrast, the investigated nanoparticles showed no significant cytotoxic effect towards normal MRC5 cells. From SAR measurements, it was found that the samples up to x = 0.2 of doped atoms have highest heating ability (Fig. 1a). The resulting value for specific absorption was in the range from 125.6 W/g to 363.3 W/g for sample $Mg_{0.2}Fe_{2.8}O_4$ at various frequencies and 200 G of magnetic field strength. After optimization of electrochemical method, the increase of magnesium concentration to the value of x = 0.4 in $Mg_xFe_{3-x}O_4$/glassy carbon paste modified electrode is followed with increase of the corresponding oxidation current of gallic acid (Fig. 1b). Working linear range from 1-39 µM was obtained with detection limit of 0.29 µM.

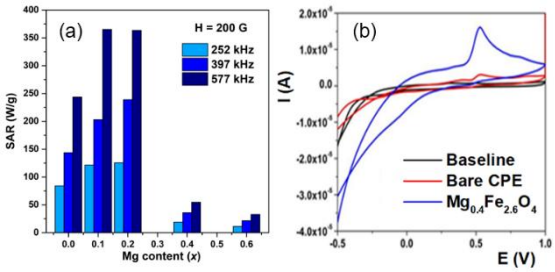

Fig. 1 (a) SAR values of the samples with different Mg content calculated by the slope method, **(b)** Cyclic voltammograms using $Mg_{0.4}Fe_{2.6}O_4$ modified electrode in the presence of 1 mM gallic acid.

The main conclusion of this work is that this two-step method of synthesis can be used to prepare doped magnetite nanoparticles of well-defined shape, relatively narrow size distribution and that examined ferrofluids can be potentially used in biomedicine through the hyperthermia therapy as well as electrochemical biosensors for gallic acid determination.

[1] D. Stanković, S. Škrivanj, N. Savić, A. Nikolić, P. Vulić, D. Manojlović, Electroanalysis 26(7) (2014) 1536-1543.

Spin Crossover Phenomenon in Iron Nitroprusside Intercalated with Pyrazine

Y. Plasencia, Y. Ávila and E. Reguera

Instituto Politécnico Nacional, Centro de Investigación en Ciencia Aplicada y Tecnología Avanzada, Unidad Legaria, Ciudad de México, México
(laplace2108@gmail.com)

Functional materials with switchable magnetic properties and memory transduction behaviour are interesting thanks to their potential technological applications [1]. In the last 20 years numerous coordination compounds with such features have been reported, however, the search for new findings in that sense has no limits. The Hoffman-like spin crossover compounds have been some of the most studied due to their laminar structure [2]. These are considered 2D compounds where each sheet is connected to the next one through organic ligands, such as pyrazine, pyridine and X-pyridine, were X = F, Cl, Br and I [3]. In these compounds, the iron atom presents an octahedral coordination while the external metal (Ni, Pt, Pd, Au, Ag) is found in a square planar environment of ligands. These compounds show a spin-crossover hysteretic behaviour and relative high transition temperatures, which depends on the involved organic molecules linked to the axial positions of the iron atom.

In this contribution, the spin-crossover behaviour for layered iron nitroprusside with pyrazine molecules intercalated between layers is discussed. Transition metal nitroprussides are recently reported [4]. These series of intercalation compounds have a 2D or 3D interconnected framework, depending on the intercalated organic ligand. When a single molecule is found linking two metal canters forming neighbouring layers, the resulting framework has 3D features. When the intercalated molecule is pyrazine (Pyz), a 3D network is formed of a formula unit . Its crystal structure is quite similar to that reported for the solids obtained with imidazole as intercalated molecule [4]. In the course of an study on $T(Pyz)_2[Fe(CN)_5NO]$ with T = divalent transition metals, we have observed the occurrence of a spin-crossover transition for the case of iron, which is discussed in this contribution.

Table 1 Hyperfine parameters for

	δ(mm/s)	Δ(mm/s)	Γ(mm/s)	A(%)
4K	0.711	0.283	0.289	40
77K	0.705	0.286	0.327	40
200K	0.668	0.281	0.392	40
255K	1.297	1.159	0.394	40

[1]Isomer shift reference scale to Sodium Nitroprusside.

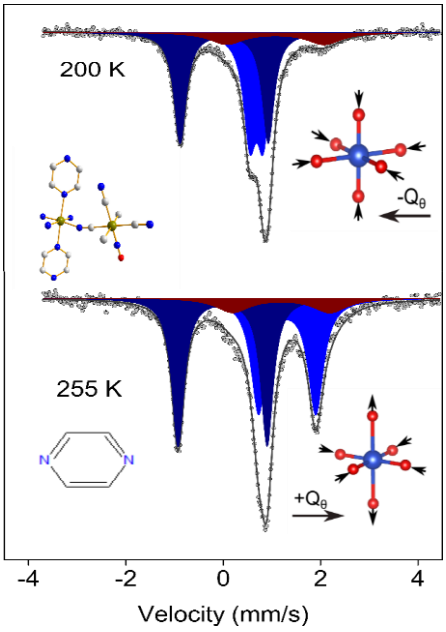

Fig. 1 Mössbauer spectra for the iron nitroprusside illustrating the occurrence of a spin-crossover transition.

Mössbauer spectroscopy is very sensitive to the spin-crossover phenomena because the hyperfine parameters isomer shift and quadrupole splitting change in an abruptly way when the iron atom goes from low spin to high spin configuration and vice versa. The Mössbauer spectra for this compound at different temperatures were recorded and their hyperfine parameters for the external iron atom are shown in Table 1. The iron of the nitroprusside ion has no change of spin configuration, it remains in a low spin state for the whole temperature range. Figure 1 shows the recorded spectra at 200 and 250 K. It is easy to notice the change in both, the isomer shift and quadrupole splitting due to a variation in the electron population of the iron atom t_{2g} orbitals. The Mössbauer study was complemented with DSC and magnetic susceptibility data, and supported with the crystal structure solution and refinement.

[1] Hollingsworth, M. D. Science 2002, 295, 2410.

[2] Iwamoto, T. In Inclusion Compounds; Atwood, J. L., Davies, J.E.D., MacNicol, D. D., Eds.; Oxford University Press: London, U.K.,1991;Vol.5,p177.

[3] V. Martínez, A.B. Gaspar, M.C. Muñoz, G.V. Bukin, G. Levchenko, J.A. Real. Chem. Eur. J. 15 (2009) 10960.

[4] D.M. Gil et al. Eur. J. Inorg. Chem. 11 (2016) 1690-1696.

Microstructural and magnetic properties of electrospun α-Fe_2O_3/$CuFe_2O_4$ nanocomposites

Ž. Petrović[a], A. Kremenović[b], M. Reissner[c], S. Musić[a] and M. Ristić[a]

[a]*Ruđer Bošković Institute, Division of Materials Chemistry, HR-10000 Zagreb, Croatia*
[b]*University of Belgrade, Faculty of Mining and Geology, Belgrade, Serbia*
[c]*Technical University of Vienna, Institute of Solid State Physics, A-1040, Vienna, Austria*
(ristic@irb.hr)

Hematite (α-Fe_2O_3) is n-type semiconductor with E_g value of ~ 2.1 eV and this material has various applications in traditional as well as advanced technologies. Recently, it has been extensively investigated as photoanode material in the photoelectrochemical (PEC) devices for water and air purification, waste water remediation, etc. A lot of efforts have been made to improve magnetic, electrical, catalytic, photocatalytic, or other properties of hematite. These properties are highly dependent on its crystal structure, particles size and morphology and can be tuned by controlling the synthesis conditions or/and doping with foreign metal ions There is also the increasing number of studies of nanocomposites of hematite and other metal oxides. These hematite materials are specifically interesting since they may exhibit new physical properties overcoming the failing of the single materials.

In the present work the nanofibers of α-Fe_2O_3/ $CuFe_2O_4$ (Fig. 1) have been synthesized using electrospinning method starting from viscous solution of polyvinylpyrrolidone (PVP) containing appropriate molar ratio of $Fe(NO_3)_3$ and $Cu(NO_3)_2$ solutions. As synthesized electrospun fibres were calcined in air at 500 °C for 1 hour and additionally at 700 °C for 1 hour. The reference electrospun α-Fe_2O_3 (Fig. 2) was synthesized at the same experimental conditions. The microstructural, magnetic and optical properties of the synthesized electrospun fibres were characterized by XRD, FE SEM, 57-Fe Mössbauer, FT-IR, UV-Vis-NIR spectroscopies and magnetometric measurements. A small amount of Fe_3O_4 was detected in the reference hematite fibres obtained at both calcined temperatures. On the other hand, the electrospun fibers containing copper ions obtained by calcination at 500 °C show the presence of α-Fe_2O_3, $CuFe_2O_4$ and γ-Fe_2O_3 phases. A small amount of Fe_3O_4 is also present. Additional heating at 700 °C of these fibres lead to the formation of hematite and cuprospinel composite. The α-Fe_2O_3/$CuFe_2O_4$ composite fibres showed enhanced magnetic and optical properties compared to reference α-Fe_2O_3 electrospun fibres.

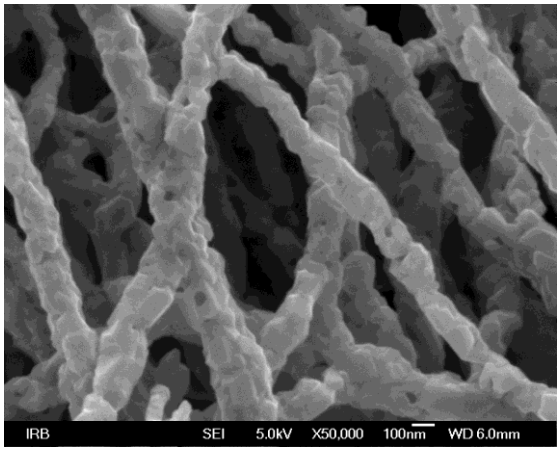

Fig. 1 FE-SEM image of α-Fe_2O_3/$CuFe_2O_4$ nanofibers calcined at 700 °C.

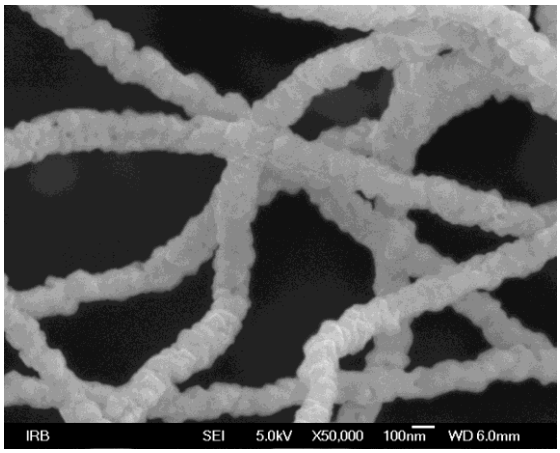

Fig. 2 FE-SEM image of α-Fe_2O_3 reference nanofibers calcined at 700 °C.

Mössbauer Studies on Nanosecond Infrared Pulsed Laser Deposition of Cobalt Ferrite Thin Films on Si (100) Substrates

M. Sánchez-Arenillas, J. De la Figuera, J.F. Marco, M. Castillejo and M. Oujja

Instituto de Química Física «Rocasolano», CSIC, Madrid 28006, Spain
(msanchez@iqfr.csic.es)

Cobalt ferrite has attracted interest in various applications such as electronic devices, ferrofluids, magnetic delivery microwave devices and high density information storage (1). Cobalt ferrite is a mixed iron (III) and cobalt (II) oxide ($CoFe_2O_4$) with a spinel-related structure (2). It can be rationalized as a cubic structure centered on the faces (FCC) of oxygen anions with the Fe (III) ions occupying the tetrahedral sites and the half of the octahedral sites, while the Co (II) ions occupy the other half of the octahedral sites (3). The electronic and magnetic properties depend strongly on the cation distribution.

Our work is focused on understanding the growth of cobalt ferrite thin films on Si (100) by several methods, in particular by pulsed laser deposition (PLD). The study is aimed at investigating the influence that the growth method has on the physicochemical properties of the obtained films and, in particular, in the cation distribution and crystal quality. For this goal we have used several characterization techniques such as X-ray Photoelectron Spectroscopy, Raman spectroscopy, X-Ray diffraction, low-energy electron diffraction and atomic force microscopy. Changes in the Fe cation distribution have been probed by Mössbauer spectroscopy. The Mössbauer spectra have been acquired for thin films in Conversion Electron Mössbauer Spectroscopy (CEMS) mode and in transmission mode for the thickest one. The latter one has been probed at both 26 and 298 K.

[1] Y.H. Hou, Y.J. Zhao, Z.W. Liu, H.Y. Yu, X.C. Zhong, W.Q. Qiu, D.C. Zeng and L.S. Wen, J. Phys.D: Appl. Phys, 43 (2010) 445003.
[2] Handbook of Magnetism and Advanced Magnetic Materials. (Wiley-Blackwell, 2007).
[3] J. Montes de Oca, L. Chuquisengo, H. Alarcón, Rev Soc Quím Perú 76 (4) (2010) 400.

Local Structural Analysis of Conductive Vanadate Glass Containing Tin or Indium by Means of Mössbauer Spectroscopy

N. Yamaguchi[a], T. Izumi[a], Y. Fujita[a], S. Masuda[a], H. Miyamoto[a], S. Kubuki[b], T. Nishida[a] and N. Oka[a]

[a]*Department of Biological and Environmental Chemistry, Kindai University, 11-6 Kayanomori Iizuka Fukuoka 820-8555, Japan*
[b]*Department of Chemistry, Graduate School of Science and Engineering, Tokyo Metropolitan University, 1-1 Minami-Osawa, Hachi-Oji, Tokyo 192-0397, Japan*
(nobuto.oka@fuk.kindai.ac.jp)

1. Introduction

Barium iron vanadate glass, *e.g.*, $20BaO{\cdot}10Fe_2O_3{\cdot}\ 70V_2O_5$ (composition in mol%), and its analogs show very high electrical conductivity at *RT* amounting to the order of 10^{-1} $S{\cdot}cm^{-1}$ after isothermal annealing at a given temperature higher than its glass transition temperature or crystallization temperature [1,2]. It is noted that the electrical conductivity (σ) is tunable from the order of 10^{-6} to 10^{-1} $S{\cdot}cm^{-1}$ by changing the condition of the annealing. It was reported that substitution of Cu^{I} ($3d^{10}$), Zn^{II} ($3d^{10}$) and Cu^{II} ($3d^{9}$) for Fe^{III} ($3d^{5}$) causes a further increase in the σ value [2].

In this study, we investigated substitution effect of Sn^{IV} ($4d^{10}$) and Sn^{II} ($5s^{2}$) for Fe^{III} ($3d^{5}$) on the local structure and the σ values measured before and after the annealing at 450 °C or 500 °C for 0-300 min.

2. Experimental

$20BaO{\cdot}x(SnO/SnO_2/In_2O_3){\cdot}(10\text{-}x)Fe_2O_3{\cdot}70V_2O_5$ glasses were prepared by a melt-quench method with weighed amounts of $BaCO_3$, Fe_2O_3, V_2O_5 and SnO, SnO_2 or In_2O_3. Each reagent mixture placed in an alumina crucible was melted in an electric muffle furnace at 1100 °C for 2 h under the ambient atmosphere. Almost black glass samples were prepared by quenching the melt on a brass mold in the air. Annealing of each glass sample was carried out at 450 or 500 °C in another electric furnace. The electrical resistivity of rectangular glass sample was determined by a conventional dc-four probe method at room temperature (*RT*), and a linear relationship was confirmed between the voltage and the electric current. The σ value was obtained by measuring the resistivity and the dimension of the sample. ^{57}Fe Mössbauer spectra were measured at *RT* by the conventional constant acceleration method with a source of 370 MBq of ^{57}Co(Rh). A foil of α-Fe was used for calibrating the velocity scale of the spectrometer and as a reference of isomer shift (δ).

3. Results and Discussion

After isothermal annealing at 500 °C for 60 min, conductivity of SnO_2-substituted vanadate glass, $20BaO{\cdot}3SnO_2{\cdot}7Fe_2O_3{\cdot}70V_2O_5$, was increased from 3.7×10^{-6} to 1.8×10^{-1} $S{\cdot}cm^{-1}$, which was a few times larger than that of $20BaO{\cdot}10Fe_2O_3{\cdot}70V_2O_5$ glass. Figure 1 shows *RT*-Mössbauer spectra of conductive vanadate glasses annealed at 500 °C for 0, 30 and 60 min. In the glass samples annealed for 60 min, quadrupole splitting (Δ) of Fe^{III} (0.57 $mm{\cdot}s^{-1}$) was smaller than that of SnO_2-free glass (0.62 $mm{\cdot}s^{-1}$), which reflected smaller distortion or higher symmetry of FeO_4 and VO_4 tetrahedra in the *3D*-network. This will cause the highly improved conductivity of SnO_2-substituted glass. Some results of ^{119}Sn Mössbauer measurements will also be discussed at the Conference.

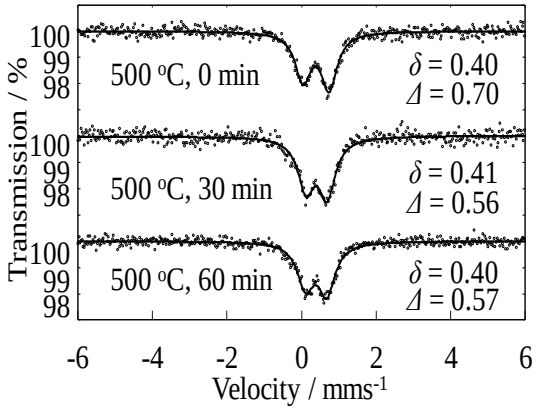

Fig. 1. ^{57}Fe Mössbauer spectra of $20BaO{\cdot}3SnO_2{\cdot}7Fe_2O_3{\cdot}70V_2O_5$ glass measured at *RT* after annealing at 500 °C for 0-60 min.

[1] K. Fukuda, A. Ikeda and T. Nishida, *Solid State Phenom*., **90/91** (2003) 215-220.

[2] T. Nishida, Y. Izutsu, M. Fujimura, K. Osouda, Y. Otsuka, S. Kubuki and N. Oka, *Pure and Appl. Chem*., **89** (2017) 419-428.

Less Than a Half-Life Remembered

F. J. Berry

School of Chemistry, The University of Birmingham, Edgbaston, Birmingham B15 2TT, United Kingdom
(f.j.berry.1@bham.ac.uk)

In this, the last contribution to MECAME 2018, Frank Berry, the person who this Conference honours, will reflect on more than forty years in solid state- and materials- chemistry with particular reference to the community of Mössbauer spectroscopists within which he has worked. A photographic record of places and people will prompt memories of the people who founded the community and were the pioneers in the fundamental science which underpinned the technique. The photographic record will track the development of Conferences and personal encounters which illustrate the evolution of the technique from an elegant experiment in solid state physics to a method of extracting features of fundamental scientific importance to a method with application in a diverse range of branches of science including industrial applications.

The presentation will focus on people and be a commentary on not only the scientific standing of numerous practitioners of the technique with expertise in different disciplines over the past half-century but a celebration of their humanity and friendship which has been a characteristic of these people and has enriched the lives of many within the community and, in a limited but real way, has contributed to a better understanding and shared enjoyment between many people from different cultures. The fact that this equates to only a fraction of what the presenter can remember is a reflection of both the dynamic nature of the community, the vibrancy of the individuals within it, the vastness of individual interests and the exceptional imagination of those individuals which has resulted in no limitation to exploitation.

This will also be an opportunity not just to look back but also to look forward with the presenter suggesting some personal qualities which younger colleagues might wish to consider as they look ahead. There will be a strong recommendation to make the most of opportunities, to take chances, and, above all, to enjoy life!

INDEX OF AUTHORS

A

Aballe L. 44
Adler P. **1**
Ágostai K. 33
Akiyama K. 31, 32, 35
Albino M. 6
Alenkina I.A. **27**
Amagasa S. 50
Ando T. 11
Androš Dubraja L. **40**
Antalffy M. 47
Antić B. 39, 46, 51
Aoki Y. 13, 35
Armstrong J.A. 49
Ávila Y. 52

B

Balogh J. **28**
Bazsó G. 15
Bernhardt B. 10
Berry F.J. **41**, **56**
Bell A.M.T. 37
Bessas D. 15
Bharut-Ram K. 7
Bingham P.A. 37
Brand R.A. 25
Brezesinski T. 40
Bošković M. 13, **42**, 46
Bujdosó L. 28

C

Castillejo M. 54
Celse J.-P. 15
Christensen M. 44
Chukin A.V. 19
Chumakov A.I. 15
Cherkezova-Zheleva Z. **43**
Clark L. 6
Ćosić V. 42

D

Dann S.E. 49
Darko B. 38
Dasireddy V.D.B.C. 7
Delgado Soria G. **44**
Dénès G. **29**
Dojčinović B. 39, 51
Dote H. 16
Dubiel S.M. **2**

F

Felser C. 12
de la Figuera J. 44, 54
Filip J. 14
Fodor F. 30, 33
Forder S.D 37
Foerster M. 44
Felner I. 27
Fujita Y. 17, 36, 55

G

Ganeshraja A.S. **4**
Garcia Y. **5**
García J.A. 20
Garitaonandia J.S. 20
Gerasimchuk N.N. 48
Girones Lopez J. 10
Goga F. 48
Golban L.-M. 48
Greaves C. 41
Grenèche J.-M. **6**
Gruner M.E. 25

H

Hah H.-Y. 41
Hahn H. 25, 40
Hanžel D. **7**
Higashinaka R. 13, 35
Homonnay Z. 13, **30**, 31, 47, 48
Huszthy P. 48

I

Ito H. 50
Ishikawa S. 31
Iwai S. 16
Izumi T. **55**

J

Jafari A. 15
Janus P. 44
Jiang L. 46
Johnson C.E. 41
Johnson J.A. 41
Jones A.H. 37
Jumas J.-C. **8**

K

Kaptás D. 28
Khan F. 7
Khanh N.Q. 15
Kamali S. 41
Kaneko M. **9**, 16
Katayama Y. **31**
Keresztes Sz. 47
Kis V. 30
Kitagawa A. 11, 26
Klencsár Z. 30
Klingelhöfer G. **10**
Kobayashi Y. **11**, 26, **32**, 50
Kobayashi J. 11, 26
Konstantinova T.S. 27
Környei J. 47
Kovács K. 30, **33**
Krehula S. 13, 31, 35, **45**, **46**
Kruk R. 25, 40
Kremenović A. 53
Ksenofontov V. **12**
Kubo M.K. 11, 26
Kubuki S. **13**, 31, 32, 35, 36, 55
Kuzmann E. 13, 27, 30, 31, **47**, **48**

L

de Laune B.P. 41
Lázár K. **34**
Leblanc M. 6
Lengyel A. 30
Lhoste J. 6
Li X. 24, 46
Likozar B. 7
Lightfoot P. 6
Lippens P.-E. 8
Lobera A. 37
López-García J. 20

M

Machala L. **14**, 38
Madamba M.C. 29
Maisonneuve V. 6
Maksimova A.A. 19
Mandziak A. 44
Marco J.F. **41**, 44, **49**, 54
Masuda S. 17, 55
Máthé Z. 34
Matsuda T.D. 13, 35
Medvedev S.A. 12
Merazig H. 29
Merkel D.G. 15

Mihara M. 11, 26
Mitar I. 46
Mitov I. 43
Miyamoto H. 17, 55
Miyazaki J. 11, 26
Morris R.V. 10
Morishita S. **35**
Muntasar A. 29
Musić S. 13, 30, 31, 35, 45, 46, 53

N

Nagatomo T. 11, 26
Nagy D.L. **15**
Naka T. 13, 35
Nakane T. 13, 35
Nakashima S. **16**
Natori D. 26
Naumov P. 12
Németh Sz. 30
Nemeth S. 31
Neumann K.U. 49
Nomura K. 31, 32, 35
Nishida N. **50**
Nishida T. 13, 17, 32, **36**, 55

O

Ognjanović M. 39, **51**
Oka N. **17**, 36, 55
Okabayashi J. **18**
Olivier-Fourcade J. 8
Oshtrakh M.I. **19**, 27
Oujja M. 54

P

Paneva D. 43
Payen C. 6
Plasencia Y. **52**
Pereiro E. 44
Pérez-Landazába J.I. 20
Perović M. 13, 42, 46
Petrova E.V. 19
Petrović Ž. 45, 53
Plazaola F. **20**
Pokol Gy. 48
Prieto J.E. 44
Prieto P. 44
Prucek R. 14

Q

Quesada A. 44

R

Ram K.B.
Raptopoulou C.P. 21
Recarte V. 20
Reguera E. 52
Reissner M. 53
Reitz C. 40
Renz F. 10
Ristić M. 13, 30, 31, 35, 45, 46, **53**
Rodionov D. 10
Rodríguez-Velamazán J.A. 20
Rüffer R. 15

S

Sajti Sz. 15
Sanakis Y. **21**
Sánchez-Alarcos V. 20
Sánchez-Arenillas M. 44, **54**
Sato M. 11
Sato S. 11, 26
Sato Y. 11, 26
Sato W. 11, 26
Schröder C. 10
Scrimshire A. **37**
Semionkin V.A. 27
Sharma V.K. **38**

Shiba S. 32
Shylin S. 12
Solti Á. 30, 33
Some K. 11
Stanković D.M. **39**, 51
Sterianou I. 37
Stewart S.J. **22**
Sun G. 46
Sunakawa K. 13, 35
Szalay R. 30, 48

T

Takahama N. 11
Takahashi K. 11
Tanigawa S. 26
Thomas M.F. 41
Tsutsui S. **23**
Tucek J. 14

U

Unzueta I. 20

V

Valvidares M. 44
Várhelyi Jr Cs. 48
Várhelyi M. 48
Vasili H.B. 44
Velasco L. 40
Velinov N. 43
Vinogradov A.V. 27

W

Wang J. 4, **24**, 46
Wang D. 25
Watanabe M. 9
Wende H. 25
Whittaker M.J. 41
Witte R. **25**, 40
Wortmann G. 12
Wu C. 46

Y

Yamada Y. 11, **26**, 50
Yamaguchi N. **55**
Yoshinami K. 16
Yuasa M. 17

Z

Zhang T. 46
Zboril R. 14, 38

Mössbauer Sources & Reference Absorbers

RITVERC™ isotope products

Mössbauer Sources

Our sources are designed for all types of Mössbauer spectrometers. Together with high quality spectral characteristics the sources have reliable capsules. Sources are certified on high-precision Mössbauer spectrometer.

^{57}Co
Matrix: Rh
Type: serial, point
Window: Be
Activity: 1-200 mCi

^{119m}Sn
Matrix: $CaSnO_3$
Type: serial
Window: Be
Activity: 2-20 mCi

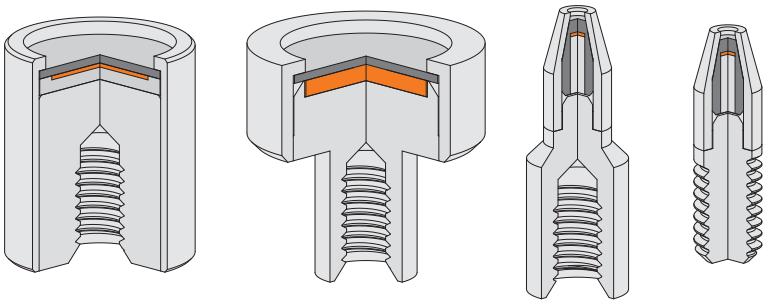

Serial Sources

Special Purpose Point Sources

Sources Grippers

Grippers are designed for mounting and dismounting of Mössbauer sources (MCo7 and MSn9) manufactured by Ritverc on a spectrometer.
Significant decrease of gamma radiation provided by tungsten shield.

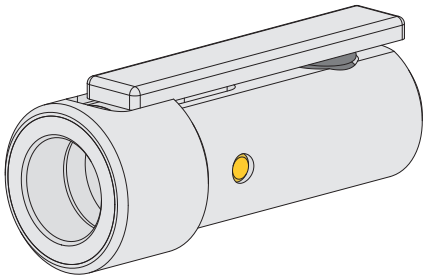

Reference Absorbers

Enriched Fe & Natural Fe reference absorbers:
- single line absorber;
- double line absorber;
- six line absorber

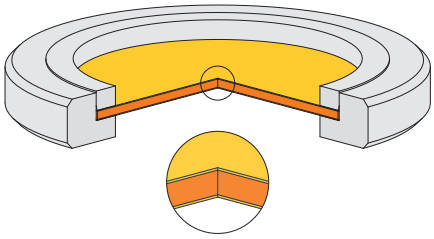

RITVERC GmbH
Mössbauer Sources & Reference Absorbers. Grippers

www.ritverc.com
info@ritverc.com
P: +7 812 297 44 63
F: +7 812 297 58 87

10, Kurchatova str.
194223, St. Petersburg,
Russia